metals

MDPI

Review

The Expanded Phases Formed in Stainless Steels by Means of Low-Temperature Thermochemical Treatments: A Corrosion Perspective

Francesca Borgioli

Department of Industrial Engineering, University of Florence, via S. Marta 3, 50139 Florence, Italy; francesca.borgioli@unifi.it; Tel.: +39-055-275-8734

Abstract: Surface engineering of stainless steels using thermochemical treatments at low temperatures has been the subject of intensive research for enhancing the surface hardness of these alloys without impairing their corrosion resistance. By using treatment media rich in nitrogen and/or carbon, it is possible to inhibit chromium compound formation and obtain supersaturated solid solutions, known as expanded phases, such as expanded austenite or S-phase in austenitic stainless steels, expanded ferrite in ferritic grades, and expanded martensite in martensitic grades. These low-temperature treatments produce a significant increase in surface hardness, which improves wear and fatigue resistance. However, the corrosion behavior of the modified surface layers remains of paramount importance. In the international literature, many studies on this topic are reported, but the results are not always univocal, and there are still open questions. In this review, the corrosion behavior of the expanded phases and the modified layers in which they are present is critically analyzed and discussed. The relationships between the phase composition and the microstructure of the modified layers and the corrosion resistance are highlighted while also considering the different test conditions. Furthermore, corrosion test methods are discussed, and suggestions are given for improving the measurements. Finally, perspectives on future directions for investigation are suggested for encouraging further research.

Keywords: stainless steels; low-temperature treatments; nitriding; carburizing; expanded austenite; S-phase; expanded martensite; expanded ferrite; corrosion resistance

Citation: Borgioli, F. The Expanded Phases Formed in Stainless Steels by Means of Low-Temperature Thermochemical Treatments: A Corrosion Perspective. *Metals* **2024**, *14*, 1371. https://doi.org/10.3390/met14121371

Academic Editors: Frank Czerwinski, Zhongyu Cui, Chao Liu and Tianliang Zhao

Received: 14 October 2024
Revised: 20 November 2024
Accepted: 26 November 2024
Published: 1 December 2024

1. Preface

Low-temperature thermochemical treatments with nitrogen and/or carbon are receiving increasing interest for improving the surface hardness of stainless steels without impairing their corrosion resistance. Using these treatments, it is possible to obtain supersaturated solid solutions, known as expanded phases, which have peculiar characteristics. Despite the relevant number of scientific papers devoted to the low-temperature treatment of stainless steels, there is still a gap in our knowledge concerning the corrosion behavior of expanded phases and of the modified surface layers in which they are present. A complete understanding of the mechanisms underlying the corrosion behavior is still lacking, and the influence of the microstructure and the phase composition of the modified surface layers on corrosion resistance in different environments is often overlooked.

This review has the aim of critically analyzing and discussing the relevant literature on the corrosion behavior of low-temperature-treated stainless steels, offering a picture as complete as possible. The review is organized into eight main sections. In the introduction (Section 2), stainless steels and low-temperature thermochemical treatments are considered. In Section 3, the characteristics of the passive layer, formed on stainless steels, and the effects of N and C on the corrosion behavior are discussed. The following sections concern the characteristics of the modified layers formed in the different stainless steel grades and

summarize the corrosion behavior studies carried out in different environments using different test conditions and methodologies. In Section 4, ferritic stainless steels are discussed. Section 5 regards martensitic stainless steels, and Section 6 describes the austenitic stainless steels. Section 7 is devoted to duplex stainless steels, and in Section 8, PH stainless steels are discussed. Finally, in Section 9, the main outcomes are summarized, highlighting the questions still open and possible future directions for investigation. The corrosion test methods are also discussed, and suggestions are given to improve the measurements.

2. Introduction

The widespread use of stainless steels is promoted by the fact that compared to low alloy steels, they remain without rust traces in many environments thanks to their resistance to general corrosion. The key alloy element for stainless steels is chromium (Cr). In fact, in these iron (Fe)-based alloys, this element is added in the amount of at least of 10.5 wt.%, and thus it promotes the formation of an adherent, continuous, non-porous, self-healing passive film, which protects the substrate from the corrosive environment [1,2].

As an alloy element, Cr tends to stabilize the body-centered cubic (b.c.c.) structure of ferrite (α-Fe and δ-Fe). A similar ferrite-stabilizing effect is given by molybdenum (Mo), niobium (Nb), titanium (Ti), and silicon (Si). On the contrary, the addition of nickel (Ni) expands the phase field of face-centered cubic (f.c.c.) austenite (γ-Fe), and therefore this phase is stable across a wider temperature range. A similar effect is given by manganese (Mn), nitrogen (N), and carbon (C). By changing the amount of the alloy elements able to stabilize ferrite or austenite, it is possible to obtain ferrite, martensite, and austenite and their related microstructures. Based on these microstructures, stainless steels are classified into five groups: ferritic, martensitic, austenitic, duplex, and precipitation-hardening [1–3].

Ferritic stainless steels are essentially Fe-Cr alloys, with a Cr content in the range of 10.5–30 wt.%, C less than 0.2 wt.%, and no or very little Ni. Therefore, their cost is reduced compared to the expensive Ni-containing grades. They are ferromagnetic and nonhardenable, and they have a ductile-to-brittle transition. Regarding mechanical properties, they have a relatively low strength, which can be improved through cold working. They have a moderate corrosion resistance in many environments, and they are resistant to chloride stress-corrosion cracking (SCC). By reducing the content of interstitial elements (N, C), grades with higher Cr (up to 30 wt.%), Mo (up to 4 wt.%), and Ni (up to 2 wt.%) have been developed. These grades, called super-ferritics, have improved corrosion resistance and excellent resistance to SCC.

Martensitic stainless steels have a composition similar to ferritic grades, but they contain less Cr (10–18 wt.%) and more C (up to 1.2 wt.%). As a consequence, the austenite phase becomes stable at high temperatures, and then, through quenching, it transforms into martensite. Successive tempering treatments can give favorable combinations of high strength and adequate toughness. The Cr content is limited, and hence a lower corrosion resistance is obtained when compared to that of ferritic and austenitic grades. By reducing the C content and adding Ni and Mo, super-martensitic grades have been developed, which have improved toughness and corrosion resistance.

In austenitic stainless steels, the austenite structure is maintained by a balance between the Cr content, as the ferrite-forming element, and the amount of austenite-forming elements, including, in particular, Ni. A Ni content $\geq$ 8 wt.% is present in the CrNi AISI 300 series austenitic stainless steels, while Ni is reduced and substituted by Mn and N in the CrMn AISI 200 series. AISI 200 series steels are cheaper and have an improved strength, but they have a lower corrosion resistance than CrNi grades. A negligible Ni content (<0.3 wt.%), counterbalanced by a significant increase in Mn (9–24 wt.%) and N (0.45–1.1 wt.%), is present in the Ni-free austenitic stainless steels. Austenitic stainless steels are nonmagnetic, and they can also be used at cryogenic temperatures. They have high ductility and toughness but relatively low yield strength, which can be increased through cold working. They usually have very good corrosion resistance in many environments, but they may be subjected to SCC in chloride ion (Cl^-)-containing environments. Mo

addition increases their resistance to localized corrosion. By increasing the Cr, Ni, and Mo content, super-austenitic grades have been produced, and they show an enhanced corrosion resistance.

Duplex stainless steels have a balanced alloy content of mainly Cr and Ni; therefore, upon using appropriate heat treatments, both austenite and ferrite are present. They are subject to ductile-to-brittle transition, but the transition temperature is lower than that of ferritic stainless steels. They have higher strength than either ferrite or austenite present alone. The corrosion resistance is comparable to that of austenitic stainless steels with a similar Cr content, but the resistance to SCC and corrosion fatigue is significantly improved.

Precipitation-hardening (PH) stainless steels are CrNi steels that contain elements, such as copper (Cu) and aluminum (Al), able to form precipitates when aging treatments are carried out. According to their microstructure after the solution-annealing heat treatment, they are classified as martensitic, semi-austenitic, and austenitic. In the aged condition, the steels of this grade have high strength and a corrosion resistance usually comparable to that of CrNi austenitic stainless steels with similar Cr and Mo content.

Even if stainless steels are often indicated as corrosion-resistant alloys, their effective corrosion resistance depends on the possibility of maintaining a fully protective passive film in different environments. The passive film may cease to be protective when the environment is too reducing, and therefore the formation of passive species is inhibited and the film dissolves in the active state. This may also occur when it is too oxidizing, as the oxidized species may be not stable and a transpassive dissolution of the film occurs [2,4]. In acidic solutions, general (uniform) corrosion may occur when stainless steels are in contact with aqueous solutions of reducing acids, such as hydrochloric acid (HCl) or sulphuric acid (H_2SO_4). In the presence of nitric acid (HNO_3), due to the oxidizing effect of this acid, a good or even excellent resistance is shown by many stainless steel grades [2]. As an example, CrNi austenitic stainless steels in annealed conditions have very good corrosion resistance in HNO_3 in concentrations from 0 to 65%, while in H_2SO_4 they have good resistance in very dilute or highly concentrated solutions, and their corrosion loss is high at intermediate concentrations [2]. In alkali solutions, stainless steels have very good corrosion resistance. All stainless steels resist general corrosion in solutions of NaOH with all concentrations up to 65 °C [2].

When the passive film is locally broken and unable to reform, localized corrosion occurs, such as pitting and crevice and intergranular corrosion [2]. The presence of Cl^- in the environment is the most common cause of pitting and crevice corrosion, as this ion is able to weaken the passive film, thus decreasing its protective effect [2,4,5]. Both pitting and crevice corrosion phenomena are autocatalytic. The small zone in which the passive film breaks down becomes anodic, while the surrounding passive steel is cathodic, and therefore metal dissolution can easily and rapidly occur. The presence of an excess of positive charge due to metal ions present within the pit tends to promote the migration of Cl^- to maintain the electroneutrality. Metal chlorides can form, and their subsequent hydrolysis causes an increase in the H^+ concentration within the pit. The acidic conditions stimulate further dissolution of the metal, and the process tends to accelerate with time [6]. Pitting and crevice corrosion phenomena are particularly harmful, as corrosion may penetrate so deeply into a metallic component that it affects its structural integrity. Intergranular corrosion generally occurs in sensitized steels when Cr compounds, such as Cr carbides, form as a consequence of a thermal treatment. The concurrent Cr depletion in the region adjacent to the precipitate may locally weaken the passive film, and corrosion phenomena may occur at grain boundaries in aggressive environments [2,4]. The combination of environments able to cause localized corrosion and tensile stress may promote SCC [2,4].

Taking into account the fact that corrosion phenomena depend on the steel (the alloy composition, the microstructure, and the surface finishing) and the environment, the corrosion resistance of stainless steels can be improved further using different strategies. From a metallurgical point of view, it is possible to act on type and amount of alloy elements and use heat treatments to form a favorable microstructure. The increase in the Cr content,

as well as the content of Ni in many grades, the addition of Mo, and the control of C have been proven to be efficient ways to obtain stainless steels with enhanced corrosion resistance in specific environments [2,7]. The effect of the Cr, Mo, and N content on the pitting corrosion of austenitic, duplex, and ferritic stainless steels is qualitatively indicated by the Pitting Resistance Equivalent Number (PREN) [4].

$$\text{PREN} = (\%\ \text{Cr}) + 3.3\ (\%\text{Mo}) + x\ (\%\ \text{N}) \quad (1)$$

where x is 0 for ferritic stainless steels, 30 for austenitic stainless steel, and 16 for duplex stainless steels. The higher the PREN, the higher the resistance to pitting in chloride solutions. Another strategy entails the possibility of adding corrosion inhibitors to the solution, but it cannot be applied in all service conditions [8].

A different approach is given by surface engineering, in which only the topmost part of a component is modified [9–11]. The need to maintain or even increase the corrosion resistance together with an improvement in the surface hardness and the tribological properties has made surface engineering a fundamental step in manufacturing to prolong the life of components. Among the different techniques, in recent years, N and/or C surface alloying using thermochemical treatments performed at low temperatures is receiving increasing interest for the surface modification of stainless steels [12–16]. When the treatment temperature is quite low (usually in the range of 300 ÷ 500 °C), the interstitial (N, C) atoms can freely diffuse, while the diffusion of substitutional atoms, such as Cr, is significantly slowed down, and these atoms can be considered relatively "immobile" in the lattice. As a consequence, the formation of Cr compounds tends to be inhibited. In these para-equilibrium conditions [17], interstitial atoms are solubilized in the Fe-based lattices well beyond the solubility limits, and supersaturated solid solutions form. The interstitial content may be up to several hundred times higher than the equilibrium solubility, and therefore a significant lattice expansion occurs. For this reason, these supersaturated solid solutions are often described as "expanded" phases: expanded ferrite, expanded martensite, and expanded austenite, or S-phase, depending on the parent phase [12,16,18]. The N and C content of these expanded phases is reported in Table 1; as a comparison, the maximum interstitial content in ferrite and austenite in the equilibrium conditions, as deduced based on Fe-N [19] and Fe-C [20] phase diagrams, is reported together with the N range for the two main Fe nitrides, γ'-Fe_4N (f.c.c.) and ε-$Fe_{2-3}N$ (hexagonal).

Table 1. N and C content in the expanded phases and in the equilibrium phases.

Phase	N (at. %)	C (at.%)	Reference
Expanded ferrite (max.)	24	10	N: [21], C: [17]
Expanded martensite (max.)	22	10	N: [22], C: [23]
Expanded austenite (max.)	38	19	N: [24], C: [25]
α-Fe (max.)	0.4	0.104	N: [19], C: [20]
γ-Fe (max.)	10.3	9.23	N: [19], C: [20]
γ'-Fe_4N	19.3 ÷ 20		N: [19]
ε-$Fe_{2-3}N$	15 ÷ 33		N: [19]

Intensive studies have highlighted that these expanded phases can be obtained in all of the stainless steels grades, and their presence can significantly improve the surface hardness, thus enhancing tribological properties and fatigue resistance. Regarding corrosion resistance, it may be maintained or even increased in Cl^--containing solutions when the modified surface layers produced by low-temperature treatments consist mainly of expanded phases. On the contrary, in Cl-free environments, as in H_2SO_4 aqueous solutions, contradictory results have been found.

Low-temperature treatments producing expanded phases have many advantages compared to other surface engineering strategies. Compared to surface treatments, which modify only the passive layer, such as anodization [26], they produce hardened surface layers, which enhance tribological properties [18,27–31] and resistance to corrosion-related me-

chanical failures, such as corrosion wear [31], corrosion erosion [32], corrosion fatigue [33], and stress corrosion cracking [34]. Compared to coating processes, low-temperature treatments produce expanded phases, which entail the modification of the parent matrix, thus avoiding coating detachment due to insufficient adhesion. The use of N and/or C gaseous precursors reduces the environmental impact compared to coating processes, such as hard chromium plating [35]. The use of low treatment temperatures compared to those used in other diffusion-based processes, such as aluminizing [36] and boriding [37], reduces the risk of component distortion and decreases energy consumption. Low-temperature thermochemical treatments can be performed using gas [38,39], plasma [40,41], and salt bath [42,43] processes or even a solid precursor [44]. Gaseous processes offer better control of interstitial atom feeding in the steel, even if the removal of the passive layer for promoting N and/or C solubilization may require an additional step [38]. Plasma-based treatments are particularly efficient, as they allow for removing the passive layer by means of ion bombardment, they have a reduced environmental impact, and they are faster and more efficient than gaseous-based processes [40]. The scaling up of the processes proposed in research papers from laboratories to production processes has been difficult, but gas, plasma, and salt bath processes are now commercially available [15].

To date, more than a thousand papers have been published in the international literature concerning the low-temperature thermochemical treatment of stainless steels, the expanded phase formation, and the characteristics of the produced modified surface layers. Many of them are about austenitic stainless steels and expanded austenite, and the reviews have had a similar focus [12,15,18,45]. Only a few reviews also concern the other expanded phases and the other stainless steels grades [12,13,16]. In spite of the paramount importance of the corrosion behavior of stainless steels, this topic is usually considered as a part of more general reviews [12,16,18,46]. Reviews specifically focused on corrosion behavior have generally considered either the nitrided and/or carburized steels [46] or only austenitic stainless steels [47]. However, an analysis of the international literature shows that there is still a gap in our knowledge on this topic, including, for example, the mechanisms underlying the corrosion behavior of expanded phases, the influence of microstructural characteristics and the phase composition of the modified surface layers on corrosion behavior in different environments, and the influence of the corrosion test conditions on the reported measurements. Extensive reviews, which also take into account these topics, are not present in the literature.

The aim of the present review is to critically discuss and analyze the main studies regarding the effects of the formation of expanded phases on the corrosion behavior of stainless steels subjected to low-temperature treatments. The characteristics of the modified surface layers are considered, and their corrosion behavior in different environments is discussed, highlighting the conditions suitable for maintaining or even enhancing the corrosion resistance of the parent alloy. The possible mechanisms underlying the corrosion behavior of the expanded phases and the influence of the corrosion test conditions on the obtained measurements are also considered.

3. The Passive Layer and the Effects of N and C Alloying on Corrosion Behavior

3.1. The Passive Layer and N and C Alloying

As the interface between the steel and the environment, the passive layer has a fundamental role in preserving the underlying metal by slowing its dissolution by many orders of magnitude. Despite its small thickness, typically about 1–3 nm [48,49], the passive layer cannot be regarded as a "rigid" layer; it is a dynamic one able to adjust its thickness and composition depending on environmental conditions [50].

In stainless steels, Cr is the key alloy element for allowing a protective passive layer to form [7]. However, the passive film does not consist of Cr oxide alone, and its composition and structure depend on alloy elements [7,51], the conditions in which it forms (for example, in air, in passivating solutions, or with electrochemical treatments) [51–54], and the corrosive environment [48,55,56]. Therefore, the conditions for passive behavior of stainless

steels depend on both the material itself (the alloy composition, the microstructure, the surface finishing) and the corrosive environment [2].

Many analysis techniques are used for evaluating the characteristics of the passive film. Auger electron spectroscopy (AES) and X-ray photoelectron spectroscopy (XPS) are ex situ techniques that give information on the chemical composition of the film, while in situ techniques, such as photoelectrochemical analysis, allow for detecting the structure evolution during the film growth. Additional information is given by electrochemical techniques, such as Mott–Schottky analysis, which allows for evaluating the semiconductive properties of the film, and electrochemical impedance spectroscopy (EIS). EIS experimental data can be modeled with an electrical equivalent circuit (EEC) in order to evaluate the properties of the passive film and obtain a physical picture of the corrosion phenomena. Stainless steels usually have Nyquist plots characterized by one or two connected semicircles, which are related to one or two time constants [47,57,58]. For one semicircle, the EEC is modeled using a resistance related to the solution in series with the parallel combination of a resistance R (charge transfer resistance) and a capacitance, or a constant phase element, C (double layer capacitance). When two (or more) semicircles are present, data are modeled with two (or more) parallel combinations of resistance and constant phase elements in series or hierarchically connected [47,58–60]. These parallel combinations are related to charging/discharging processes occurring at the electrode/electrolyte interface and the processes occurring in the oxide, but the attribution to a high or a low time constant is not univocal.

Analysis of the passive film of stainless steels has shown that it has a complex structure. Cr(III) oxide, Cr_2O_3, and, eventually, Cr hydroxide are mainly detected in the inner part in contact with the metal substrate, and this region has a *p*-type semiconductivity. In the outer region, at the film–electrolyte interface, which has an *n*-type semiconductivity, Fe(II)/Fe(III) oxides and hydroxides are observed [61,62].

The relative amount of Cr and Fe oxides depends not only on the alloy composition but also the corrosion environment. In acid aqueous solutions, Fe oxides have a higher dissolution rate than that of Cr oxide, so the surface film strongly enriches in Cr in the passive range. As the transpassive range is reached, the oxidation of Cr(III) into Cr(IV) with the formation of soluble $Cr_2O_7^{2-}$ occurs, and therefore the Cr content decreases [49]. In alkaline solutions, Fe oxides are less soluble, and the enrichment of Cr in the passive film is lower [49].

Together with Cr and Fe, other alloy elements of stainless steels may play a role in the passive film. In Ni-containing alloys, such as austenitic grades, Ni is considered crucial for the formation of the passive film, but its presence in the film itself is still a matter of debate [7]. An enrichment of metallic Ni beneath the passive layer was detected by Fredriksson et al. [63], while other authors observed Ni in the form of oxides/hydroxides in the passive film [64,65]. Mo is added to improve the pitting corrosion resistance in Cl^--containing solutions, and various mechanisms have been proposed to explain its beneficial role, while also taking into account that Mo oxides are detected in the passive film [7].

The addition of N and/or C as alloy elements affects the composition of the passive layer, even if it does not change its two-layer structure. As an example, the alloy elements and the N, C, and O content vs. the depth in the passive layer of nitrided and carburized austenitic stainless steel specimens are shown in Figure 1.

An enrichment of N atoms at the metal–film interface is detected in N-containing austenitic stainless steels [66,67]. Similarly, in N-rich expanded austenite, a substantial increase in N atoms in the inner Cr oxide/hydroxide region is observed, while in the outer region, where Fe oxides/hydroxides are present, only a small amount of N is detected [68,69] (Figure 1a). A change in the semiconductive behavior is also registered, with a decrease in acceptor and donor density and a decrease in the flat band potential, which is particularly significant for N-rich expanded austenite [67,70].

In the case of C alloying, as in C-rich expanded austenite (Figure 1b), a very high C content is detected at the surface, but it is difficult to say whether it is either present in

the oxide film, or due to contamination or a carbon soot. C content tends to markedly decrease at a depth of about 0.5 nm, and then it is higher in the Cr-oxide-rich inner part of the passive layer [71]. The Cr content in the passive layer of C-added austenitic stainless steels is registered to increase [72], decrease [73], or remain identical [71] compared to that of untreated steel. As observed for N alloying, a change in the semiconductive behavior is observed, and a decrease in acceptor and donor density is registered, even if it is smaller than that observed with N alloying [74].

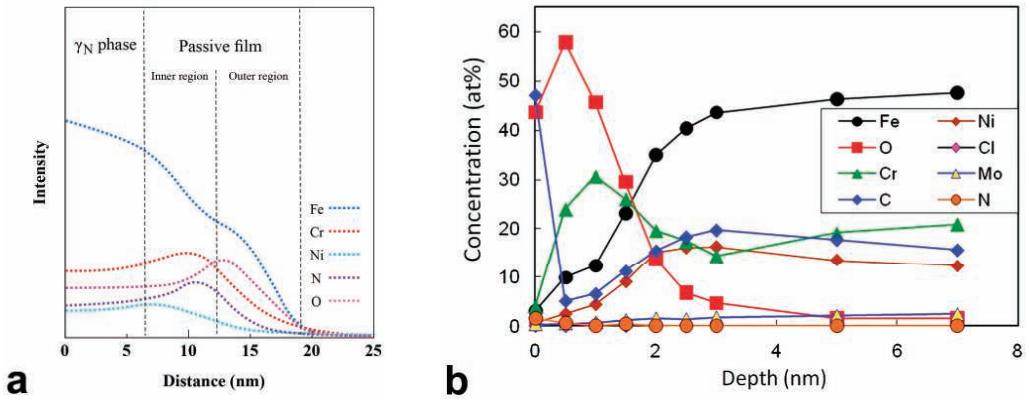

Figure 1. Alloy element and N, C, and O content vs. depth in the passive film and in the substrate: (**a**) nitrided AISI 304, in contact with a borate buffer solution at pH 7.7 (for further details, see [69]) (reprinted with permission from Ref. [69]. Copyright 2021 Elsevier); (**b**) carburized AISI 316L, in contact with 0.6 M NaCl solution (for further details, see [71]) (reprinted with permission from Ref. [71]. Copyright 2012 Elsevier).

3.2. Effect of N and C on Corrosion Behavior

The effect of N and C on corrosion behavior has been discussed in depth in other reviews [7,47]. Here, the main mechanisms are summarized. Pourbaix E-pH diagrams for interstitial N [75] and C [75] and for an Fe-17Cr steel [76] are depicted in Figure 2.

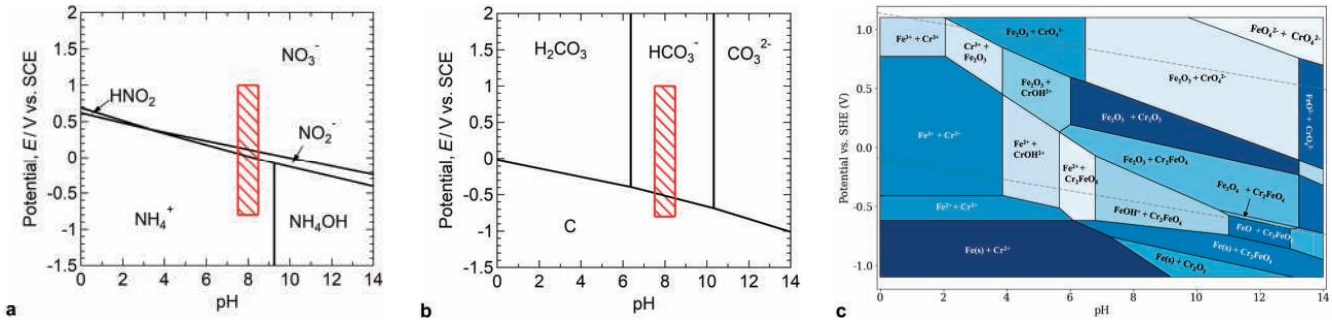

Figure 2. E-pH diagrams: (**a**) interstitial N/H_2O and (**b**) C/H_2O (for further details, see [75]) (reproduced under the terms of the CC-BY license. [75] Copyright 2020, The Authors, published on behalf of The Electrochemical Society by IOP Publishing Limited); (**c**) Fe-17Cr/H_2O (for further details, see [76]) (reproduced under the terms of the CC-BY license. [76] Copyright 2023, The Authors, published on behalf of The Electrochemical Society by IOP Publishing Limited).

3.2.1. Nitrogen

N addition is usually performed on austenitic, duplex, and martensitic stainless steels [77]. It has been proposed that a N-alloyed steel is considered "high N" when the N content is higher than 0.4 wt.% in austenitic steels and 0.08 wt.% in martensitic steels [77,78]. In austenitic stainless steels, N may be added in a small amount in traditional steels, as in AISI 316LN (~0.1–0.16 wt.%), while a larger content is present in high-N austenitic stainless

steels and in Ni-free austenitic stainless steels (0.45–1.1 wt.%) as a substitute of Ni together with Mn [78,79].

N alloying increases the tensile properties [77,78] and affects the corrosion resistance, enhancing, in particular, the resistance to localized corrosion phenomena [7,77,78]. N widens the passive range and improves the resistance to SCC and intergranular corrosion [7,66,78].

Different hypotheses have been put forward to explain the improvement of corrosion resistance to localized corrosion phenomena when N is present.

Local alkalinization is the main mechanism that is proposed for explaining the increase in corrosion resistance in both N-containing stainless steels [7,66,80] and in N-rich expanded phases [81,82]. During the early stages of the corrosion process, N atoms may be released, and they may react with H^+ and form ammonium ions (NH_4^+) [66]:

$$N + 4H^+ + 3e^- \rightarrow NH_4^+ \quad (2)$$

As a consequence, protons are consumed, and then the pH value locally increases, so the repassivation is promoted in incipient pits and crevices [7,66]. The local pH increase was indeed detected in situ for nitrided AISI 316L tested in solutions of 0.1 M Na_2SO_4 + 0.4 M NaCl acidified down to pH 2.4 [81]. The presence of NH_3 and NH_4^+ was observed through XPS analysis on the outermost layer, which was anodically formed on N-rich expanded austenite in a 3 wt.% NaCl solution [68]. It was hypothesized that, as the oxides formed, N was released at the surface and it was able to form NH_3. Thus, it was supposed that the formation of ammonium ions occurred with a two-step hydrolysis mechanism, with a first step during which N hydrolyzed to NH_3 and then NH_3 hydrolyzed to NH_4^+ [82].

At high potential values, nitrates (NO_3^-) and nitrites (NO_2^-) are able to form, and they may act as inhibitors [66,75,83].

Another mechanism supposes that N, in form of negatively charged N ($N^{\delta-}$), may hinder the migration of Cl^- toward the metal surface, exerting a repulsive action [7].

The N enrichment at the interface between the passive layer and the metallic substrate may create a barrier layer that improves the bonding at the oxide–metal interface such that the anion attack is hindered [67]. In Fe-N alloys, from first-principle calculations, it was observed that interstitial N causes a decrease in the occupied states around the Fermi level such that system bonding is enhanced and the active dissolution of Fe is suppressed [75]. In the N-rich expanded austenite, formed in austenitic stainless steels, a preferential bond between Cr and N was observed through different analysis techniques [84–86] and supposed on the basis of first principle calculation [87]. It was hypothesized that this strong Cr-N bond can restrict Cr migration at the interface between the N-rich metal matrix and the passive film [69,88]. Some authors observed both Cr-N and Fe-N preferential bonds [68,88], and therefore a restriction of Fe migration can also be supposed.

Another mechanism may be related to the change in semiconductive properties of the passive film. In the outer region of the passive film, having an *n*-type behavior, the dominant donor species is oxygen vacancy [89,90]. For N-rich expanded austenite, a significant decrease in donor density is observed, as mentioned above, so that the conductivity of the film is lower, and it is hypothesized that it allows for obtaining a more stable and protective film [82].

On the basis of the experimental results reported in the literature, it may be supposed that all of these mechanisms contribute to varying degrees to mitigating local corrosion phenomena when N-rich expanded phases are present. In the presence of Cl^--containing solutions, at first, N can hinder the passive film dissolution caused by the weakening effect of Cl^- in different ways. The presence of N within the oxide film increases its stability and protectiveness thanks to the decrease in donor density, and it creates a barrier layer, which enhances the bonding at the oxide–metal interface, thus hindering the anion attack. Moreover, negatively charged N may repel the migration of Cl^- toward the metal surface. When the passive film is broken, N present in the oxide film and in the solid solution in the expanded phases is released, and it causes a local alkalization of the acidic pit environment in a two-step hydrolysis, as suggested by Tong et al. [82]. At first, N hydrolyzes to NH_3

with a very fast reaction rate, which is mainly affected by the concentration of released N. In the second step, NH_3 further hydrolyzes to NH_4^+ with a slow reaction rate, which is greatly affected by the pH value of the solution. The lower the pH value, the faster the reaction and the consumption of H^+. The formation of NH_4^+ increases the pH value in the pit, promoting repassivation. Moreover, the fairly strong Cr-N and Fe-N bonds restrict the migration of Cr and Fe, counteracting their dissolution. In the polarization curves, this beneficial role of N can be inferred by the increase in the corrosion potential, the widening of the passive range with high pitting potential, and the decrease in the anodic current density in the passive branch.

The repassivation kinetics of metastable pits in free corroding conditions can be studied by monitoring the open circuit potential (OCP) vs. time. As an example, OCP values for untreated (with a freshly polished surface) and nitrided (air-grown passive film) AISI 316L specimens are depicted in Figure 3. The OCP of the untreated alloy usually has sharp decreases and increases in the potential value due to metastable pit nucleation and repassivation phenomena. The nitrided steel usually has higher potential values with fewer pit nucleation events, but the repassivation kinetic tends to be slower, in accordance with the slow rate of NH_4^+ hydrolysis.

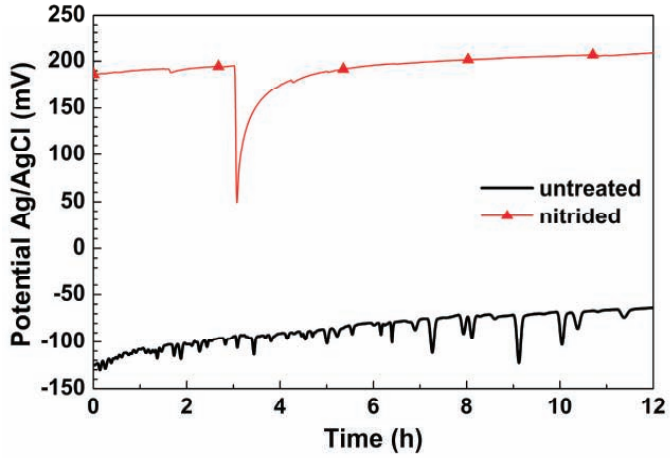

Figure 3. Open circuit potential vs. time for AISI 316L specimens: untreated (freshly polished) and nitrided at 380 °C for 3 h (air-grown passive film) (for further details on the treatment, see Ref. [91]) (solution: 5 wt.% NaCl, aerated) (adapted from Refs. [47,91]).

The formation of N-rich expanded phases tends to widen the pH range in which the stainless steel is passive. As an example, the potential pH diagrams in 3 wt.% for untreated and nitrided 1Cr18Ni9Ti with an expanded austenite (N max: 32 at.%) layer [92] are shown in Figure 4. N-rich expanded austenite extends the immunity and the perfect passivity regions, while the imperfect passivity and pitting regions are reduced.

The effect of N-alloying is still a matter of debate when the corrosion environment causes general corrosion, as in H_2SO_4 aqueous solutions. For N-containing stainless steels, both positive [93,94] and negative [95] effects are observed. Similarly, when N-rich expanded phases form, different behaviors are observed. Some authors report that the corrosion resistance is maintained or even increased [96–98], while for other authors, the corrosion resistance is decreased [97,99]. As a matter of fact, the corrosion resistance in H_2SO_4 aqueous solutions seems to strictly depend on the microstructure of the modified surface layers, i.e., on the formation of other phases together with the expanded phases.

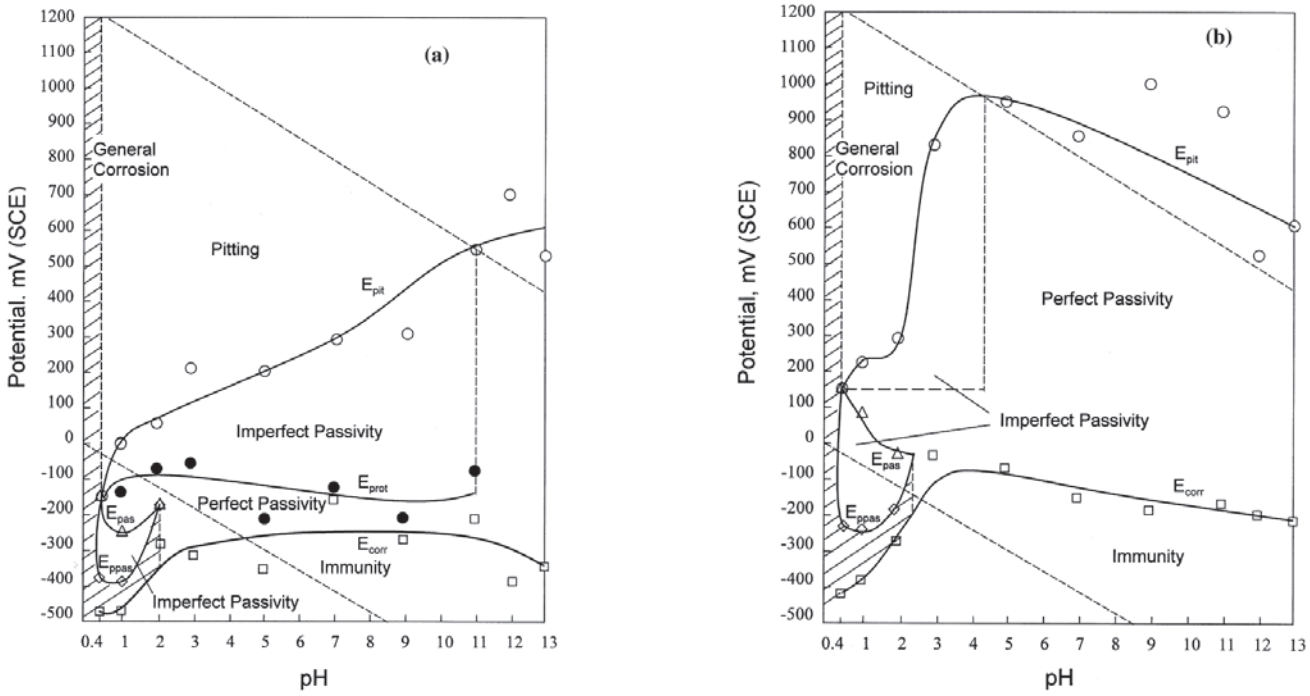

Figure 4. Potential pH diagrams for 1Cr18Ni9Ti: (**a**) untreated steel; (**b**) nitrided (380 °C, 4 h) steel with N-rich expanded austenite layer (solution: 3 wt.% NaCl) (for further details, see Ref. [92]) (reprinted with permission from Ref. [92]. Copyright 2000 Elsevier).

3.2.2. Carbon

C alloying is performed to enhance the mechanical properties of stainless steels, because it promotes the austenite formation and thus the martensite formation in martensitic stainless steels, and it forms hard carbide precipitates. However, when corrosion resistance is considered, C is harmful [2,7] and a low C content is used for reducing the risk of sensitization and obtaining a stable passive layer [2,7].

The study of corrosion behavior of Fe-C alloy (C: 0.34 wt.%) in boric–borate solution pointed out that the formation of HCO_3^- improves the corrosion resistance. Another effect that may contribute to the corrosion resistance was inferred by first principle calculation for the Fe-C system. A more stable electronic structure occurs in the presence of C, so the active dissolution of Fe is suppressed [75].

When C-rich expanded phases form, an improvement in the localized corrosion resistance is observed [74,100]. The mechanism responsible for this beneficial effect is not clear.

At first, Martin et al. [101] hypothesized that C atoms were mobile in the passive film and enhanced/maintained the oxygen vacancy motion. A further observation that in carburized AISI 316L a transition from an *n*-type semiconductivity to a *p*-type semiconductivity occurred suggested that a more stable passive film was formed [102]. Thinner passive layers were detected in low-temperature carburized AISI 316L compared to those of the untreated steel [71,73]. On the basis of this observation, Heuer et al. [71] hypothesized that the occurrence of a thinner passive film at a given potential reduced the effect of the thickness undulation of the film itself, which could promote dielectric breakdown and the nucleation of pits. Niu et al. [73] observed that the near-surface regions of carburized AISI 316L had a lower Cr and oxygen vacancy concentration as the C content was higher, and they hypothesized that C hindered the film formation due to strong Cr-C bonding and that it also formed a barrier to Cr transfer in the oxide. A decrease in donor density in the passive layer of carburized austenitic stainless steel was also observed by other authors [74,100], and it was related to a decrease in oxygen vacancy concentration, which promoted a more stable and protective film. The presence of strong localized (covalent)

bonds between C and metal atoms (Fe, Cr, Ni) was suggested by the analysis performed using a density-functional theory (DFT) calculation by Li et al. [103]. The metal–C bonds were 1.4–2.0 times stronger than the metal–metals bonds, and therefore it was hypothesized that C was able to reduce the metal dissolution rate, even if, for these authors, the passive film seemed to be weakened by C.

It has to be taken into account that the formation of a more or less protective passive layer may also be influenced by the presence of carbon soot, which usually forms in carburizing treatments, and by the formation of carbide precipitates.

At present, a complete picture of what happens when a C-rich expanded phase is put into contact with a Cl^--containing solution is not present in the international literature. It may be hypothesized that at first C hinders passive film dissolution with mechanisms similar to N atoms by changing the semiconductivity properties of the film and hindering Cr and Fe dissolution thanks to the strong metal–C bonds. When localized corrosion phenomena begin, these strong metal–C bonds counteract Cr and Fe dissolution. Moreover, on the basis of the C/H_2O potential–pH diagram (Figure 2b), it may be supposed that HCO_3^- forms. Therefore, the pH value within the pit is increased, thus restoring the conditions for forming a stable passive layer.

When general corrosion, such as that produced in H_2SO_4 aqueous solutions, is considered, C-rich expanded phases and, in particular, expanded austenite seem able to reduce the susceptibility to corrosion [104].

4. Ferritic Stainless Steels

For the FeCr ferritic stainless steels, the interstitial-rich phase, formed as a consequence of low-temperature treatment, is usually indicated as "expanded ferrite". N-rich and C-rich expanded ferrites are also designated as "α_N" and "α_C", respectively. The main properties of ferritic stainless steels subjected to low-temperature nitriding and carburizing are reported in Table 2.

Table 2. Main characteristics of the modified surface layers obtained on ferritic stainless steels through nitriding or carburizing. (References for the indicated values are reported in the text).

Properties			Nitriding	Carburizing
Formation temperature (without formation of Cr compounds) (°C)			<380	<470
Max. interstitial content in expanded ferrite (at. %)			24	10
Max. surface hardness ($kg_f\ mm^{-2}$)	-	Expanded ferrite only	1090	1000
	-	With Fe-nitride precipitates	1200	-
	-	With a continuous layer of ε-$Fe_{2-3}N$	1500	-
Localized corrosion resistance (Cl^--containing solutions)	-	Expanded ferrite only	good	good
	-	With ε_N'/Fe-nitride precipitates	poor	-
	-	With a continuous layer of ε-$Fe_{2-3}N$	good	-
Corrosion resistance in H_2SO_4 solutions	-	Expanded ferrite only	good	-
	-	With ε_N'/Fe-nitride precipitates	poor	-

4.1. Microstructure and Characteristics of the Modified Layers

In the ferritic stainless steels, the formation of a modified surface layer consisting mainly of expanded ferrite is more difficult, which is different from what occurs in austenitic stainless steels for expanded austenite. In fact, the formation of the supersaturated solid solution of N in ferrite is competitive to that of the ε-$Fe_{2-3}N$ nitride, so both phases are easily formed.

Depending on the nitriding conditions, three different microstructures may form: (i) a modified layer consisting of expanded ferrite [105], (ii) a modified layer consisting of both expanded ferrite and Fe-based nitrides and/or N-rich h.c.p. ε'-martensite (expanded

ε′-martensite, ε_N') [105–109], and (iii) a modified layer with a continuous layer of ε-nitride on an inner layer in which expanded ferrite and nitrides are present [110].

The surface microstructure of nitrided samples has an etched appearance, with the grains well-delineated and small reliefs at the grain boundaries, suggesting the occurrence of localized plastic deformations [108,111] (Figure 5a).

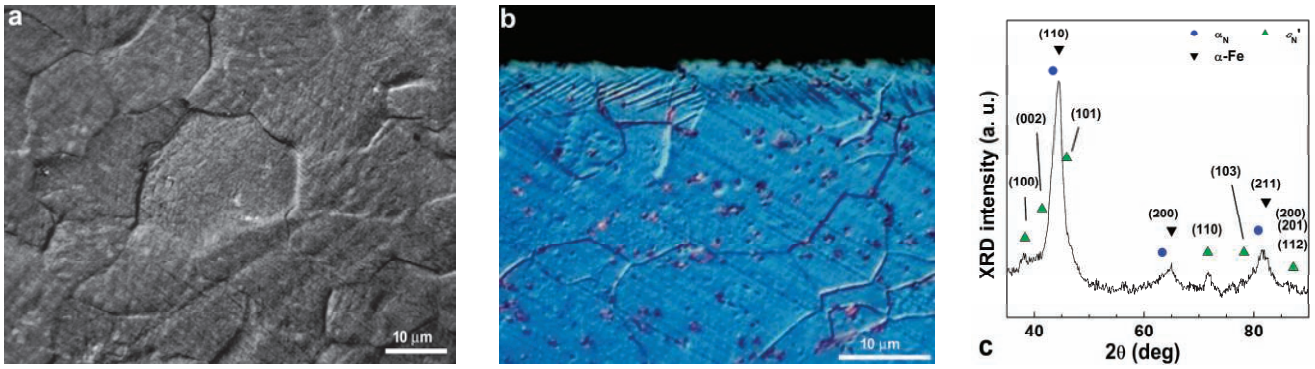

Figure 5. Plasma-nitrided AISI 430 ferritic stainless steel (380 °C, 10^3 Pa, 5 h): (**a**) surface morphology, (**b**) cross-section microstructure, (**c**) XRD pattern (for further details, see [108]) (adapted from Ref. [108]).

The cross-section microstructure of the modified surface layers depends on the treatment conditions. When N-rich expanded ferrite is the main phase, the modified layer is almost featureless due to the higher corrosion resistance of this phase compared to the substrate [17,105,108,111], but a clear interface with the substrate is not always present [112,113]. Below this layer, needle-like structures are observed, which extend into the substrate [105,112] (Figure 5b). Larisch et al. [112] interpreted these structure as deformation bands due to the N-supersaturation, while other authors [105,109] supposed that they were related to the precipitation of Fe nitrides. By using different analysis techniques (light microscopy, scanning electron microscopy (SEM), electron backscatter diffraction (EBSD), and X-ray diffraction (XRD)) on plasma-nitrided AISI 430, it was shown that the needle-like structures can be related to a hexagonal close-packed (h.c.p.) phase, which has significantly lower lattice parameters than those of the ε-$Fe_{2–3}N$ nitride [108] (Figure 5c). It was suggested that this phase can be regarded as a N-rich h.c.p. ε′-martensite, ε_N', which forms from expanded ferrite as a consequence of a b.c.c. to h.c.p. displacive transformation due to the high compressive stress induced by the huge N solubilization in the ferritic matrix. This "expanded" ε′-martensite is analogous to the N-rich h.c.p. ε′-martensite, ε_N', which forms together with expanded austenite in low-temperature nitrided austenitic stainless steels, and it may be the precursor of the ε-nitride. When Fe-based nitrides are able to form, their presence is usually detected through XRD analysis, but they are not easily observable in the microstructure [105,106,112]. The formation of expanded austenite from expanded ferrite is also observed [114].

The high ε-nitride content may promote the formation of a more or less continuous layer. Kishimoto and Nishimoto [109] carried out dc plasma nitriding with a metal screen on AISI 430 at 360 and 380 °C and observed a very high N content (up to about 40 at.%) when the treatment duration was 15 h. The formation of an ε-nitride layer may be supposed, even if it was not easily detectable through microscopy analysis.

The comparison of the featureless, unetched layer with the thickness of the hardened layer suggests that the diffusion, and hence the hardening effect, of N atoms extends far beyond this layer [105].

When nitrocarburizing is performed, expanded ferrite is able to form a uniform layer, but the precipitation of carbides and nitrides may also occur depending on treatment conditions [113,115]. Similarly, low-temperature carburizing produces a C-rich expanded ferrite, but the precipitation of carbides may also occur [17].

It has to be taken into account that the formation of expanded ferrite with or without Fe-based nitride/carbides depends on both the treatment conditions (temperature, duration, N and/or C feeding) and the steel composition. To avoid further precipitation of Cr-based compounds, temperatures lower than 450 °C for nitriding and nitrocarburizing treatments [16,116,117] and lower than 470 °C for carburizing treatments [17] are usually reported. However, at nitriding temperatures as low as 380 °C, CrN was not detected using a 28 h treatment duration, while it could form when the duration was increased up to 40 h [112].

When expanded ferrite forms, the concentration profiles of N and C have the same trend [17,21], which is similar to that of a complementary error function. A maximum N content of ~24 at.% is detected in expanded ferrite [21], while in C-rich expanded ferrite, a maximum C content of ~10 at. % is registered [17].

The thermal stability of a low-temperature nitrided UNS S44400 super-ferritic stainless steel was studied by Schbicheski Kurelo et al. [114]. When the modified layer consisted of expanded ferrite (300 °C, 3 h), this phase did not decompose at 450 °C up to 106 min, even if its lattice parameter became smaller due to N diffusion. When the nitriding treatment produced both expanded ferrite and expanded austenite (300 °C, 6 h), during the heat treatment at 450 °C, expanded austenite tended to decompose into CrN and α-Fe. Taking into account the treatment temperature and the time limits for avoiding CrN formation (380 °C, t < 40 h), it may be supposed that the modified layers have good long-term stability at temperatures lower than 100 °C.

The modified surface layers can significantly increase the surface hardness. When N-rich expanded ferrite forms, microhardness values of about ~1090 $kg_f\ mm^{-2}$ are registered [105], and a further increase up to ~1200 $kg_f\ mm^{-2}$ occurs when Fe-based nitrides are also present [106]. When a more or less continuous layer of ε-nitride forms, values as high as ~1500 $kg_f\ mm^{-2}$ are measured [109]. On carburized samples, microhardness values greater than 1000 $kg_f\ mm^{-2}$ are registered [17]. The microhardness profiles depend on the phases present in the modified surface layers. The presence of expanded ferrite together with no amount or a negligible amount of Fe-based compounds allows for obtaining a fairly smooth hardness profile [17,105]. When a large amount of Fe-based compounds forms, a more or less extended plateau with high hardness values is observed at the surface, followed by a steep decrease to matrix hardness values [115].

Further details regarding the characteristics and properties of expanded ferrite and the modified layers formed on ferritic stainless steels are reported in [12,13,16].

4.2. Corrosion Behavior in the Presence of Cl^-

The corrosion behavior of ferritic stainless steels subjected to low-temperature treatments is usually tested in NaCl solutions when the effect of Cl^- has to be evaluated, i.e., the susceptibility to localized corrosion phenomena. As expected, the corrosion resistance is closely related to the microstructure of the modified surface layers.

EIS analysis carried out at the open circuit potential (OCP) allows for obtaining information on the resistance of the steel to general corrosion. Different behaviors are observed when the modified surface layers consist of N-rich expanded ferrite only or expanded ferrite and ε_N' [108] (Figure 6a). For plasma-nitrided AISI 430 tested in 3.5 wt.% NaCl, EIS data suggested the presence of two time constants, which were modeled with two parallel R-C elements hierarchically connected. The high frequency (HF) time constant was related to charging/discharging at the electrode/electrolyte interface, while the low frequency (LF) time constant was related to the processes occurring in the oxide layer. The specimens, having a N-rich (max ~4.3 at.%) modified layer, which consisted of expanded ferrite (indicated as α_N), showed markedly higher impedance and polarization resistance and lower capacitance of the oxide layer in comparison with those of the untreated steel. These data suggest that a more protective and thicker oxide film formed. On the contrary, when ε_N' was present together with expanded ferrite (nitriding at 380 °C, 5 h) in a N-rich (max ~13.4 at.%) 10-μm thick layer (sample indicated as $\alpha_N + \varepsilon_N'$), lower impedance values

were detected, and therefore it may be hypothesized that a thinner and less protective oxide layer was formed. These data were not fully confirmed when potentiodynamic polarization tests were performed (Figure 6b). The samples in which expanded ferrite alone formed had higher corrosion potential, lower corrosion current density, and lower anodic current density in the passive branch compared to those of the untreated steel, but the pitting potential was lower. These data suggest that, in spite of the greater protectiveness of the oxide film, the small thickness of the nitrided layer and the fairly low N content were not able to fully counteract the localized corrosion phenomena. When a heterogeneous modified layer formed consisting of expanded ferrite and ε_N', a significant decrease in the corrosion resistance was registered.

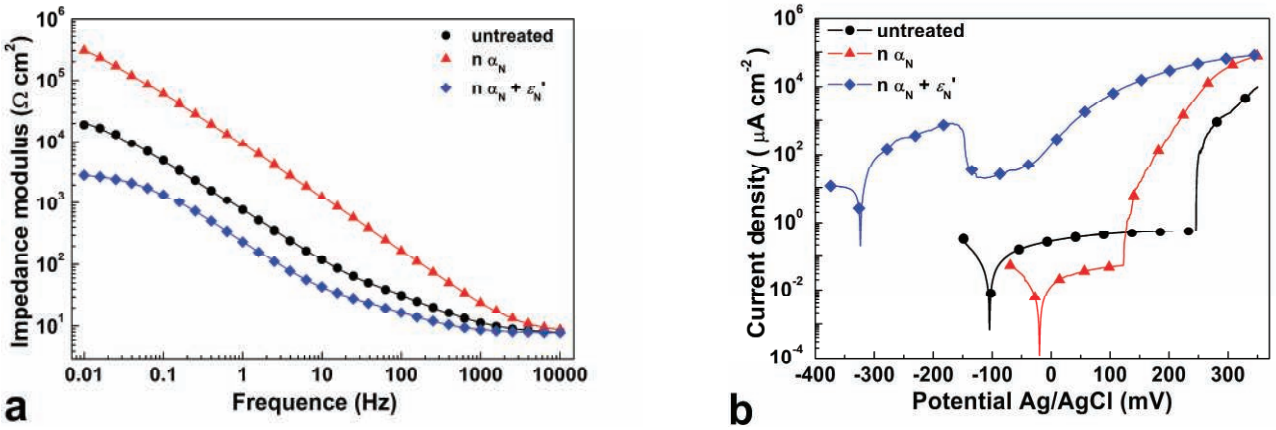

Figure 6. Plasma-nitrided and untreated AISI 430 ferritic stainless steel: (**a**) Bode plots (impedance) and (**b**) potentiodynamic polarization curves (solution: 3.5 wt.% NaCl, aerated) (phases present in the modified layers: n α_N: expanded ferrite; n α_N + ε_N': expanded ferrite + ε_N') (for further details, see [108]) (adapted form Ref. [108]).

Other EIS data were reported by Luiz et al. [106] for a super-ferritic stainless steel, UNS S44400, subjected to plasma nitriding using plasma immersion ion implantation (PIII) at 400 °C and tested in a 3.5 wt.% NaCl solution. In these conditions, both expanded ferrite and ε and γ′ Fe-based nitrides were detected through XRD analysis, so a heterogeneous modified surface layer might be hypothesized. The Nyquist plots for durations up to 30 days showed semicircles, which tended to become wider as the duration was longer. In Bode plots, similar impedance values were observed. The presence of two time constants was clearly observable in the phase angle plot. Hence, an EEC with two time constants was chosen for modeling experimental data. The HF time constant was related to the passive film formation and the LF time constant represented the charge and mass transfer phenomena through the passive film to the double layer. The polarization resistance of nitrided samples slightly increased during the first day, and then it reached nearly constant values up to 30 days. The values were significantly higher than those of the untreated steel, which increased up to 15 days and then decreased. Therefore, it was hypothesized that N, both solubilized in expanded ferrite and as nitride, having a high corrosion resistance, contributed to the stability and protection effect of the passive film. Regarding the passive film capacitance, slightly lower values were observed in comparison to those of the untreated steel.

The study by Luiz et al. [106] also gives useful information regarding the time evolution of OCP of this sample type. OCP values increased markedly during the first day, and then they had a slower increase up to a maximum at 15 days and tended to decrease. The OCP values were significantly higher than those of the untreated steel, and therefore a better corrosion resistance may be supposed. This hypothesis was confirmed by the cyclic polarization tests, during which significantly higher pitting and repassivation potential values were registered.

The treatment of the same UNS S44400 super-ferritic stainless steels with different PIII nitriding conditions by Schbicheski Kurelo et al. [105] allowed for appreciating the effect of different contents of nitride precipitates in the modified surface layers on the corrosion resistance in 3.5 wt.% NaCl solution. In Figure 7, potentiodynamic polarization curves of untreated and nitrided specimens and their surface morphologies after the corrosion test are reported. When the samples were treated at 300 °C, significantly higher corrosion and pitting potential values and lower anodic current density in the passive branch were registered compared to those of the untreated alloy, and only micrometric pits occurring near inclusions were observable after the tests. After a passive–transpassive transition, a further reduction in the anodic current values was observed as a secondary passivation region, probably due to the precipitation of corrosion products. Samples nitrided at 350 °C had comparable corrosion and pitting potential values but higher anodic current density values, which became even higher and comparable to those of the untreated alloy for the samples treated at 400 °C. Similarly, more pits were present on the surface after the tests. Even if nitrides were not detected through XRD analysis, it was hypothesized that an increasing amount of these phases was able to form when the treatment temperature increased. The precipitation of these nobler Fe-based nitrides in the N-rich expanded ferrite could cause micro-galvanic effects, which decrease corrosion resistance. Therefore, the better corrosion behavior (300 °C) may be ascribed to modified layers consisting of N-rich expanded ferrite, while worse behavior (400 °C) may be due to a heterogeneous microstructure formed by expanded ferrite and nitride precipitates. The deleterious effect of nitride or carbonitride precipitates is also reported by other authors [113,118], with a possible worsening of the corrosion resistance [113,118,119].

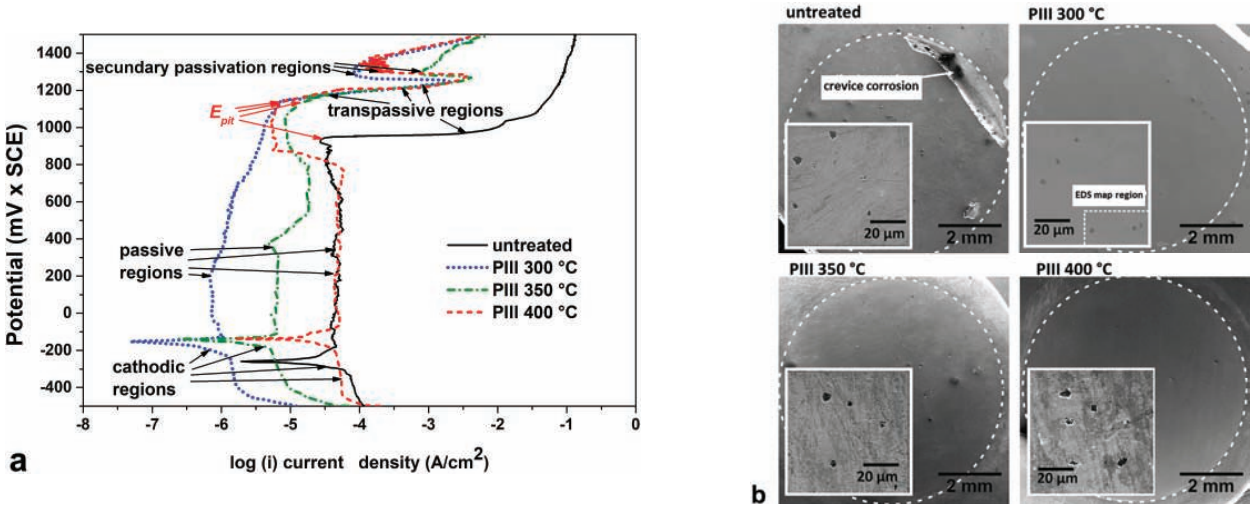

Figure 7. PIII nitrided UNS S44400: (**a**) potentiodynamic polarization curves, (**b**) surface morphology of the samples after the polarization test (solution: 3.5 wt.% NaCl) (phases present in the modified layers: PIII 300 °C: expanded ferrite; PIII 350 °C: expanded ferrite (+ nitrides); PIII 450 °C: expanded ferrite (+ nitrides)) (for further details, see [105]) (reprinted with permission from Ref. [105]. Copyright 2020 Elsevier).

A further increase in corrosion resistance is observed when an almost continuous layer of ε-nitride was able to form. Kishimoto and Nishimoto [109] observed a significant increase in the pitting potential for AISI 430 specimens nitrided at 360 and 380 °C for 15 h when tested in a deaerated 3.5 wt.% NaCl.

The influence of the treatment conditions was also highlighted by Spies [46]. Not only the nitriding temperature but also the treatment duration have an effect on the corrosion resistance. For example, for AISI 430 nitrided at 420 °C and tested in a 0.5 M NaCl solution, a treatment duration of 8 h allowed for an increased pitting potential in comparison to that of the untreated steel. Using a longer duration (20 h), the corrosion and pitting potential

significantly decreased due to the formation of large amounts of Cr nitride precipitates. The corrosion behavior is also influenced by the initial microstructure of the untreated steel [120].

The corrosion resistance of a modified layer with a continuous surface layer consisting of ε nitride was tested with the ferri/ferro-cyanide test (3 g NaCl + 0.1 g $K_3Fe(CN)_6$ in 100 mL distilled water), and it was reported to be excellent [110].

As expected, the formation of a large amount of Cr nitrides/carbonitrides causes a marked decrease in corrosion resistance [113,118,119].

The improved resistance of C-rich expanded ferrite to localized corrosion can be inferred by the resistance to chemical etching with Marble's reagent [17].

4.3. Corrosion Behavior in Cl-Free Solutions

The influence of the microstructure of the modified surface layers and, in particular, the formation of heterogeneous structures consisting of expanded ferrite and Fe-based nitrides is also observed in H_2SO_4 solutions.

Spies [121] and Spies et al. [46] reported a significant increase in the corrosion potential and a decrease in the passive current density for treatments that presumably were not able to produce significant amounts of nitrides (250 °C/39 h, 300 °C/60 h up to 420 °C/36 h) on AISI 430 when tested in 0.05 M H_2SO_4. On the contrary, when AISI 409 steel was nitrided in the range of 350–500 °C for 3 h and then tested in 0.1 M H_2SO_4, only a slight increase in the corrosion potential but a significant increase in the anodic current density were registered compared to those of the untreated alloy [122].

These results highlight that suitable conditions for obtaining improved corrosion resistance are strictly related to the steel composition, the modified surface layer's composition, and the solution with which the treated steel is put into contact.

5. Martensitic Stainless Steels

Even if martensite is a supersaturated solid solution and is thus an "expanded" phase, the term "expanded martensite" is usually used to indicate the expanded phase that forms in martensitic stainless steels with low-temperature treatment. The symbols α_N' and α_C' are also used to indicate N- or C-rich expanded martensite, respectively. The main properties of martensitic stainless steels subjected to low-temperature nitriding and carburizing are reported in Table 3.

Table 3. Main characteristics of the modified surface layers obtained on martensitic stainless steels through nitriding or carburizing. (References for the indicated values are reported in the text).

Properties		Nitriding	Carburizing
Formation temperature (without formation of Cr compounds) (°C)		200–350	200–450
Max. interstitial content in expanded martensite (at. %)		22	10
Max. surface hardness ($kg_f\ mm^{-2}$)	- Expanded martensite only	1120	970
	- With Fe-based compounds	1400	1530
	- With a continuous layer of ε-$Fe_{2-3}N$	1560	-
Localized corrosion resistance (Cl^--containing solutions)	- Expanded martensite only	good	good
	- With Fe-based compounds (low amount)	acceptable	acceptable
	- With Fe-based compounds (high amount)	poor	poor
	- With a continuous layer of ε-$Fe_{2-3}N$	good	-

5.1. Microstructure and Characteristics of the Modified Layers

As observed for ferritic stainless steels, in martensitic stainless steels, the formation of an expanded martensite is competitive with the formation of nitride precipitates. Expanded austenite may also form when retained austenite is present.

The surface morphology has an etched appearance when plasma treatments are used, and reliefs at grain boundaries are observable [123–125] (Figure 8a).

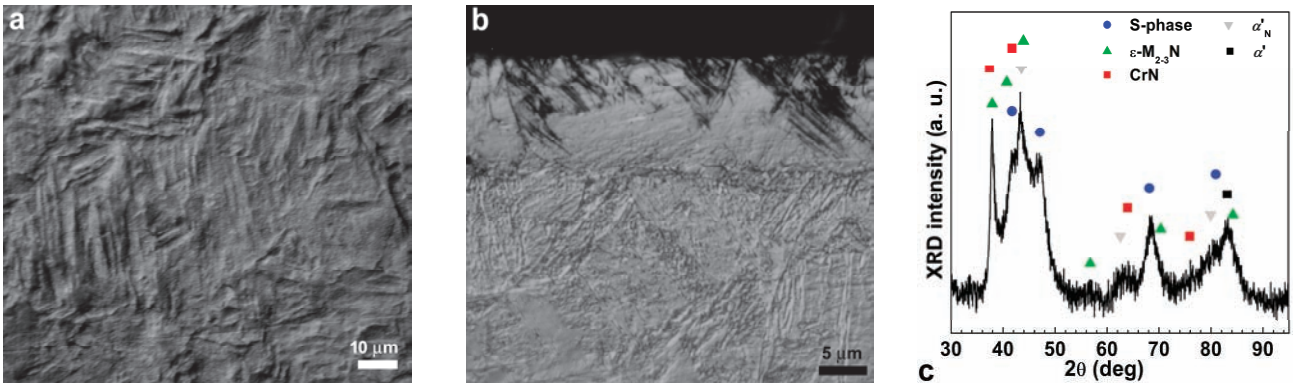

Figure 8. Plasma-nitrided AISI 431 martensitic stainless steel (400 °C, 500 Pa, 5 h): (**a**) surface morphology, (**b**) cross-section microstructure, (**c**) XRD pattern (for further details, see [125]) (adapted from Ref. [125]).

The cross-section microstructure of the modified surface layers is almost featureless, and it does not have a strong etched interface with the substrate (Figure 8b). This characteristic is observed when Cr nitrides are not able to form, but it occurs independently on the phases present in the layer. Authors report the formation of layers consisting of expanded martensite only [126], layers consisting of expanded martensite and Fe-based nitrides [106,126–130], or of expanded martensite, expanded austenite (S-phase), and ε-nitride [124,125] (Figure 8c). When Fe-based nitrides are present in fairly low amounts, they are observed as acicular precipitates in the expanded martensite matrix [123]. As the Fe-nitride content increases, a continuous layer forms, and the microstructure consists of an outer compound layer, in which nitrides, in particular ε-$Fe_{2–3}N$, are present, and an inner diffusion layer, in which expanded martensite is observed [129]. It has to be taken into account that the whole hardened layer extends beyond the unetched part of the modified layer. Similar microstructures are observed in the nitricarburized samples [124], where the carbonitride ε-$Fe_{2–3}$(N, C) can form instead of ε-nitride [131].

Low-temperature carburizing produces C-rich expanded martensite, which is observable as a thin, almost featureless layer with a thicker "diffusion layer" below [132,133].

It has to be taken into account that martensitic stainless steels are subjected to quenching and tempering, which influence the microstructure and the mechanical properties of the bulk. As a matter of fact, the characteristics of the modified surface layers and the phases formed in them depend on the previous heat treatment history of the steel. The low-temperature treatments can be performed after quenching, so tempering and surface treatment are carried out in a single step, or surface treatment can follow the tempering step. The effect of previous heat treatments was reported by Figueroa et al. [134], who highlighted that different tempering steps influenced the amount of retained austenite and hence the possibility of forming expanded austenite together with expanded martensite, Fe-based nitrides, and even CrN. Recently, Toscano et al. [135] suggested a novel approach to low-temperature nitriding of martensitic stainless steels. The authors performed a hybrid treatment on ASTM CA6NM martensitic stainless steel consisting of an austenitization step followed by cooling down to a temperature that enabled low-temperature nitriding in the metastable austenite field, thus avoiding martensite transformation. In the obtained modified surface layers, N-rich expanded austenite and ε-nitride were present. A further cooling down to room temperature allowed for the transformation of the bulk material into martensite or bainite depending on the nitriding duration.

In order to avoid the formation of Cr compound precipitates, which deteriorate the corrosion resistance, treatment conditions (temperature, duration, N and/or C feeding) should be also chosen on the basis of the steel composition and its previous heat treatment history. The temperature limit for avoiding the formation of Cr-rich precipitates is usually indicated as ~350 °C for nitriding [13,136], ~400 °C for nitrocarburizing [136], and ~450 °C

for carburizing [136]. However, exceptions to these "critical" temperatures are present in the literature. For example, Dalibon et al. [130] carried out dc pulsed plasma nitriding of quenched and tempered AISI 420 at 390 and 420 °C for durations ranging from 4 to 10 h in a 20% N_2–80% H_2 atmosphere, and they detected expanded martensite and Fe-based nitrides but no CrN. Similarly, no Cr-compound formation was detected upon nitriding or nitrocarburizing at 420 and 440 °C for 2 h [29]. For gas nitriding of quenched AISI 420 stainless steel, Tang et al. [137] carried out nitriding treatments at different temperatures and times and obtained a temperature–time–precipitation curve for CrN. On the basis of these data, the authors performed nitriding treatments in the "incubation time" for CrN at 500 °C for 0.5 h while maintaining the cooling rate in order to reduce CrN precipitation. They succeeded in obtaining thick, modified layers with a very small amount of CrN precipitates.

The concentration profile of interstitial atoms in the modified surface layers has a shape very close to a complementary error function when expanded martensite is the main phase and nitrides are present in negligible amounts [138]. When a fairly large amount of nitrides forms, a high N content is present at the surface, followed by a first sharp decrease, a plateau, and then a smoother decrease [139]. In martensitic stainless steels, a maximum N content of ~20 at.% is detected in expanded martensite [138]. A maximum C content of ~10 at% is detected in the C-rich expanded phase [23].

The thermal stability of modified surface layers containing expanded martensite can be inferred from the treatment temperature and the time limits for avoiding the formation of Cr-based compounds. For AISI 420 martensitic stainless steel treated at 400 °C, the threshold limit for sensitization is 4 h for nitriding [140] and more than 36 h for carburizing [133]. It may be supposed that at temperatures lower than 100 °C, the modified surface layers formed on martensitic stainless steels have good long-term stability.

Surface microhardness depends on the microstructure and the phase composition of the modified surface layers. Values of ~1120 $kg_f\ mm^{-2}$ are registered for a layer consisting of N-rich expanded martensite alone, with a further increase up ~1400 $kg_f\ mm^{-2}$ when nitride precipitates are present in expanded martensite [126]. With the formation of a more or less continuous outer layer of ε-nitride, values as high as ~1560 $kg_f\ mm^{-2}$ are reported [106]. For carburized samples, surface microhardness values of about 970 $kg_f\ mm^{-2}$ are registered [132], and an increase up to ~1530 $kg_f\ mm^{-2}$ is reported [141], probably due to the strengthening effect of carbide precipitates. The microhardness profiles depend on the phases present in the modified surface layer. When expanded martensite alone forms in nitrided specimens, the hardness profile is fairly smooth, but when a large amount of nitrides is present, a more or less extended surface region with very high hardness values is observed, followed by a steep decrease to matrix values [126]. The carburized specimens usually show fairly smooth profiles [142].

Further details regarding the characteristics and properties of expanded martensite and the modified layers formed on martensitic stainless steels are reported in [12,13,16].

5.2. Corrosion Behavior in the Presence of Cl^-

Low-temperature-treated martensitic stainless steels are usually tested in NaCl solutions. As expected, their corrosion behavior depends on the microstructure and phase composition of the modified surface layers.

The good corrosion resistance of modified layers consisting of expanded martensite, such as those obtained at ultra-low temperatures (200 and 250 °C), may be inferred by the high resistance to chemical etching with Vilella's reagent [126].

Modified layers consisting mainly of expanded martensite obtained with arc discharge plasma nitriding (440 °C, arc current: 100, 110 A) on annealed AISI 420 steel were tested in a 3.5 wt.% NaCl solution by Li et al. [143]. With these treatment conditions, a slight increase in corrosion resistance was observed by means of EIS analysis and polarization curves, even if after the tests only micrometric pits were observed. It is not clear whether these results were due to either the previous heat treatment history and the nitriding parameters, and hence the obtained microstructure, or the test conditions.

The change in stability of the passive film formed on the modified surface layer of a PIII nitrided (400 °C) UNS S41426 super-martensitic stainless steel when put into contact with 3.5 wt.% NaCl solution up to 30 days was studied by Luiz et al. [106]. The modified surface layers consisted of expanded martensite and Fe-based nitrides. In the Nyquist plot, the semicircles became wider as the time increased up to 7 days, and then they slightly decreased (Figure 9a). The obtained values for polarization resistance were significantly higher than those of the untreated alloy; they increased for the first 2 days, and then they remained almost constant. On the contrary, for the untreated steel, marked variations occurred in the first 7 days, and then the values tended to decrease, suggesting a decrease in the stability and protectiveness of the passive film. The calculated capacitance of the passive film remained almost constant up to 30 days. These authors also evaluated the OCP variations over a 30-day duration, and, for the nitrided steel, they registered a sharp initial increase during the first day and then fairly constant values, with a slightly decreasing trend after 7 days. These OCP values were significantly higher than those of the untreated steel, which had unstable behavior during the test period, suggesting that dissolution and repassivation phenomena occurred. Therefore, this type of modified surface layer seemed to improve the stability of the passive film over time. Further details about the corrosion behavior of this sample type were obtained through cyclovoltammetry tests [106]. In the voltammogram of the nitrided sample, at the beginning, the anodic current density values remained low, as the sample was in a passive state, and then a linear and smooth increase in the anodic current density was registered due to the initial dissolution and breakdown of the passive film (Figure 9b). This trend was not typical for localized corrosion, for which an abrupt increase in the anodic current was observed, such as in the untreated stainless steel, and it was hypothesized that it might be related to a more uniform corrosion. An increase in the anodic current density, which might be ascribable to localized corrosion, occurred only at higher potential values. When the reverse scan was performed, repassivation seemed hindered, presumably due to the formation of a corrosion product layer. Only when the corrosion products underwent a dissolution the substrate was it able to repassivate. The potential for the passive–transpassive transition to occur was higher for the nitrided steel in comparison with the untreated one, but the repassivation potential was lower, suggesting that the "compound" layer had good protectiveness but it was difficult to repassivate. After the test, the surface of the nitrided specimen was similar to a sample subjected to chemical etching, and only few pits were present (Figure 9c), suggesting that uniform corrosion predominated, while large pits were present on the surface of the untreated steel.

Using a quenched UNS S41426 super-martensitic stainless steel, Schibicheski Kurelo et al. [129] performed tempering and nitriding in a single step. By nitriding at 300 °C for 3 h, the authors obtained a modified surface layer in which expanded martensite and a low amount of γ' nitride were present. When tested in a 3.5 wt.% NaCl solution, this sample type had a significantly higher corrosion potential than that of the reference samples, i.e., samples tempered at only 400 °C for 3 h. Even if no clear passive branch was registered, after the test, only a few pits were observed on the surface of the samples. By increasing the nitriding temperature at 350 °C, a larger amount of nitride was formed, so a more heterogeneous surface structure was supposed to be present. As a consequence, the corrosion potential shifted to a less noble value, even if it was higher than that of the untreated alloy, and more pits were observable at the surface. The good corrosion resistance of the modified layers consisting of expanded martensite with a small amount of nitrides was also assessed by other authors [29,130,144]. As an example, short nitriding and nitrocarburizing treatments (420 and 440 °C, 2 h) on AISI 420 martensitic stainless steel produced modified surface layers mainly consisting of expanded martensite and ε- and γ'-nitrides or carbonitrides, which had an improved corrosion resistance in 3.5 wt.% NaCl solution [29] (Figure 10a). Even the presence of very small amounts of CrN did not impair the corrosion resistance [137].

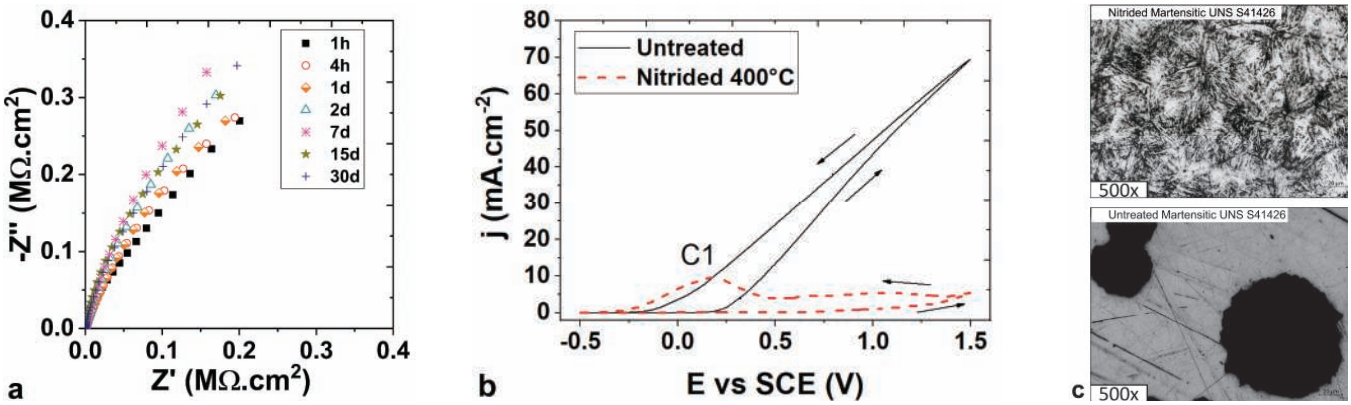

Figure 9. PIII nitrided UNS S41426 super-martensitic stainless steel (400 °C): (**a**) Nyquist plots registered at OCP for different times, (**b**) voltammograms of untreated and nitrided specimens, and (**c**) surface morphology of untreated and nitrided specimens after the polarization test (solution: 3.5 wt.% NaCl, aerated) (phases present in the modified layer: expanded martensite, ε- and γ′-nitrides) (for further details, see [106]) (reprinted with permission from Ref. [106]. Copyright 2021 Elsevier).

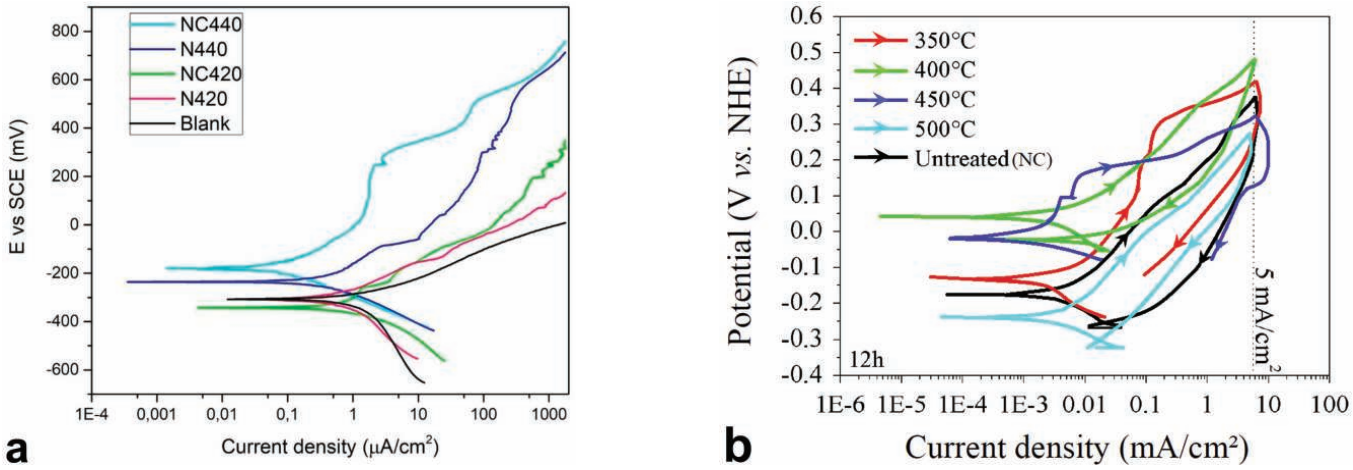

Figure 10. AISI 420 martensitic stainless steels: (**a**) potentiodynamic polarization curves of untreated (blank), nitrided (N420, N440), and nitrocarburized (NC420 and NC440) specimens (solution: 3.5 wt.% NaCl) (phases present in the modified layers: N420 and N440: expanded martensite + ε- and γ′-nitrides; NC420 and NC440: expanded martensite + ε- and γ′-nitrides + Fe_3C) (for further details, see [29]) (reprinted with permission from Ref. [29]. Copyright 2024 Elsevier). (**b**) Potentiodynamic polarization curves of untreated and carburized specimens (solution: 3.5 wt.% NaCl) (phases present in the modified layers: 350–450 °C: expanded martensite + Fe-based carbides; 500 °C: α-Fe + Fe- and Cr-based carbides) (for further details, see [133]) (reprinted with permission from Ref. [133]. Copyright 2019 Elsevier).

The formation of a heterogeneous surface with a fairly large amount of Fe-based nitrides dispersed in the expanded martensite matrix tends to impair corrosion resistance. In fact, nitrides are nobler than the expanded martensite, and micro-galvanic effects occur, causing the formation of many small pits [124,129]. As a consequence, corrosion potential values even lower than those of the untreated steel are registered, as well as fairly large anodic current density values [124,125,130,143]. The passive branch in the nitrided samples, which is short but clearly observable in the polarization curve of the untreated alloys, often becomes shorter or hardly detectable [129].

A clear improvement in the corrosion resistance is observed when a continuous layer of ε-nitride forms on top of an inner "diffusion" layer, in which expanded martensite and eventually Fe-nitrides are also present [129,143,145]. An EIS analysis of nitrided samples

tested in 3.5 wt.% NaCl showed a wider semicircle in the Nyquist plot in comparison with the untreated alloy and higher impedance values [143]. An increase in the corrosion potential when an almost continuous layer of ε-nitride formed was also observed for AISI 420 martensitic stainless steel subjected to arc discharge plasma nitriding (440 °C, 1 h, arc current: 130 A) [143]. The presence of a continuous ε-nitride layer (plasma nitriding; 350 °C, 15 h) also allowed for obtaining good corrosion resistance in a 5% NaCl + H_2SO_4 solution at pH 3, as assessed by Xi et al. [146] by means of a salt fog spray test (duration: 120 h) and potentiodynamic polarization.

An improvement in the corrosion resistance is also registered when ε-nitride is formed together with expanded austenite due to the transformation of retained austenite [125,134]. In particular, it was observed that the combination of ε-nitride, expanded austenite, and expanded martensite present in the modified surface layers of nitrided (400 °C, 5 h) AISI 431 steel caused a decrease in the corrosion potential when tests were carried out in a 5 wt.% NaCl solution, but the anodic dissolution rate was reduced. After the tests, the surface was slightly colored, and shallow pits were observable, suggesting that even for this sample type a combination of uniform and localized corrosion phenomena occurred [125].

A decrease in the corrosion resistance is also observable for nitrocarburized martensitic stainless steels with heterogeneous surface microstructures [124]. When a large amount of ε-$Fe_{2–3}$(N,C) carbonitride forms, improved corrosion resistance is observed [29].

The C-rich expanded martensite allows for increasing the corrosion resistance. Scheuer at al. [133] reported that for the carburized AISI 420 samples, in which the precipitation of Cr carbides was avoided, the OCP values in a 3.5 wt.% NaCl solution were usually higher than those of the untreated steel, even if they had its same decreasing trend. An increase in the corrosion potential was observed, and small pits were present on the surface after the tests. The authors reported a significant improvement in the corrosion resistance for samples subjected to carburizing treatments at low temperatures (up to 450 °C) and over short durations (up to 12 h) (Figure 10b). The increase in the treatment temperature or the duration caused the formation of large amounts of Fe carbides or even Cr carbides, which could reduce the corrosion resistance in comparison with the untreated alloy. The occurrence of intergranular corrosion was observed when Cr carbides formed along grain boundaries [133]. Carburizing treatment (450 °C, 8 and 12 h) was also effective in mitigating tribocorrosive effects, such as those due to slurry erosion and liquid impingement erosion when AISI 420 steel was exposed to a 3.5 wt.% NaCl solution [32]. The carburizing treatment of AISI 410 steel at 450 °C for 20 h produced an increased amount of carbides, which formed a thin layer on the surface, but corrosion resistance was almost maintained compared to that of the untreated steel [147].

Thus, the results present in the literature point out that an improved corrosion resistance can be obtained by modified surface layers consisting of either expanded martensite without or with a low amount of Fe-based precipitates (nitrides/carbides) or a continuous layer of Fe-based nitrides/carbonitrides above the expanded martensite. The conditions for obtaining such modified layers depend on the steel composition, the previous heat treatment history (quenching with/without tempering), and low-temperature treatment parameters. An attempt to summarize the effects of the treatment temperature and duration on the corrosion resistance in NaCl solutions of nitrided, nitricarburized, and carburized martensitic stainless steels was recently reported by Scheuer et al. [148].

When CrN begins to form with the other phases, corrosion resistance degrades [124,134,148,149]. It is interesting to note that upon using nitriding temperatures comparable to those used for the nitriding of low alloy steel (460–500 °C), a thick compound layer rich in both Fe- and Cr-based nitrides is able to form, and it has a good corrosion resistance in both 3.5 wt.% NaCl solution and 1% HCl acidic water solution [145].

5.3. Corrosion Behavior in Cl-Free Solutions

The corrosion behavior of martensitic stainless steels in aqueous H_2SO_4 solutions is reported in the international literature (see, for example, [150]). However, to the author's knowledge, no study on low-temperature-treated martensitic stainless steels is present.

6. Austenitic Stainless Steels

For austenitic stainless steels, the "expanded" phase formed in low-temperature thermochemical treatments is usually indicated as "expanded austenite", "S-phase" (referring to the shift of its diffraction peaks compared to those of the untreated austenite), γ_N for the N-rich one, and γ_C for the C-rich one.

The main characteristics of the modified surface layers obtained on austenitic stainless steels through nitriding and carburizing are summarized in Table 4. Further information is present in dedicated reviews [12,18,47].

Table 4. Main characteristics of the modified surface layers obtained on austenitic stainless steels through nitriding or carburizing. (References for the indicated values are reported in the text).

Properties		Nitriding	Carburizing
Formation temperature (without formation of Cr compounds) (°C)		300–450	300–550
Max. interstitial content in expanded austenite (at. %)		38	19
Max. surface hardness ($kg_f\ mm^{-2}$)		1450	1000
Localized corrosion resistance (Cl^--containing solutions)	- Expanded austenite only	very good	good
	- With ε_N'/Fe-based compounds (low amount)	good	acceptable
	- With Fe-based compounds (high amount)	poor	poor
Corrosion resistance in H_2SO_4/sulfite solutions	- Expanded austenite only	good	good
	- With ε_N'/Fe-based compounds	poor	-

6.1. Microstructure and Characteristics of the Modified Layers

The solubilization of interstitial atoms (N, C) well beyond the solubility limit (often indicated as "colossal" supersaturation) in the austenite lattice causes local plastic deformations, which are even observable at the surface [151–157] (Figure 11a). As a consequence, after the treatment, an increase in surface roughness is usually observed [152].

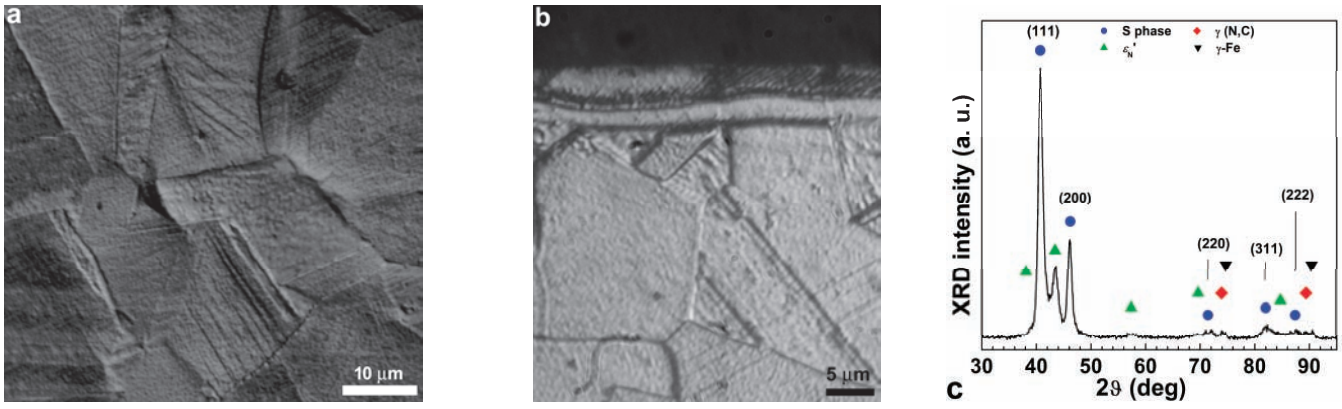

Figure 11. Plasma-nitrided AISI 202 austenitic stainless steel (380 °C, 130 Pa, 5 h): (**a**) surface morphology, (**b**) cross-section microstructure, (**c**) XRD pattern (for further details, see [158]) (adapted from Ref. [158]).

When the cross-sections or tapered sections are examined after chemical etching, the modified surface layer is continuous, fairly homogeneous, and separated from the matrix by a strong, etched line (Figure 11b). In nitrided and nitrocarburized samples, two layers are often observed [91,159–162], while in carburized specimens, only one layer

is detected [73,163]. The effect of local plastic deformations caused by expanded austenite formation is observable as slip lines extending from the surface into the inner part of the outer modified layer [164]. The extension and the number of these slip lines depend on the steel composition and the nitriding conditions [91,151,165]. In particular, they are more numerous in Mn-rich austenitic stainless steels, such as AISI 200 series steels or Ni-free austenitic stainless steels [60,91,164,166], and when the N content in the modified layer is high.

The main constituent of the modified surface layer is expanded austenite (Figure 11c). This phase has been described as a supersaturated solid solution of N and/or C in the f.c.c. lattice, but recent studies have shown that the picture is more complex. Preferential bonding between Cr and N atoms is detected [85], and the formation of Cr-N short-range ordered (SRO) regions is observed [86]. In the outer part of the modified layer, where the N content is higher, long-range ordered (LRO) regions, with a γ'-Fe_4N-like order and named $\gamma_N{}'$, are present together with SRO regions [167–171]. As the N content decreases, only SRO regions are present in a disordered expanded austenite [168]. The LRO $\gamma_N{}'$ regions are small ordered domains separated by antiphase boundaries, and their size decreases as the Cr content increases and when the N content is lower [171]. Peculiar features are observed, such as anisotropic growth with a pancake-like antiphase domain distribution [172].

The occurrence of local plastic deformations due to the huge N solubilization is related to the formation of a strain-induced phase, called N-induced h.c.p. ε'-martensite, $\varepsilon_N{}'$, which is a solid solution of N in the h.c.p. ε'-martensite [167,173]. It is a matter of debate whether this phase can be considered strictly a martensite phase formed from expanded austenite through a martensitic shear transformation above a critical N concentration [174] or whether it is simply due to a cluster of stacking faults [175]. The h.c.p. structure is coherent with the matrix, and it has the Shoji–Nishiyama orientation relationship, which is characteristic of the f.c.c.-to-h.c.p. martensitic transformation, $\{111\}_{fcc}//\{0001\}_{hcp}$ and $[1\bar{1}0]_{fcc}//[11\bar{2}0]_{hcp}$ [173,176]. However, multilayer stacking faults are indeed observed in the nitrided layer, and their thickness and width are related to the N content, plastic deformation, and the strain gradient [177]. In the formation of this h.c.p. phase, the N has a dual role. As a solubilized element, it causes the expansion of the f.c.c. cell, which is also accommodated by plastic strain [177], and it decreases the stacking fault energy, promoting the formation of extended stacking faults [176,177]. Therefore, the formation of $\varepsilon_N{}'$ depends on both the N content and the alloy elements, and it tends to be promoted in steels with a low stacking fault energy, such as those with a fairly high Mn content [91,165,176]. This fact should be taken into account as the presence of this phase may influence corrosion resistance.

The presence of $\gamma_N{}'$ regions and $\varepsilon_N{}'$ is also detected in nitrocarburized steels [178]. In addition to the fact that $\gamma_N{}'$ may originate γ'-nitride, $\varepsilon_N{}'$ may originate ε-nitride when an ordering of N atoms occurs together with a distortion of the lattice [179].

The presence of an inner layer in the nitrided zone is well-assessed when nitrocarburizing treatments are carried out, and it is ascribed to the formation of C-rich expanded austenite [161,162]. An inner layer is observed also in nitrided steels with both low [91,165,180] and fairly high [60,91,158] C content, and it is related to an expanded austenite with a lower expansion, γ(N,C) [164]. Different hypotheses are put forward in order to explain this phenomenon, including a local increase in C atoms [181], local high residual stresses [182], and the effect of the N concentration profile [160]. The formation of a low-expansion f.c.c. phase, which transformed into expanded austenite, was observed by means of in situ XRD analysis during low-energy ion implantation of N on AISI 316Ti [183]. The formation of a layered structure in which expanded austenite had two distinct lattice expansions was registered in both AISI 316Ti and Ni-rich (24–26 wt.%) AISI 904L super-austenitic stainless steel, and it seemed to be dependent on nitriding conditions [184].

Nitrides may be present as precipitates, especially along the grain boundaries or the slip lines, and they are observable as strong etched regions in the cross-section [151,164]. Differently from what is observed for ferritic and martensitic stainless steels, in austenitic stain-

less steels, ε-nitride does not form a more or less continuous layer when low-temperature nitriding is performed, probably as a consequence of the larger N amount that can be solubilized in austenite compared to in ferrite or martensite. The formation of CrN may cause the transformation from austenite to ferrite due to the loss of Cr from the matrix [176]. In order to avoid the formation of Cr compounds, nitriding should be performed at temperatures lower than 450 °C [78,185], and carburizing should be performed at temperatures lower than 550 °C [185]. However, the formation of Fe and Cr compounds also depends on the steel composition and the treatment conditions (duration, N and/or C feeding) [60,151,156,163,186]. As an example, for nitriding, the temperature at which nitrides can form tends to decrease as the Mn content increases and the Ni content decreases [60,125,165,166].

The concentration profile of interstitial atoms is dependent on the treatment type. When nitriding is carried out, the obtained N concentration profile has a characteristic step-like trend, with high values near the surface, followed by a nearly constant plateau with lower values and then a steep decrease to matrix values [12,18,160,184]. The carburized specimens have a C profile with an initial steep decrease in the C concentration near the surface, followed by a smooth decrease to matrix values [12,18,100,161]. Nitrocarburizing allows for obtaining a smoother profile due to the presence of a N-rich expanded austenite near the surface and a C-rich expanded austenite in the inner part of the modified layer [161,162]. The maximum interstitial content of expanded austenite is ~38 at.% for N [24] and ~19 at.% for C [25].

As a non-equilibrium phase, expanded austenite tends to decompose and transform into CrN and α-Fe when the service temperature is too high. The incubation time for the decomposition of N-rich expanded austenite ranges from minutes at 500 °C to thousands of hours at 300 °C [187]. For C-rich expanded austenite, the incubation time for the formation of carbides is thousands of hours at 350 °C [188]. As the service temperature decreases further, the incubation time becomes longer.

Low-temperature thermochemical treatments produce modified surface layers with a significant increase in hardness. Nitrided steels can reach ~1450 $kg_f\ mm^{-2}$ [189], and the microhardness profile maintains the step-like trend of the N concentration [18,190]. Carburized steels can reach ~1000 $kg_f\ mm^{-2}$ [191], and the obtained microhardness profile shows a gradual decrease [18,190]. When nitrocarburizing is performed, high microhardness values at the surface with a smooth hardness profile can be attained [18,190].

6.2. Corrosion Behavior in the Presence of Cl^-

In the international literature, many studies are reported regarding the corrosion behavior of low-temperature-treated austenitic stainless steels in environments containing Cl-ions. Most of them include tests in NaCl aqueous solutions, both aerated and deaerated, but they also report tests in mixed saline solutions, such as NaCl + Na_2SO_4, and solutions simulating body fluids (phosphate-buffered saline (PBS) solution, Ringer's solution, simulated body fluid (SBF) solution, etc.), $FeCl_3$ solutions, and HCl solutions. An overview of the studies is reported in [47]; here, the main results are summarized.

The EIS analysis gives important information regarding the corrosion behavior of the N and/or C alloyed modified surface layers. When Nyquist plots are considered for nitrides samples tested in NaCl solutions, wider semicircles are observed compared to those of untreated steel, so a better corrosion resistance is hypothesized [70,91,158] (Figure 12a). Similarly, higher impedance values are registered in the Bode plots of samples with an expanded austenite layer [70,91,158]. Regarding phase angle plots, both one [192] and two [60,70,91,158] time constants are observed. When the overall polarization resistance is considered, a higher value is measured for the nitrided samples compared to that of the untreated alloys [60,70,91].

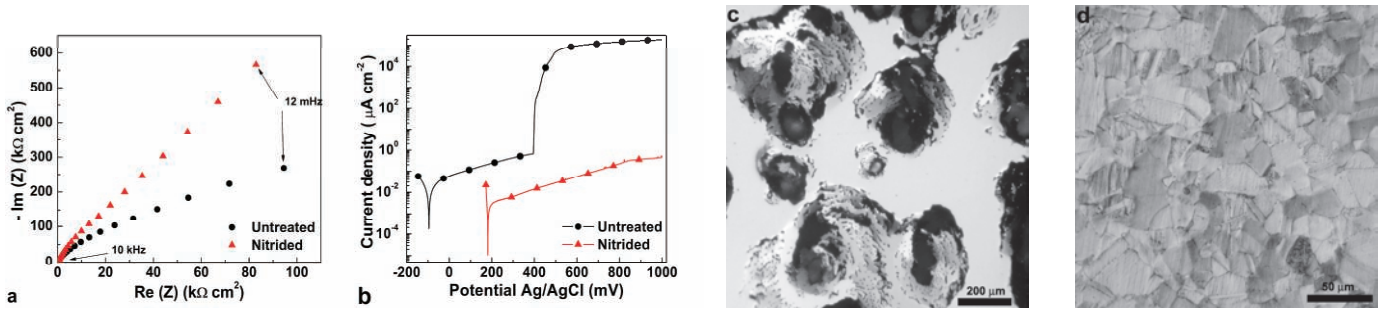

Figure 12. Plasma-nitrided (380 °C, 130 Pa, 5 h) and untreated AISI 202 austenitic stainless steel: (**a**) Nyquist plots, (**b**) potentiodynamic polarization curves, and surface morphology after the polarization test for untreated (**c**) and nitrided (**d**) specimens (solution: 5 wt.% NaCl, aerated) (phases present in the modified layers: expanded austenite + ε_N' + γ(N, C)) (for further details, see [158]) (adapted from Ref. [158]).

The change in the electrochemical behavior over time was studied in nitrided high-Mo UNS S31254 super-austenitic stainless steel tested in a 3.5 wt.% NaCl aerated solution [106]. When the Nyquist plots registered for times ranging from 1 h to 30 days were compared, it was observed that the semicircles became wider and wider up to 7 days, and then they were smaller. The polarization resistance was at the maximum for 7 days, and then it tended to decrease, but it remained comparable to that of the untreated steel. The capacitance of the passive film was evaluated, and it was slightly lower than that of the untreated steel, and therefore it may be hypothesized that the passive film was stable and that the relevant dissolution processes did not occur.

As reported before, the formation of N-rich expanded austenite can cause the concurrent formation of ε_N'. The EIS analysis suggests that the presence of this phase does not significantly influence the corrosion resistance. Wider Nyquist plots and higher impedance values are observed in nitrided samples compared to those of the untreated alloys, even in steels that tend to promote the formation of ε_N', such as AISI 202 and Ni-free P558 [91]. However, when fairly high amounts of ε_N' form, as in Ni-free P558 austenitic stainless steel plasma-nitrided at 380 °C for 3 h, the phase angle plot has three inflections, which can be related to three time constants [91]. A similar trend is observed for inhomogeneous surfaces or a porous oxide layer, and it is therefore supposed that the heterogeneous surface consisting of both expanded austenite and ε_N' influences the properties of the passive film. Nevertheless, improved corrosion resistance is observed.

The increase in impedance values for nitrided austenitic stainless steels is observed not only in NaCl solutions but also in mixed saline solutions, such as PBS solution [193] and SBF solution [194], which are usually used for simulating body fluids.

The increase in impedance values is also registered for austenitic stainless steels subjected to nitrocarburizing [157] and carburizing [73,74,100], suggesting that both N and C surface alloying with the formation of expanded austenite improves the corrosion resistance in Cl^--containing solutions.

On the contrary, the formation of large amounts of nitrides impairs the corrosion resistance, as suggested by narrower semicircles in Nyquist plots [60,178,194].

Information regarding the behavior in free corroding conditions can be obtained based on the trend of OCP values over time. For untreated austenitic stainless steels, the characteristic OCP trend has sharp decreases and increases due to the formation of metastable pits and their repassivation. In nitrided samples tested in NaCl solutions, higher OCP values are usually observed, with an increasing trend [189,195] and the presence of fewer events due to pit nucleation. The repassivation kinetic tends to be slower [91,189,195]. Equilibrium conditions are attained after a fairly long time (hours) [91]. The evaluation of OCP values for times up to 30 days for the nitrided UNS S31254 super-austenitic stainless steel showed that OCP values quickly increased in the first day, followed by a slower

increase up to 15 days, and, afterwards, a slight decrease at 30 days, suggesting a slow dissolution of the passive film for periods longer than 15 days [106].

The formation of N-rich expanded austenite can significantly increase the localized corrosion resistance in NaCl solutions. The potentiodynamic polarization curves of nitrided austenitic stainless steels have higher corrosion potential and pitting potential values, together with lower anodic current density in the passive branch, compared to those of the untreated alloys [12,70,91,92,106,125,180,196] (Figure 12b). After the tests, a significant difference is observed between the surface of the nitrided specimens and that of the untreated alloys (Figure 12c,d). For the nitrided steels, the surface shows the presence of a few fairly small pits, or it is fairly untouched, with some micrometric pits; on the contrary, large pits are observed for the untreated steels [91,164,195,196].

The increase in surface roughness, the occurrence of local plastic deformations at the surface, and the formation of ε_N' due to expanded austenite formation do not adversely affect the corrosion resistance, which is different from what is observed on N-containing austenitic stainless steels subjected to cold working [197]. The improvement in the corrosion resistance is observed even for the steels that tend to promote the formation of ε_N', such as AISI 202 [91,164,165], Ni-free P558 [60,91], and high-Mn Fe-17Cr-20Mn-0.5N steel [166]. As an example, the potentiodynamic polarization curves of AISI 316L, AISI 202, and Ni-free P558, both untreated and nitrided (380 °C, 340 Pa, 3 h), are depicted in Figure 13. Even the fairly high ε_N' content in nitrided P558 does not impair the enhancement of corrosion resistance due to N-rich expanded austenite. On the contrary, the transformation of ε_N' into ε-nitride causes a decrease in the corrosion resistance, as observed by Lei et al. [97]. These authors compared the behavior of nitrided 1Cr18Ni9Ti specimens containing expanded austenite only with those of samples containing expanded austenite + ε_N' and expanded austenite + ε-nitride (solution: 1 wt.% NaCl). They registered a significant (and comparable) increase in the pitting potential for samples with expanded austenite with/without ε_N', while for samples containing expanded austenite + ε-nitride, the pitting potential was lower than that of the untreated steel.

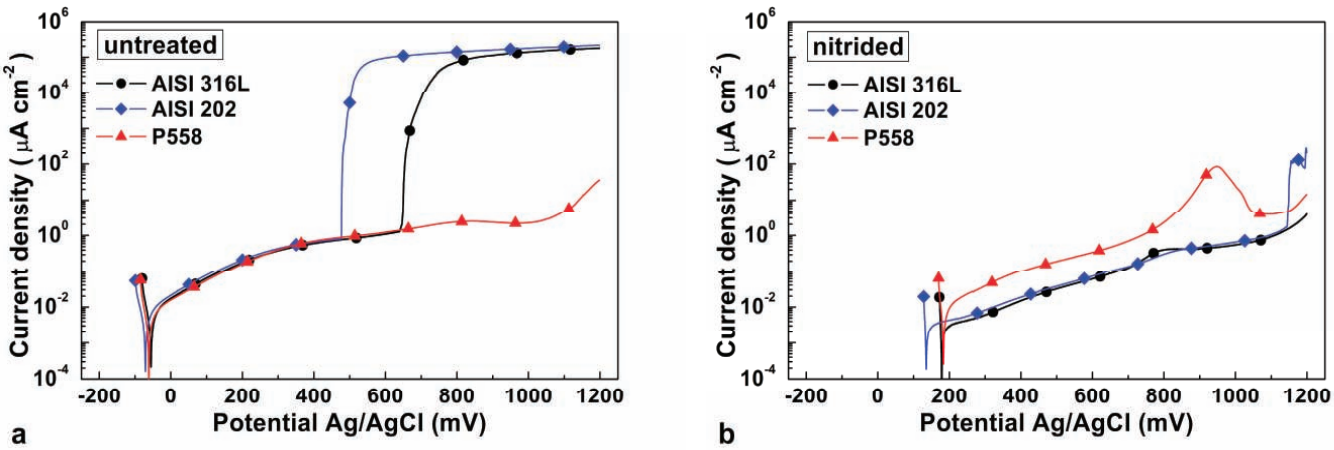

Figure 13. Potentiodynamic polarization curves of AISI 316L, AISI 202, and Ni-free P558: (**a**) untreated, (**b**) nitrided (380 °C, 340 Pa, 3 h) (solution: 5 wt.% NaCl, aerated) (phases present in the modified layers: expanded austenite + ε_N' + γ(N, C); the ε_N' content increases as AISI 316L < AISI 202 < Ni-free P558) (for further details, see [91]) (adapted from Ref. [91]).

The presence of N-rich expanded austenite is also beneficial when MnS inclusions are present in the steel [198]. It is well-known that MnS inclusions are pit initiation sites in austenitic stainless steels [199], and it is observed that in nitrided austenitic stainless steels, they also tend to initiate corrosion where they are present. However, the inclusions act as channels, so corrosion phenomena occur in the untreated substrate where the electrolyte penetrates, while no pits or crevices are observed in expanded austenite. Therefore, the formation of a modified surface layer thick enough to embed inclusions is desirable.

Studies on the effect of alloy elements were also carried out [91,125,165,200]. In particular, the synergy between Mo and N in impairing corrosion phenomena should be taken into account, and Mo-containing steels have an enhanced corrosion resistance after nitriding [91,165,200].

The effect of surface finishing was also studied, and it was shown that nitrided steels with a surface roughness comparable to a 2D finishing (Ra ~ 0.2 μm) maintained very good corrosion resistance [158].

The ability of modified layers consisting of expanded austenite to repassivate can be assessed using different techniques (cyclic potentiodynamic and galvanostatic techniques). It has to be taken into account that different test conditions influence the extension of the damage and the possibility of repassivation. The comparison of literature data suggests that repassivation can occur when the depth of pits or crevices is not too large [91,97,106].

Potential pH diagrams were obtained by Zhu and Lei [92] for untreated and nitrided AISI 1Cr18Ni9Ti steels tested in 3 wt.% NaCl solutions with pH values in the range of 0.4–13. N-rich expanded austenite allowed for extending the immunity and perfect passivity regions, and it reduced imperfect passivity and pitting zones. A significant increase in pitting corrosion resistance was observed in the pH range of 4–11.

The improvement in the localized corrosion resistance for nitrided specimens is also observed when crevice corrosion is assessed. As an example, tests carried out in a 10 wt.% NaCl solution at 55 °C showed that untreated AISI 316L had the first signs of crevice corrosion after only 3 days. When nitriding was performed at 400 °C for 5 h, and a 10-μm thick expanded austenite layer was obtained, no observable corrosion phenomena were observed up to 60 days [195]. An enhancement of corrosion resistance to crevice phenomena was also observed when nitrided AISI 316 (430 °C, 20 h) was tested in a 3 wt.% $FeCl_3$ solution at pH 3 [155].

The presence of nitrides together with expanded austenite may affect corrosion behavior. Low amounts usually do not impair corrosion resistance, and the pitting potential is usually higher and the surface damage is smaller than those of the untreated steel, even if a lower corrosion potential is registered [151,158,164,165,195,201]. However, in crevice tests, this improvement is not observed [195]. The formation of large amounts of Cr- and Fe-based nitrides causes the decrease in corrosion resistance [60,164,186,201–203].

The enhancement of corrosion resistance for low-temperature nitrided austenitic stainless steels is also reported when the steels are tested in mixed saline solutions, such as those simulating body fluids, such as PBS [193,204–206], Ringer's solution [201,207], and SBF solution [194]. The increase in the pitting corrosion resistance is also observed in a 0.4 M NaCl + 0.1 M $NaSO_4$ solution at pH 3 for nitrided AISI 304L [98].

Low-temperature nitriding is also effective in increasing the critical pitting temperature. An increase from 40 to 65 °C was registered for nitrided AISI 316L steel [208].

Overall, literature data suggest that N-rich expanded austenite can exert a protective effect, and its ability to hinder localized corrosion phenomena increases as the content of solubilized N increases and when the modified surface layer is thicker and nitride precipitates are not present in a significant amount. Therefore, the treatment parameters (temperature, time, N feeding) have a critical role, and they have to be carefully chosen as a function of the used alloy for producing a N-rich, nitride-free, and thick modified surface layer.

When both N and C alloying is performed in nitrocarburizing treatments, an enhancement of corrosion resistance is observed. In the polarization curves, higher corrosion and pitting potential values are registered, and the anodic current in the passive branch is lower [157,190,209–212]. When compared to nitrided specimens, slower pit formation was observed for AISI 316L samples, which were nitrocarburized with the active screen technique. Therefore, it was hypothesized that N and C acted in combination in hindering the corrosion process [211]. An improved corrosion resistance is also detected when tests are carried out in Ringer's solution [213]. However, the formation of large amounts of nitrides and carbonitrides impairs corrosion resistance [178].

Low-temperature carburizing is effective for increasing corrosion resistance in different Cl^--containing environments, such as NaCl solutions [15,74,100,214,215], NaCl + HCl solutions [74], $FeCl_3$ solutions [214,216], and Ringers' solution [213,216]. However, the results reported in the literature often depend on the presence or absence of the upmost layers, in which a carbon soot may form and carbides may be present. As an example, Sun [74] carried out cyclic polarization tests on carburized AISI 316L specimens in aerated 0.5 M (3 wt.%) NaCl solution (Figure 14a). The first test was performed after removing the first 2 μm of the modified layer and then repeated by progressively removing the modified layer in order to correlate the typical potential values (corrosion potential, breakdown potential, repassivation potential) with the C content. It was observed that repassivation occurred in all of the tests, and the repassivation potential was fairly high at a depth up to about 18 μm. Corrosion resistance was significantly improved when the C content was higher than ~0.25 wt.% (~1.1 at.%), without a significant dependence on the C concentration. On the contrary, Li et al. [103], who tested the corrosion resistance of carburized AISI 316 foils in aerated 0.6 M (3.5 wt.%) NaCl solution after ultrasonically cleaning them in deionized water to remove soot, observed a lower breakdown potential than that of the untreated steel, followed by a pseudo-passivity region (Figure 14b). During the reverse scan, the carburized specimens did not fully repassivate, and a pseudo-passivity region was registered. The authors concluded that the passive film formed on carburized specimens had a low resistance to breakdown and a low ability to repassivate. However, the assessment of the pit growth stability using 1D pit electrodes, which are able to create a single pit, highlighted that carburized specimens had a high rate of dissolution in the transpassive region, but the pit dissolution current density was about 11 orders of magnitude smaller than that of the untreated alloy, and stable pit growth did not occur. Therefore, it was suggested that the improved pitting corrosion resistance of carburized samples was due to the low ability to stabilize the pit growth.

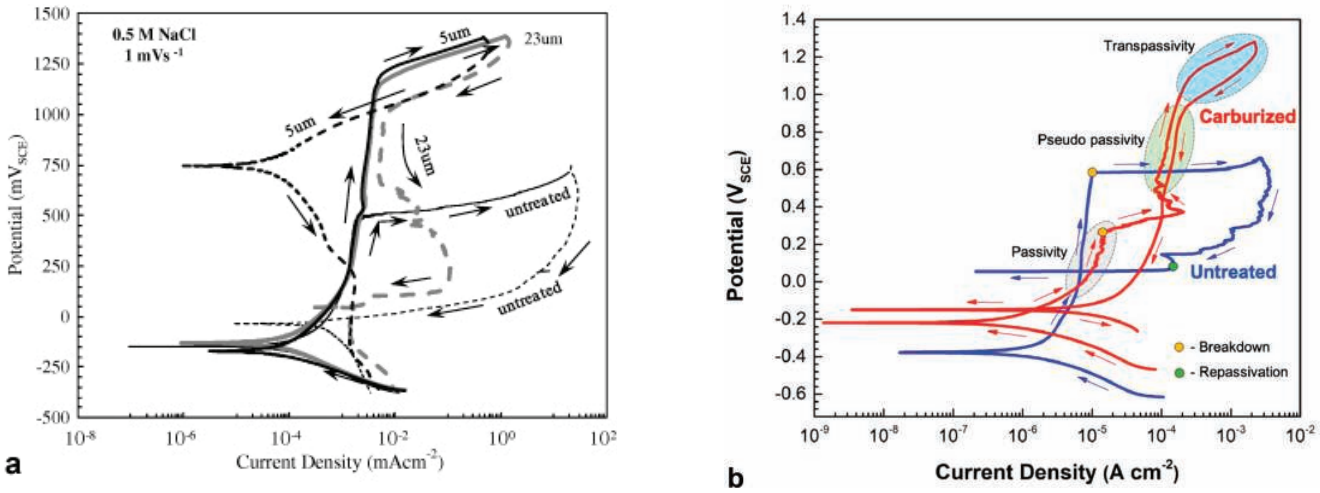

Figure 14. Cyclic polarization curves of carburized and untreated austenitic stainless steel specimens: (**a**) carburized AISI 316L at different depths (solution: 0.5 M NaCl) (phase present in the modified layer: expanded austenite) (for further details, see [74]) (reprinted with permission from Ref. [74]. Copyright 2010 Elsevier); (**b**) carburized AISI 316 (solution: 0.6 M NaCl) (phase present in the modified layer: expanded austenite) (for further details, see [103]) (reprinted with permission from Ref. [103]. Copyright 2021 Elsevier).

The enhancement of resistance to pitting corrosion phenomena is also observable when the critical pitting temperature is considered. An increase from 16.9 to 79.1 °C was registered for carburized AISI 316 [15].

The improvement of corrosion resistance to crevice phenomena thanks to low-temperature carburizing is observed using $FeCl_3$ solutions [214,216].

The formation of carbides at the surface causes a decrease in corrosion resistance, and smaller passive branches with high anodic current density values are registered [100].

HCl solutions are usually harmful to stainless steels [2]. The good corrosion resistance of the modified surface layers containing expanded austenite even in HCl solutions can be inferred by the difficulty of etching this phase when the HCl-containing chemical etchants for stainless steels are used. Corrosion tests in HCl solutions highlight that both nitriding [217] and carburizing [103,218,219] at low temperature increase the corrosion resistance.

6.3. Corrosion Behavior in the Presence of Cl-Free Solutions

The corrosion behavior of modified surface layers containing N- and/or C-rich expanded austenite is studied in different Cl-free environments, such as H_2SO_4 solutions, Na_2SO_4 solutions, borate solutions, and HF solutions. An overview of these studies is reported in [47].

As recalled above, austenitic stainless steels have good corrosion resistance in very dilute or highly concentrated H_2SO_4 solutions, while they suffer high corrosion loss at intermediate concentrations. The possibility of improving the corrosion resistance of austenitic stainless steels in H_2SO_4 solutions thanks to low-temperature thermochemical treatments has gained increasing attention for certain applications, such as bipolar plates in proton exchange membrane fuel cells (PEMFCs) [43,220–222]. The corrosion resistance of N-rich expanded austenite in H_2SO_4 solutions is usually comparable to that of the untreated alloys [96] or even higher [222]. However, it is particularly sensitive to the presence of other phases, such as ε_N' or nitrides, which form a heterogeneous surface layer together with expanded austenite, causing a decrease in corrosion resistance [97,222]. As an example, Lei et al. [97] tested nitrided 1C318Ni9Ti samples with modified layers with different compositions in a 0.5 M H_2SO_4 solution. The authors observed that for the specimens with expanded austenite alone, the polarization curves were comparable to those of the untreated steels, while the simultaneous presence of ε_N' caused an increase in the passive current values by one to two orders of magnitude. The presence of nitrides caused a further increase.

On the basis of literature data regarding corrosion behavior in sulphate solutions, it can be suggested that the high anodic reactivity observed when N-rich expanded austenite forms [31,99,118,222,223] may be related not only to the passive film that forms in this environment but also to the presence of a heterogeneous structure at the surface due to the presence of ε_N' and/or nitrides together with expanded austenite. As an example, Kuczynska-Wydorska and Flis [223] studied corrosion behavior at various depths for nitrided AISI 304L and AISI 316L (425 °C, 30 h) in a 0.1 M Na_2SO_4 solution acidified to pH 3. The authors observed that for the near surface part of the modified layer with a ~7–14 wt.% (22–35.7 at.%) N content, anodic current density values were much higher than those of the untreated steels in the active, passive, and transpassive regions, suggesting a decrease in corrosion resistance. Taking into account the treatment conditions, it may be hypothesized that ε_N' and eventually nitride precipitates formed. In deeper zones of the modified layer with N content lower than 7 wt.% (~22 at.%), the anodic current density values were slightly higher than those of the untreated alloys, and they were lower in the passive and transpassive regions. For these zones, the presence of expanded austenite alone may be hypothesized, suggesting that it has the ability to maintain or even increase the corrosion resistance.

A model for relating the thickness of the nitrided layer to the corrosion resistance in H_2SO_4 solution was developed by Reinders and Bräuer [224]. By starting with iso-thickness maps, which related the thickness of the modified layer to the treatment temperature and the time, the authors performed potentodynamic tests in 0.05 M H_2SO_4 at 80 °C and obtained the corrosion data used for quantifying a "corrosion resistance value" or CRV. The superposition of the maps with the CRV allowed them to identify suitable treatments for maintaining good corrosion resistance in H_2SO_4 solutions.

When low-temperature carburizing is considered, good corrosion resistance is observed after the removal of the outermost layer, which usually has poor corrosion resistance [104]. The polarization curves of both untreated and carburized samples have the typical active–passive–transpassive trend, but the carburized samples have very small anodic peaks, higher corrosion potential values, and lower corrosion current density [31,104]. Corrosion potential and corrosion current density tend to increase and decrease, respectively, as the C content increases, while the anodic current in the passive branch and the transpassive potential are not significantly influenced by the C content [104]. Carburized AISI 316L also has good corrosion resistance in boiling 16% H_2SO_4 solution [225].

The corrosion behavior in borate buffer solution at different pH values has also been studied for nitrided austenitic stainless steels, and the experimental results highlight that N-rich expanded austenite maintains good corrosion resistance, even in this environment [69,82,88]. Good corrosion resistance is also observed for carburized specimens [226].

Modified surface layers consisting mainly of N-rich expanded austenite allowed 904L super-austenitic stainless steel to have good corrosion resistance in 0.1 M HF solution [227]. However, strict control of the nitriding conditions was required in order to avoid the precipitation of Fe- and Cr-based nitrides, which impaired corrosion resistance [227,228].

7. Duplex Stainless Steels

7.1. Microstructure and Characteristics of the Modified Layers

Duplex stainless steels consist of austenite grains in a ferritic matrix with different compositions owing to the partitioning of alloy elements during cooling. Slow cooling allows ferrite to become richer in ferrite-stabilizing elements, such as Cr and Mo, while austenite becomes richer in austenite-stabilizing elements, such as Ni and Mn.

When a low-temperature thermochemical treatment is carried out on a duplex stainless steel, the interstitial atoms (N, C) diffuse faster in the b.c.c. ferrite than in the f.c.c. austenite, and therefore different thicknesses of the modified layers in the different phases are observed [112,229]. The supersaturation of interstitial atoms can produce both expanded austenite and expanded ferrite [229–231], or it can also cause the transformation of ferrite into expanded austenite [27,106,112,232,233].

The surface morphology of the low-temperature-treated duplex stainless steels is similar to that of austenitic stainless steels treated in comparable conditions, even when both expanded ferrite and expanded austenite form [111]. Grain boundaries are well-delineated and shear lines and reliefs are observed in austenite grains, while ferritic grains remain fairly smooth.

When both expanded ferrite and expanded austenite form, the cross-section microstructure has a typical appearance (Figure 15a). The part of the modified layer containing expanded austenite is usually thinner than the part in which expanded ferrite is present [111,229,234], and it has a characteristic arc-like shape, becoming thicker close to the ferrite boundary [111,229]. As observed for the other stainless steel types, the modified surface layer produced on duplex stainless steels is fairly unetched compared to the matrix, and it is separated from the matrix by a strong etched line, as occurs for austenitic stainless steels. Slip lines are observable in the expanded austenite regions, while in expanded ferrite regions, deformation bands are present due to the high compressive stresses occurring during the formation of the expanded phases [229]. Moreover, Fe-based nitride precipitates may form in the expanded ferrite regions due to the greater tendency of ferrite to form Fe-based nitrides compared to austenite [231,235,236].

The microstructure of the modified layers formed on carburized duplex stainless steels is similar to that observed on nitrided samples, with possible differences in the thickness of the layer formed on previous ferrite and austenite grains [237].

Modified surface layers consisting of expanded austenite alone can also form [27,106,232,238,239]. For nitrided steels, the thickness of the expanded austenite is different in the austenite grains and the previous ferrite matrix [232], while for nitricarburized steels, comparable thickness is registered [234]. In the cross-section microstructure of the

modified layer of nitrided (300–400 °C) UNS S32750 super-duplex stainless steel, some authors observed the usually two-layer microstructure in the austenite grains, while only one etched line was observed in the ferrite grains [238,239]. Many slip lines were observed in expanded austenite formed in previous austenite grains, and these deformed zones promoted nitrides precipitation [239]. With the nitrocarburizing treatment, both N- and C-rich expanded austenite phases are reported to form [234].

The ferrite part of the modified layers has a higher tendency to form precipitates owing to the presence of fairly large amount of nitride- or carbide-forming elements, such as Cr [230,240,241]. Thus, to avoid the precipitation of Cr-based nitrides/carbides, the treatment temperature should be lower than that usually employed for the low-temperature treatment of austenitic stainless steels. Temperatures lower than 430 °C should be employed for the nitriding treatment [240], and temperatures lower than 480 °C should be employed for the carburizing treatment [241]. However, even if some treatments, such as nitriding, are performed at temperatures lower than 430 °C, previous annealing treatments may also influence the formation of nitrides [242], as well as mechanical surface treatments, such as shot-peening [243]. When a fairly high treatment temperature is used, the formation of compound precipitates can be avoided using a shorter treatment duration. As an example, Shen et al. [233] obtained a 3-µm thick expanded austenite layer without detectable nitride precipitates by nitriding 2205 duplex stainless steel at 460 °C for 1 h with hollow cathode discharge assistance.

Regarding the interstitial content in the expanded phases, the only consensus regards the fact that ferrite and austenite regions solubilize different concentrations of N and C. Conflicting results are reported, with the austenite part having either a higher [240] or a lower [229] content of interstitials than the ferrite part. When nitriding is performed, N concentration profiles are similar to those observed for nitrided austenitic stainless steels, with high values near the surface and then a fairly steep decrease to matrix values [230,236,244]. The C profiles in previous ferrite and austenite grains were measured for cast 2205 steel, which was carburized at 380 °C for 150 h [237]. The ferrite grains had a high C content (up to ~22 at.%) at the surface, which decreased smoothly to a depth of about 10 µm, and then it had a steep decrease to matrix values. In austenite grains, a slightly lower (~18 at.%) C concentration was registered, and the C profile was smooth, which is similar to that observed in low-temperature carburized austenitic stainless steels.

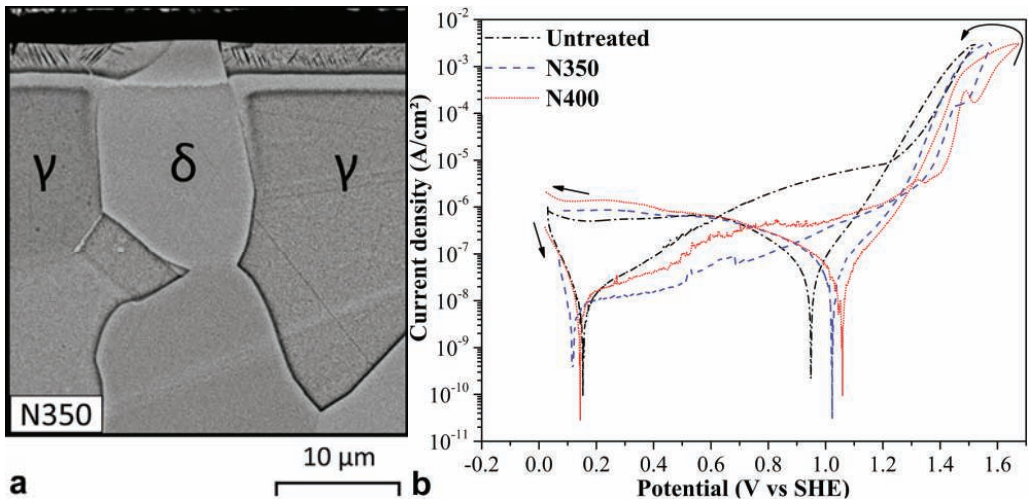

Figure 15. UNS S232750 super-duplex stainless steel: (**a**) cross-section microstructure of a nitrided (450 °C, 4 h) specimen (for further details, see [239]) (reprinted with permission from Ref. [239]. Copyright 2024 Elsevier); (**b**) cyclic potentiodynamic polarization curves of untreated and nitrided specimens (350, 400 °C, 4 h) (solution: 3.5 wt.% NaCl) (phase present in the modified layer: expanded austenite) (for further details, see [238]) (reprinted with permission from Ref. [238]. Copyright 2021 Elsevier).

Differences are also observed in the microhardness values of the expanded austenite and the expanded ferrite [240,245]. Values as high as ~1510 kg_f mm^{-2} are registered for nitrided samples [231] and ~1500 kg_f mm^{-2} for carburized ones [237]. For nitrided specimens, the microhardness profile is comparable to the N profile, with high values in the modified layers and a steep decrease to matrix values [111]. The microhardness profiles in previous ferrite and austenite grains of carburized cast 2205 steel (380 °C, 150 h) were similar to the C profiles, with a step-like trend in the ferrite grains and a smoother profile in the austenite grains [237].

Further details regarding the characteristics and properties of the modified layers are reported in [12,16].

7.2. Corrosion Behavior in the Presence of Cl^-

The modified surface layers formed on duplex stainless steels usually have good corrosion resistance in Cl^--containing solutions both when they consist of expanded austenite together with expanded ferrite and when only expanded austenite is present.

When the modified layers consist of expanded austenite and expanded ferrite, the presence of two phases with different interstitial and alloy element contents does not impair corrosion resistance. An increase in corrosion resistance is observed as long as nitrides do not precipitate in expanded ferrite. Chiu et al. [230] studied the corrosion behavior of UNS S31803 active screen plasma-nitrided at 420 °C in a 3.5 wt.% NaCl solution by means of the potentiodynamic method. When the treatment duration was 10 h, higher corrosion potential values and lower anodic current density in the passive branch were observed, but increasing the nitriding duration caused an increase in the anodic current density values due to the presence of nitride precipitates.

A good corrosion resistance of this modified surface layer type was also observed in mixed NaCl acidic solution (5 wt.% NaCl + 0.5 M CH_3COOH + 0.1 $Na_2S_2O_3$) at pH 2.7 on 2205 duplex stainless steel nitrided at 400 °C for 15 h, with an increase in the corrosion potential and a decrease in the anodic current density in comparison with the untreated alloy [39]. A similar result was found when CO_2 was added.

When the modified surface layers consisted of expanded austenite, in the cyclic potentiodynamic polarization curves of nitrided samples, Calabokis et al. [238] registered corrosion potential values comparable to those of the untreated alloy. However, for nitrided samples, the anodic current density in the passive branch was lower, and the potential values at which passive–transpassive transition occurred were higher, as well as the repassivation potential (Figure 15b). These results suggest a higher corrosion resistance and a greater repassivation capability of nitrided samples. A similar result was found by Alphonsa et al. [234] for modified surface layers obtained on a 2205 duplex stainless steel through nitriding and nitrocarburizing at 350 and 450 °C and consisting mainly of expanded austenite. An EIS analysis showed a higher polarization resistance, and the potentiodynamic curves showed slightly higher corrosion potential, lower anodic current density values in the passive branch, and higher pitting potential. Moreover, the authors reported that the pits formed on the austenite grains for both nitrided and untreated specimens were probably due to the lower Cr and Mo content of the austenite grains. However, interstitial alloying aided passivation, and the density and size of the pits lowered. Zhao and Wang [244] registered higher corrosion potential values and lower anodic current density in the passive branch when 2205 duplex steel was nitrided at 420 °C for durations up to 10 h, and after the test, they observed no significant corrosion attack at the surface of these nitrided sample types. When the treatment duration was increased up to 18 h, the corrosion resistance was lower than that of the untreated steel.

When a 2-μm thick modified layer formed on an SAF 2507 super-duplex stainless steel, the corrosion potential was comparable to that of the untreated alloy, but higher anodic current density values in an extended passive branch were observed [27].

Very good stability and protectiveness of the passive film formed on the PIII nitrided UNS S32205 super-duplex stainless steel in a 3.5 wt.% NaCl solution were assessed for a duration up to 30 days by Luiz et al. [106].

Studies on crevice corrosion performed with the PD-PS-PD (potentiodynamic–potentiostatic–potentiodynamic) technique in a 3.5 wt.% NaCl solution showed a higher corrosion resistance of the nitrided steel, with lower corrosion depth [238].

An increase in the critical pitting temperature of nitrided UNS 31803 steel from 70 to 85 °C was registered by Spies et al. [208], but it is not clear if it was ascribable to modified layers consisting of expanded austenite alone or to expanded austenite with expanded ferrite.

Therefore, literature data suggest that the modified layers can exert their protective role when N-rich and thick modified layers are produced without the formation of nitrides. In fact, as expected, when Cr-based nitrides and carbides form, a decrease in corrosion resistance is observed [230,234,246].

Carburized samples also have good corrosion resistance. Studies on duplex 2205 stainless steel carburized at 350 and 380 °C and tested in 0.6 M NaCl solution showed that the polarization curves were comparable to that of the untreated steel [237]. Crevice corrosion tests performed holding the specimens at +300 mV for 1 week in natural sea water with a specially designed holder registered no crevice formation for the carburized samples during the test duration, while on the untreated alloy, a crevice initiated within the first hours.

7.3. Corrosion Behavior in Cl-Free Solutions

The corrosion resistance of low-temperature nitrided duplex stainless steels is influenced by the presence of nitride precipitates when tested in H_2SO_4 solutions. A poor corrosion resistance in 0.05 M H_2SO_4 solution was registered for the UNS 31803 duplex stainless steel nitrided for fairly long times (420 °C, 20 and 32 h) or at higher temperatures (460 °C, 9 h), which were conditions able to produce a fairly high amount of precipitates in comparison with the untreated steel [208].

On the contrary, the formation of a N-rich expanded austenite layer can also improve corrosion resistance in H_2SO_4 solutions. Shen et al. [233] observed a significant increase in corrosion potential and a decrease in corrosion current density for nitrided (460 °C, 1 h) 2205 duplex stainless steel when tested in 0.5 M H_2SO_4 + 2 ppm F^- solutions at 70 °C and bubbled with air to simulate the cathodic environment of a PEMFC and with H_2 to simulate the anodic environment. For both testing conditions, the potentiodynamic polarization curves of the nitrided samples shifted towards nobler potential values and lower anodic current density compared to those of the untreated alloy.

8. Precipitation Hardening Stainless Steels

8.1. Microstructure and Characteristics of the Modified Layers

Precipitation hardening stainless steels need an aging treatment for obtaining the required mechanical properties. Therefore, this thermal treatment can be carried out before the low-temperature surface treatment [149] or together with it as a single process [247–249]. The microstructure and phase composition of the obtained modified layers depend on both the surface treatment conditions and the initial microstructure of the steel.

Most of the studies present in the international literature concern martensitic PH stainless steels. The microstructure of martensitic PH stainless steels, which are solution-treated and aged, consists of martensite with/without retained austenite, with dispersed precipitates. When low-temperature treatments are carried out, interstitial atoms are solubilized in the Fe-based phases, and therefore expanded martensite forms with/without expanded austenite. In nitrided 17-4 PH stainless steels, an expanded martensite layer was obtained using treatment temperatures lower than 370 °C [250,251]. The formation of a small amount of expanded austenite together with expanded martensite was observed in plasma-nitrided (350 °C, 10 h) 17-4 PH stainless steel [252], as well as in plasma-nitrided (360 °C, 10 h) Corrax® (Uddeholm, Hagfors, Sweden) stainless steel [149], due to the

presence of retained austenite. As the treatment temperature increases, Fe-based nitrides tend to form together with the expanded phases. As an example, the presence of γ'-Fe_4N was detected in 17-4 PH stainless steel plasma-nitrided at 420 °C for 5 h [252]. When the treatment duration was increased up to 10 h or more (420 °C), or the treatment temperature was higher (500 °C), CrN also formed.

The effects of subsequent plastic deformation after solution treatment and aging on the characteristics of the nitrided layers are also studied. Machining processes, such as mechanical grinding, produce a work-hardened surface layer with an increased density of dislocations, grain fragmentation, and a high surface roughness, which may influence the characteristics of the nitrided layers. Han et al. [253] compared the nitriding behavior of ground and polished 17-4 PH stainless steel specimens. Grinding produced a work-hardened layer with an upper nanograin layer and an inner refined grain layer. When nitriding (410 °C, 1 h) was performed, the obtained modified layer was thick, and it mainly consisted of γ'-Fe_4N together with a small amount of expanded martensite. On the contrary, nitriding of polished samples produced a thinner, N-rich expanded martensite layer. It was hypothesized that the nanograin microstructure and the high dislocation density promoted N diffusion and the formation of N-rich nitride. The microstructure and the phase evolution of plasma-nitrided (390–430 °C, 1–30 h) 17-4 PH stainless steel with a work-hardened layer were also studied [254]. With the used treatment conditions, the nitrided layer mainly consisted of γ'-nitride. When a low treatment temperature (390 °C) and a short time (1–3 h) were employed, expanded austenite and expanded martensite formed. As the nitriding temperature and duration increased, the expanded phases tended to transform in nitrides, and CrN precipitation occurred. The influence of the nanocrystalline structure on the plasma nitriding behavior of 17-4 PH stainless steel was studied by Liu et al. [255]. The solution-treated and aged steel was subjected to an ultrasonic rolling process (USRP) in order to produce a nanocrystalline structure, and then it was plasma-nitrided (350 °C, 16 h). In the USRP samples, the modified layers had a higher N content (12.4 at.%), and they consisted of γ'-nitride, which partially transformed in α-Fe, together with a small amount of CrN. In the samples, which were only solution-treated and aged, the nitrided layer had a lower N content (9.99 at.%), and expanded martensite, Fe-based nitrides, and CrN were detected.

Simultaneous aging and nitriding is an effective method for obtaining a hardened surface layer on a strengthened bulk [247,256]. The influence of previous thermal treatments (solution treatment or solution treatment + aging) on the characteristics of the modified layer was studied by Pinedo et al. [256] for 17-4 PH stainless steel nitrided at 400 ° for 20 h. The nitrided layers produced using the two different thermal routes were similar, and they consisted of expanded martensite. However, when solubilization and aging were performed before nitriding, a significantly thicker layer (9.2 μm) with a higher N content was obtained compared to that produced through solution treatment + nitriding (5.7 μm). By using thermodynamic calculation, it was shown that Cu influenced N solubility in the steel, which decreased as the Cu content increased. Therefore, when the steel was in the solubilized state, the nitrided layers had a lower N content (max 1.9 wt.%), while in the aged conditions, the formation of Cu-rich coherent precipitates ensured a higher N content (max 3.8 wt.%) in the martensite matrix.

The influence of different amounts of martensite and retained austenite present in the initial microstructure on the characteristics of the modified layers of Nanoflex® (Sandvik, Stockholm, Sweden) PH stainless steel was studied by Bottoli et al. [257]. The authors combined annealing and plastic deformation treatments for producing different contents of retained austenite and then performed nitriding (400–420 °C, 20 h) treatments for obtaining surface hardening and aging in a single step. When martensite was the initial prevalent phase, the nitrided layer was thick and fairly homogenous, and it consisted of expanded martensite. CrN precipitates formed when nitriding was performed at 420 °C. When both martensite and retained austenite were present, both expanded martensite and expanded austenite formed, and the modified layer was inhomogeneous due to the

slower N diffusivity and higher N solubility limit in austenite compared to martensite. When austenite was prevalent, an expanded austenite layer formed, and it was thinner than the expanded martensite layer obtained with the same nitriding conditions. The effects of gas nitriding (425–475 °C) on Nanoflex® PH stainless steel were also studied by Kochmański et al. [258]. Three different pre-treatments were considered, solution treatment (A), solution treatment + cold working (B), and solution treatment + cold working + aging (C), which produced a martensite matrix with retained austenite. Samples under condition A, which had the highest retained austenite content, also had the thinnest nitrided layers, while the thickest layers were observed in the samples under condition C. For all of the sample types, the modified surface layers had a layered structure, with a thin subsurface zone in which nanometric nitrides (usually ε-nitride) were detected and an inner thickest zone consisting of expanded martensite and expanded austenite. In this zone, the formation of nitride precipitates was avoided when nitriding was performed at temperatures lower than 450 °C in an atmosphere containing no more than ~50% NH_3. A C enrichment was observed near the interface with the bulk.

N solubilization during nitriding treatments may also cause the transformation of (expanded) martensite into (expanded) austenite. Frandsen et al. [22] gas-nitrided (406 °C, 16.5 h) solubilized Corrax® PH stainless steel with a martensite microstructure with a negligible amount of retained austenite, and they obtained modified layers consisting of a fairly large amount of expanded austenite together with expanded martensite.

When nitricarburizing treatments are carried out, a N-richer outer layer and an inner C-rich inner layer tend to form. Bottoli et al. [257] nitrocarburized (420 °C, 80 h) solubilized Nanoflex® PH stainless steel and observed the formation of an expanded martensite layer, which was richer in N in the outer part of the modified layer and richer in C near the substrate. The formation of a modified layer consisting of N-rich and C-rich expanded martensite, together with a small amount of expanded austenite, was also observed in nitrocarburized (400 °C, 24 h) 17-4 PH stainless steel specimens obtained through selective laser melting (SLM) [249]. The N and C profiles suggested that at the outermost surface, both N-rich and C-rich expanded martensite were present. As depth increased, the C content decreased and an expanded martensite richer in N formed. C-rich expanded martensite was prevalent in the inner part of the nitrocarburized layer. The formation of ε-(carbo)nitride together with expanded martensite was also detected [259]. An expanded martensite layer consisting mainly of expanded martensite without relevant amounts of nitrides and carbonitrides was obtained by Lee [259] on an AISI 630 (17-4) PH stainless steel using a combination of nitriding and nitrocarburizing treatments.

Low-temperature carburizing produces modified layers consisting of C-rich expanded phases. Heuer et al. [260] observed a fairly thick (~50 μm) etch-resistant layer in carburized (380 °C, 150 h) 13-8Mo PH stainless steel. The XRD analysis showed the presence of expanded austenite, which formed from retained austenite, and of a phase that was indicated as a para-equilibrium carbide with the same metal chemistry of the bulk. However, the peak position suggests that this "carbide" might be C-rich expanded martensite. The high C content at the surface (~19 at.%) suggests that C-rich expanded austenite tended to form in the outermost layer. When a large amount of expanded austenite was able to form, a modified layer with a two-layer microstructure was clearly observed in carburized (508 °C, 19 h) Corrax® PH stainless steel [22]. The outer layer consisted mainly of C-rich expanded austenite, while the inner layer was composed of C-rich expanded martensite. A similar microstructure was also observed on Nanoflex® PH stainless steel, even if it was not as clear as for Corrax®.

In semi-austenitic PH stainless steels, martensite, austenite, and residual δ-ferrite (formed during alloy solidification) are usually detected. When low-temperature treatments are performed, all of these phases can solubilize interstitial atoms well beyond the solubility limit, thus forming expanded phases [261–263].

In austenitic PH stainless steels, which have an austenite matrix after aging, expanded austenite forms. Esfandiari et al. [264] studied the effect of plasma nitriding (350–500 °C,

5–30 h) on the characteristics of solution-treated and aged A286 PH stainless steel. An expanded austenite layer similar to that formed in austenitic stainless steels was observed in samples nitrided at 350 °C for 10 h. When the treatment temperature was increased up to 420 °C, a similar modified layer formed, but when longer treatment durations or higher treatment temperatures were employed, nitrides were detected. A different approach was that of Fernandes et al. [265] and Christiansen et al. [266]. These authors took advantage of the strong nitride forming elements present in the A286 PH stainless steel, i.e., Al and Ti, and they performed the nitriding treatment after the solution treatment. These elements have a higher affinity for N than Cr, and therefore the formation of CrN was hindered. As a consequence, a nitriding temperature as high as 500 °C and treatment durations up to 60 h could be employed for forming an expanded austenite layer without CrN precipitates [265]. When a subsequent aging step was performed, a minor precipitation of CrN at grain boundaries occurred, while expanded austenite tended to transform into a precipitate-rich austenite with a low N content.

8.2. Corrosion Behavior in the Presence of Cl^-

The corrosion resistance of low-temperature-treated PH stainless steels depends on the microstructure of the modified surface layers. In Cl^--containing solutions, the formation of modified layers consisting of expanded martensite or expanded austenite alone improves corrosion resistance, similarly to what is observed for martensitic and austenitic stainless steels.

Expanded martensite layers, such as those produced by Lee [259] on AISI 630 martensitic PH stainless steel using a combination of nitriding and nitrocarburizing treatments, had an enhanced corrosion resistance in 3.5 wt.% solution. Higher corrosion potential and pitting potential values were detected compared to those of the untreated alloy (Figure 16a). It has to be noted that the corrosion resistance was also improved compared to that of nitrided specimens in which Cr nitrides formed. Similarly, when an expanded austenite layer formed, as in nitrided solution-treated and aged A286 austenitic PH stainless steels, higher corrosion resistance was observed (Figure 16b) [264].

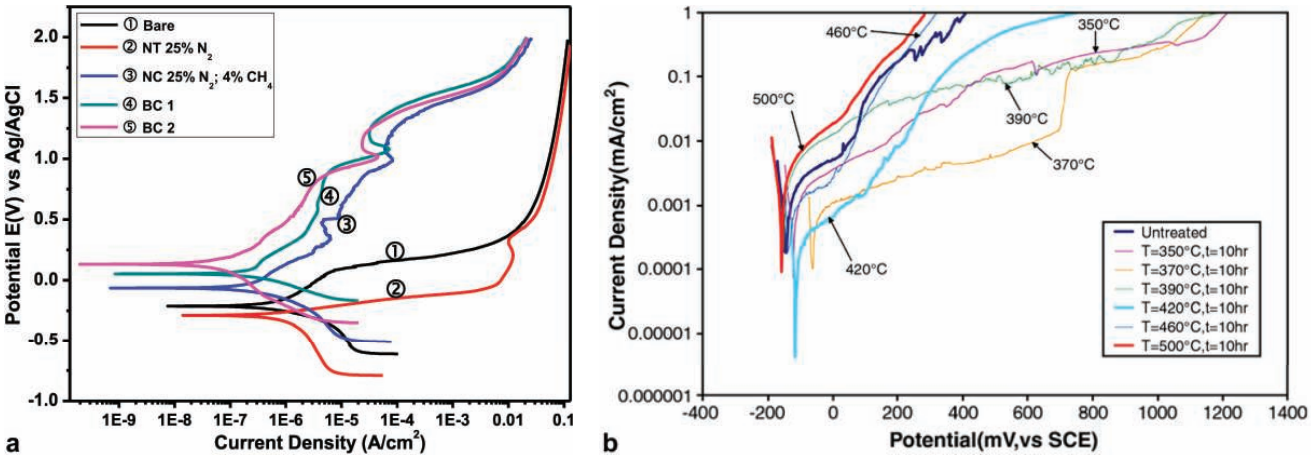

Figure 16. Potentiodynamic polarization curves of PH stainless steels: (**a**) AISI 630 martensitic PH stainless steel untreated (bare) and treated (400 °C, 15 h) with different treatments (NT, nitrided (phases: expanded martensite + Cr_2N); NC, nitrocarburized (phases: expanded martensite + ε carbonitride + Cr_2N); BC, combination of nitriding and nitrocarburizing treatments (phase: expanded martensite) (solution: 3.5 wt.% NaCl) (for further details, see [259]) (reprinted with permission from Ref. [259]. Copyright 2019 Elsevier); (**b**) A286 austenitic PH stainless steel untreated and nitrided (350–500 °C, 10 h) (solution: 3.5 wt.% NaCl) (phases present in the modified layer: 350–420°C: expanded austenite; 460–500 °C: expanded austenite + γ′ nitride + Cr nitrides) (for further details, see [264]) (reprinted with permission from Ref. [264]. Copyright 2007 Elsevier).

The formation of a C-rich layer, perhaps consisting of expanded austenite, in carburized (380 °C) 13-8Mo martensitic stainless steel improved the corrosion resistance in 0.6 NaCl solution [260].

The formation of a heterogeneous surface layer consisting of different expanded phases (expanded martensite and austenite) or expanded phases and nitrides may negatively affect the corrosion resistance. In fact, due to the different interstitial content of these expanded phases and the different nobility, micro-galvanic couples may form, and local corrosion phenomena may be enhanced.

When the modified surface layers consist of both expanded martensite and expanded austenite, different behaviors are reported. Bernardelli et al. [248] tested nitrided 15-5 martensitic PH stainless steel in 0.5 M NaCl solution. The authors observed a significant shift towards nobler values for the polarization curves of samples treated at 390 °C for 2 and 6 h, with modified layers consisting of expanded martensite and a fairly large amount of expanded austenite. This marked improvement was not registered by Brühl et al. [149] on nitrided (360 °C, 10 h) Corrax® martensitic PH stainless steel tested in 3.5 wt.% NaCl solution. The modified layer consisted of expanded martensite with a minor amount of expanded austenite. The nitrided samples had a corrosion potential comparable to that of untreated alloy, but they had a higher tendency to form metastable pits and more difficult repassivation than the untreated alloy. However, a salt spray fog test (5 wt.% NaCl, pH 6.8, 32 °C, 100 h) highlighted that after nitriding, corrosion resistance was preserved. On the contrary, a decrease in corrosion resistance, with lower corrosion potential and higher corrosion current density than those of the untreated alloy, was observed in plasma-nitrocarburized SLM 17-4 PH stainless steel [249]. Even in this case, the modified surface layers consisted of expanded martensite and a small amount of expanded austenite. The decrease in corrosion resistance in a 3.5 wt.% solution was detected in nitrocarburized specimens both in the as-printed state and after a solution treatment.

The influence of pre-treatments on the corrosion resistance of gaseous nitrided Nanoflex® PH stainless steel was tested by Kochmański et al. [258] in 3 wt.% NaCl solution and Ringer's solution using the potentiodynamic method. As described above, the modified surface layers consisted of a thin outermost layer of nanometric-size nitrides on a thicker layer consisting of expanded martensite and expanded austenite. The experimental results suggest that corrosion resistance was influenced mainly by the nitriding conditions. Regarding the tests in NaCl solution, a slight decrease in the corrosion potential value was observed for specimens nitrided at 425 °C with 50% NH_3 compared to that of the untreated steels. When the treatment temperature or NH_3 content were higher, the formation of nitride precipitates caused a further decrease in the corrosion potential. On the contrary, the corrosion potential of samples nitrided at 425 and 450 °C was comparable to that of the untreated steel when tested in Ringer's solution. However, a wider passive range and an increase in the pitting potential value were detected for the nitrided samples compared to those of the untreated steel, irrespective of the test solution. A loss of corrosion resistance was observed when nitriding was carried out at temperatures above 450 °C due to the formation of larger amounts of Fe- and Cr-based nitrides.

Mechanical treatments, which produce a nanocrystalline structure, may also influence the corrosion behavior of nitrided specimens. By using the scanning vibrating electrode technique (SVET) for assessing the corrosion behavior, Liu et al. [255] observed that 17-4 PH stainless steel with a surface nanocrystalline structure had greater corrosion resistance in 5 wt.% NaCl solution due to a more homogenous structure in which fairly large (~100 nm) precipitates, characteristic of solution-treated and aged specimens, were not present. When nitriding was carried out, in the solution-treated and aged samples, the formation of a large amount of nitride precipitates and the presence of many Cr-depleted zones promoted pitting corrosion. In the nanocrystalline samples, the alloy elements had a more uniform distribution, thus reducing the possibility of pitting corrosion. However, CrN tended to precipitate at grain boundaries where micro-defects were present, and therefore intergranular corrosion was promoted.

The formation of Fe-based nitride precipitates caused a decrease in corrosion resistance in nitrided martensitic PH stainless steels [259], as well as in austenitic PH stainless steels [264]. However, when a more or less continuous layer of (carbo)nitride was present, an improvement in the corrosion resistance was registered [259]. When Cr-based nitrides were also formed, a further decrease in the corrosion resistance was observed [259,264].

8.3. Corrosion Behavior in Cl-Free Solutions

Studies on the corrosion resistance of low-temperature-treated PH stainless steels are few. Copper sulfate spot ($CuSO_4 \cdot 5H_2O$) is used for assessing the effectiveness of passivation, and it was applied to nitrided Corrax® PH stainless steel [149]. The modified layer consisted of expanded martensite and a low amount of expanded austenite, and it maintained the corrosion behavior of the untreated alloy.

A significant decrease in corrosion resistance was observed in plasma-nitrocarburized SLM 17-4 PH stainless steel when tested in 4.9% H_2SO_4 solution, and this behavior was ascribed to the heterogeneous modified surface layer consisting of expanded martensite and expanded austenite [249].

9. Expanded Phases, Corrosion Environments, and Corrosion Tests

9.1. On Expanded Phases, Treatment Conditions, and Corrosion Environments

The overview of the international literature shows that the N- and C-rich expanded phases have improved corrosion resistance in many environments. This ability is due to the presence of interstitial atoms in the solid solution. N and C are present both in the passive layer, usually in the inner part, and in the bulk, and they efficiently act to maintain the passive film and restore it when corrosion phenomena occur. Different hypotheses have been proposed in order to explain the positive effect of N and C on the corrosion behavior, but open questions are still present, particularly regarding the mechanisms that allow C atoms to enhance corrosion resistance. Moreover, the combined effect of N and C, as present in nitrocarburized stainless steels, has not been clarified so far.

Ideally, an interstitial-rich and thick expanded phase layer can have improved corrosion resistance in both Cl^--containing solutions and Cl-free environments. However, the "real" thermochemical treatments (nitriding, carburizing, nitrocarburizing) are seldom able to produce monophasic modified surface layers, even if the formation of Cr compounds is avoided. In nitride and nitrocarburized ferritic and martensitic stainless steels, Fe-based nitrides and nitrocarbides are easily formed together with the expanded phases. In nitrided and nitrocarburized austenitic stainless steels, the huge N solubilization in the austenite matrix causes local plastic deformations, which induce the formation of a N-rich h.c.p. martensite, ε_N'. When carburizing treatments are carried out, the precipitation of Fe-based carbides may occur in all of the stainless steel grades. The formation of heterogeneous modified surface layers has different effects on the corrosion behavior of the treated stainless steels depending on the phases formed together with the expanded phases, their amount, and the corrosion environment.

For austenitic stainless steels, when the alloy is put into contact with a Cl^--containing solution, the formation of ε_N' usually does not impair the enhancement of corrosion resistance due to the presence of N-rich expanded austenite. It may be supposed that the passive film remains protective in spite of the heterogeneous surface, and, if the film is locally broken, the release of N atoms allows the alkalization of the solution within the pit, thus promoting repassivation. On the contrary, a decrease in corrosion resistance is observed when the steel is in the presence of H_2SO_4 solutions. It is not clear whether this effect is promoted by the formation of (sub)micrometric galvanic couples between the two phases or by the local plastic deformations at the surface. As a matter of fact, strict control of the microstructure is needed for components employed in H_2SO_4-containing solutions. If nitriding is chosen as the surface-hardening treatment, at least two strategies are possible. One is the choice of the steel composition, which tends to inhibit the formation of ε_N'. Steels with high stacking fault energy, such as Fe-19Cr-35Ni-1.2Si [166], fulfill

this requirement. As an example, the tendency to form ε_N' increases according to the sequence AISI 316L < AISI 304L < AISI 202 < Ni-free P558 [91,165]. A similar trend was observed concerning the formation of nitride precipitates [60,165]. Therefore, the nitriding temperature has to be decreased when Mn-rich austenitic stainless steels are treated to avoid the formation of large amounts of ε_N'/nitrides, and the N feeding has to be controlled. Another strategy is to limit the maximum N content to avoid the occurrence of large local plastic deformations. A reduced N content can be obtained by decreasing N feeding in the treatment. However, the maximum surface hardness is also limited.

When low-temperature carburizing is performed on austenitic stainless steels, the maximum C content is lower than that attained with N, and therefore minor local plastic deformations occur. As a matter of fact, a C-rich h.c.p. ε' martensite phase has not been reported so far, while Fe-based carbides have been often detected. The carbides may form micro-galvanic couples with the surrounding C-rich expanded austenite and influence the corrosion behavior. The removal of the outermost carbide-rich zone usually allows for attaining good corrosion resistance in both Cl^--containing solutions [74] and in H_2SO_4 solutions [104]. The corrosion behavior is influenced by the passive layer that forms when the carburizing treatment ends. In fact, carburizing may produce carbon soot on the surface, which hinders uniform passivation. Carbon soot or carbon contamination should be carefully removed in order to promote the formation of a uniform and protective passive layer.

The formation of ε_N' is also observed in low-temperature nitrided ferritic stainless steels due to a b.c.c.-to-h.c.p. martensitic transformation. Its presence, together with expanded ferrite, can cause a decrease in corrosion resistance in Cl^--containing solutions, probably because micro-galvanic couples form.

In stainless steel grades with a ferritic and martensitic microstructure, the formation of expanded phases is competitive with the formation of Fe-based nitrides or carbonitrides. Nitrides and carbonitrides are usually nobler than the expanded phases, and thus micro-galvanic couples can easily form in different environments. Modified layers containing expanded phases with negligible amounts of nitrides or carbonitrides preserve or even increase the corrosion resistance in solutions with/without Cl^-. This microstructure of the modified layers can be attained using fairly low treatment temperatures and by reducing the interstitial atom supply. On the contrary, the presence of large amounts of (carbo)nitride precipitates may significantly decrease the corrosion resistance. However, the formation of a continuous outer layer consisting of ε-nitride or ε-carbonitride has a beneficial effect, and high corrosion resistance is attained. A continuous nitride layer can be obtained by increasing the treatment temperature and the interstitial atom supply.

Therefore, treatment conditions have to be carefully chosen in order to obtain modified surface layers with the desired properties. As a matter of fact, the microstructure and phase composition of the modified surface layers depend not only on the treatment temperature and duration, which are usually taken into account, but also on N and/or C feeding and the steel composition. As an example, by changing the treatment pressure in plasma glow-discharge treatments, the electric parameters are changed, and so are the N and C feeding. The lower the pressure, the higher the amount of interstitial atoms that can diffuse in the steel [151,267]. However, in plasma treatments, pressures that are too low tend to promote sputtering [151,267]. In order to better control the characteristics of the modified surface layers, hybrid processes have been proposed [140,259,268], and they have the potential to become the treatments of choice for producing better-tailored modified surface layers. The use of combinations of different processes (nitriding and nitrocarburizing) has been successfully employed for obtaining an expanded martensite layer with a negligible amount of (carbo)nitride precipitates in AISI 630 martensitic PH stainless steel [259]. Sequential treatments combining nitriding, carburizing, or nitrocarburizing steps have been proposed for AISI 420 martensitic stainless steel [140], and they proved to produce thicker and/or harder surface layers depending on the treatment type and the sequence. An active screen

process using a solid carbon screen has given promising results for the nitrocarburizing of AISI 316L stainless steel [268].

The steel composition also plays an important role. As an example, in austenitic stainless steels, Mn promotes the formation of ε_N' and nitrides. Al and Ti additions have been proposed for hindering CrN formation [266]. The possibility of tailoring the steel composition in order to hinder the formation of the phases that may be detrimental to the corrosion resistance (CrN, ε_N', (carbo)nitrides) is an additional way to improve the properties of low-temperature-treated stainless steels further on.

9.2. On Corrosion Tests

The analysis of the international literature shows that conflicting results are reported by different authors. These inconsistencies may be due to the use of different steels or different treatment conditions, including not only temperature and time but also N and/or C feeding, as recalled above. Another factor that can contribute to obtaining different results is the corrosion test methodology.

First of all, the conditions of the passive film can influence the measurement. Passive films can be naturally grown in the air, mechanically removed and then grown in the test solution, or partially/totally removed through electrochemical methods and then grown in the test solution, and all of these films are expected to give different results. A passive film naturally grown in the air may be similar to that of service components, while a film grown in the test solution may give an indication of the corrosion behavior when the whole film is partially/totally removed and reforms in the service environment. The presence of carbon contamination or a carbon soot, such as that easily formed through carburizing treatments, may also influence the characteristics of the passive film and hence the corrosion behavior.

Secondly, the delay before the measurement can have an important influence on the experimental results. Usually, a 1-h delay is used in order to obtain equilibrium conditions. However, the analysis of OCP values vs. time shows that for low-temperature-treated stainless steels, the equilibrium conditions may be attained over fairly long times (several hours) [47]. This fact should be taken into account when choosing the delay time.

Another test parameter that can cause different results when potentiodynamic polarization plots are compared is the scan rate. According to the ASTM G5-14 [269] norm, a scan rate of 0.6 V/h (0.166 mV/s) should be used. However, scan rates of 1 mV/s are used by many authors. It was observed that the scan rate influences the measurements of corrosion potential and corrosion current density [270], as well as the pitting potential [271].

Cyclic potentiodynamic polarization measurements are employed for assessing the ability of treated stainless steels to repassivate. Good and poor abilities have been found, even for alloys with similar surface treatments. These conflicting results can be ascribed to the different extents of the damage produced on the samples through this technique. Strict control of the extent of the damage is very difficult, and wide and/or deep damage may be impossible to repassivate. A useful alternative for measuring repassivation or the protection potential is the galvanostatic technique [272]. With this technique, better control of the extent of the damage is possible, and it has been shown that nitrided austenitic stainless steels samples are able to repassivate when the extent of the pit or the crevice is not too great [91].

10. Conclusions

Low-temperature thermochemical treatments are becoming treatments of choice for enhancing surface hardness and wear and fatigue resistance without impairing the corrosion resistance of stainless steels. The analysis of the international literature allows the following main conclusions to be drawn.

- The high content of N and C atoms in the expanded phases has a beneficial effect by modifying both the passive layer and the bulk. As a consequence, the expanded phases have very good corrosion resistance in many environments.

- The microstructure and phase composition of the modified surface layers formed on stainless steels depend on the treatment process technique, the conditions (treatment temperature, time, N and/or C feeding), and the alloy composition.
- The highest protection effect of expanded phases is obtained when they form interstitial-rich, precipitate-free, and thick modified layers.
- The formation of other phases together with the expanded phases, such as N-rich expanded h.c.p. ε'-martensite, $\varepsilon_N{}'$, and Fe-based compounds, has different effects on the corrosion resistance of the different stainless steel grades.
- For austenitic stainless steels, N-rich expanded austenite has very good corrosion resistance in many environments. The concomitant formation of $\varepsilon_N{}'$ does not impair the excellent corrosion resistance of expanded austenite in Cl^--containing solutions, but it worsens the corrosion resistance in H_2SO_4 or sulfite solutions. C-rich expanded austenite maintains very good corrosion resistance in both of the environments. Therefore, for applications in H_2SO_4 solutions, the possible choices may be either nitrided austenitic stainless steels with a reduced N content or carburized austenitic stainless steels.
- For stainless steel grades with a ferritic or a martensitic microstructure, higher corrosion resistance was observed when the expanded phases formed without or with a negligible amount of Fe-based compounds or when ε-(carbo)nitride formed a continuous outer layer, which has great protectiveness. Multiphase heterogeneous modified surface layers usually have lower corrosion resistance.

From a scientific point of view, many questions are still open, and they can stimulate future research activity. The mechanisms that allow N and C to improve the corrosion resistance of expanded phases in different environments and the eventual limit of the interstitial atom content for such improvement are not fully elucidated, nor is the influence of the treatment process techniques and conditions or the alloy composition on the characteristics of the modified surface layers. These are all important topics that need to be clarified for optimizing low-temperature thermochemical processes and producing on stainless steels modified surface layers with characteristics tailored for the specific service environment.

From a technological point of view, a more extensive use of low-temperature thermochemical treatments on stainless steel components can benefit from the studies on hybrid or combined treatments and the development of stainless steels with an alloy composition able to promote the formation of the expanded phases.

Funding: This research received no external funding.

Conflicts of Interest: The author declares no conflicts of interest.

References

1. Washko, S.D.; Aggen, G. Wrought Stainless Steels. In *ASM Handbook*; ASM International: Materials Park, OH, USA, 1997; Volume 1, pp. 841–907.
2. Grubb, J.F.; DeBold, T.; Fritz, J.D. Corrosion of Wrought Stainless Steels. In *ASM Handbook*; Cramer, S.D., Covino, B.S., Jr., Eds.; ASM International: Materials Park, OH, USA, 2005; Volume 13B, pp. 54–77. [CrossRef]
3. Lai, J.K.L.; Shek, C.H.; Lo, K.H. *Stainless Steels: An Introduction and Their Recent Developments*; Bentham Science Publishers Ltd.: Beijing, China, 2012; ISBN 978-1-60805-305-6. [CrossRef]
4. McGuire, M.F. *Stainless Steels for Design Engineers*; ASM International: Materials Park, OH, USA, 2008; ISBN 978-0-87170-717-8.
5. Wang, Z.; Seyeux, A.; Zanna, S.; Maurice, V.; Marcus, P. Chloride-induced alterations of the passive film on 316L stainless steel and blocking effect of pre-passivation. *Electrochim. Acta* **2020**, *329*, 135159. [CrossRef]
6. Frankel, G.S. Pitting Corrosion. In *ASM Handbook*; ASM International: Materials Park, OH, USA, 2003; Volume 13A, pp. 236–241.
7. Sun, J.; Tang, H.; Wang, C.; Han, Z.; Li, S. Effects of Alloying Elements and Microstructure on Stainless Steel Corrosion: A Review. *Steel Res. Int.* **2022**, *93*, 2100450. [CrossRef]
8. Aslam, R.; Mobin, M.; Zehra, S.; Aslam, J. A comprehensive review of corrosion inhibitors employed to mitigate stainless steel corrosion in different environments. *J. Mol. Liq.* **2022**, *364*, 119992. [CrossRef]
9. Schneider, M.J.; Chatterjee, M.S. Introduction to Surface Hardening of Steels. In *ASM Handbook*; Dosset, J.L., Totten, G.E., Eds.; ASM International: Materials Park, OH, USA, 2013; Volume 4A, pp. 389–397. [CrossRef]
10. Ramezani, M.; Mohd Ripin, Z.; Pasang, T.; Jiang, C.-P. Surface Engineering of Metals: Techniques, Characterizations and Applications. *Metals* **2023**, *13*, 1299. [CrossRef]

11. Davis, J.R. Surface Engineering of Stainless Steels. In *ASM Metal Handbook*; ASM International: Materials Park, OH, USA, 1994; Volume 5, pp. 741–761. [CrossRef]
12. Dong, H. S-phase surface engineering of Fe-Cr, Co-Cr and Ni-Cr alloys. *Int. Mater. Rev.* **2010**, *55*, 65–98. [CrossRef]
13. Cardoso, R.P.; Mafra, M.; Brunatto, S.F. Low-temperature Thermochemical Treatments of Stainless Steels—An Introduction. In *Plasma Science and Technology—Progress in Physical States and Chemical Reactions*; Mieso, T., Ed.; InTech: Rijeka, Croatia, 2016; pp. 107–130, ISBN 978-953-51-2280-7. [CrossRef]
14. Casteletti, L.C.; Neto, A.L.; Totten, G.E. Nitriding of Stainless Steels. *Metallogr. Microstruct. Anal.* **2014**, *3*, 477–508. [CrossRef]
15. Collins, S.R.; Williams, P.C.; Marx, S.V.; Heuer, A.; Ernst, F.; Kahn, H. Low-Temperature Carburization of Austenitic Stainless Steels. In *ASM Handbook*; Dosset, J., Totten, G.E., Eds.; ASM International: Materials Park, OH, USA, 2014; Volume 4D, pp. 451–460.
16. Borgioli, F. The "Expanded" Phases in the Low-Temperature Treated Stainless Steels: A Review. *Metals* **2022**, *12*, 331. [CrossRef]
17. Michal, G.M.; Gu, X.; Jennings, W.D.; Kahn, H.; Ernst, F.; Heuer, A.H. Paraequilibrium Carburization of Duplex and Ferritic Stainless Steels. *Metall. Mater. Trans. A* **2009**, *40*, 1781–1790. [CrossRef]
18. Borgioli, F. From Austenitic Stainless Steel to Expanded Austenite-S Phase: Formation, Characteristics and Properties of an Elusive Metastable Phase. *Metals* **2020**, *10*, 187. [CrossRef]
19. Wriedt, H.A.; Gokcen, N.A.; Nafziger, R.H. The Fe-N (Iron-Nitrogen) system. *Bull. Alloy Phase Diagr.* **1987**, *8*, 355–377. [CrossRef]
20. Okamoto, H. The C-Fe (carbon-iron) system. *J. Phase Equilibria* **1992**, *13*, 543–565. [CrossRef]
21. Manova, D.; Thorwarth, G.; Mändl, S.; Neumann, H.; Stritzker, B.; Rauschenbach, B. Variable lattice expansion in martensitic stainless steel after nitrogen ion implantation. *Nucl. Instrum. Methods Phys. Res. Sect. B Beam Interact. Mater. Atoms* **2006**, *242*, 285–288. [CrossRef]
22. Frandsen, R.B.; Christiansen, T.; Somers, M.A.J. Simultaneous surface engineering and bulk hardening of precipitation hardening stainless steel. *Surf. Coat. Technol.* **2006**, *200*, 5160–5169. [CrossRef]
23. Baniasadi, F.; Bahmannezhad, B.; Nikpoor, N.; Asgari, S. Thermal stability investigation of expanded martensite. *Surf. Coat. Technol.* **2016**, *300*, 87–94. [CrossRef]
24. Christiansen, T.; Somers, M.A.J. Controlled dissolution of colossal quantities of nitrogen in stainless steel. *Metall. Mater. Trans. A* **2006**, *37*, 675–682. [CrossRef]
25. Christiansen, T.L.; Ståhl, K.; Brink, B.K.; Somers, M.A.J. On the Carbon Solubility in Expanded Austenite and Formation of Hägg Carbide in AISI 316 Stainless Steel. *Steel Res. Int.* **2016**, *87*, 1395–1405. [CrossRef]
26. Herath, I.; Davies, J.; Will, G.; Tran, P.A.; Velic, A.; Sarvghad, M.; Islam, M.; Paritala, P.K.; Jaggessar, A.; Schuetz, M.; et al. Anodization of medical grade stainless steel for improved corrosion resistance and nanostructure formation targeting biomedical applications. *Electrochim. Acta* **2022**, *416*, 140274. [CrossRef]
27. Dib, J.; Strubbia, R.; Abdelnabe, J.P.; Prieto, G.; Gómez, B.; Méndez, C.; Ares, A.; Hereñú, S. Improved tribological behaviour of super duplex stainless steel through plasma nitriding at ultra-low temperature without prior polishing. *Surf. Coat. Technol.* **2024**, *483*, 130806. [CrossRef]
28. Gumuslu, T.; Kaba, M.; Atar, E.; Cimenoglu, H. Effect of low-temperature nitriding on impact-sliding wear behavior of an austenitic stainless steel at room and sub-zero temperatures. *Tribol. Int.* **2023**, *185*, 108560. [CrossRef]
29. Dalibón, E.L.; Dalke, A.; Biermann, H.; Brühl, S.P. Short time nitriding and nitrocarburizing of martensitic stainless steel. *Surf. Coat. Technol.* **2024**, *485*, 130931. [CrossRef]
30. Manfrinato, M.D.; Rossino, L.S.; Kliauga, A.M.; Escobar-Hernández, J.E.; Melo-Máximo, L.; Rodríguez-Castro, G.A.; Morón, R.C. Effect of Treatment Temperature on the Cyclic Spherical Contact Behavior of Plasma Nitrided and Nitrocarburized AISI 321 Steel. *Mater. Res.* **2024**, *27*, e20240021. [CrossRef]
31. Sun, Y.; Bailey, R. Comparison of Wear Performance of Low Temperature Nitrided and Carburized 316L Stainless Steel under Dry Sliding and Corrosive-Wear Conditions. *J. Mater. Eng. Perform.* **2023**, *32*, 1238–1247. [CrossRef]
32. Mainardi, V.A.; Cardoso, R.P.; Brunatto, S.F.; Scheuer, C.J. Tribocorrosion behavior of low-temperature plasma-carburized AISI 420 martensitic stainless steel: Investigating the synergy between corrosion and erosion in slurry and liquid impingement environments. *Surf. Coat. Technol.* **2024**, *477*, 130373. [CrossRef]
33. Wang, K.S.; Che, H.L.; Lei, M.K. Corrosion-fatigue properties of plasma-based low-energy nitrogen ion implanted AISI 304L austenitic stainless steel in borate buffer solution. *Surf. Coat. Technol.* **2016**, *288*, 30–35. [CrossRef]
34. Zhang, X.; Wang, J.; Fan, H.; Yan, J.; Duan, L.; Gu, T.; Xian, G.; Sun, L.; Wang, D. Stress Corrosion Behavior of Low-temperature Liquid-Nitrided 316 Austenitic Stainless Steel in a Sour Environment. *Metall. Mater. Trans. A* **2018**, *49*, 356–367. [CrossRef]
35. Wang, S.; Ma, C.; Walsh, F.C. Alternative tribological coatings to electrodeposited hard chromium: A critical review. *Trans. IMF* **2020**, *98*, 173–185. [CrossRef]
36. Li, W.; Chen, H.; Li, C.; Huang, W.; Chen, J.; Zuo, L.; Ren, Y.; He, J.; Zhang, S. Microstructure and tensile properties of AISI 321 stainless steel with aluminizing and annealing treatment. *Mater. Des.* **2021**, *205*, 109729. [CrossRef]
37. Günen, A.; Gürol, U.; Koçak, M.; Çam, G. A new approach to improve some properties of wire arc additively manufactured stainless steel components: Simultaneous homogenization and boriding. *Surf. Coat. Technol.* **2023**, *460*, 129395. [CrossRef]
38. Somers, M.A.J.; Christiansen, T.L. Gaseous processes for low temperature surface hardening of stainless steel. In *Thermochemical Surface Engineering of Steels*; Mittemeijer, E.J., Somers, M.A.J., Eds.; Woodhead Publishing: Oxford, UK, 2015; pp. 581–614, ISBN 978-0-85709-592-3. [CrossRef]

39. Dan, N.E.; Hussain, P.B.; Shaik, N.B.; Bakthavatchalam, B.; Mohapatra, R.K.; Behera, A. Improved Surface Morphology and Corrosion Resistance Performance of 2205 Duplex Stainless Steel by Low Temperature Gas Nitriding. *J. Bio- Tribo-Corros.* **2022**, *8*, 100. [CrossRef]
40. Lebrun, J.P. Plasma-assisted processes for surface hardening of stainless steel. In *Thermochemical Surface Engineering of Steels*; Mittemeijer, E.J., Somers, M.A.J., Eds.; Woodhead Publishing: Oxford, UK, 2015; pp. 615–632, ISBN 978-0-85709-592-3. [CrossRef]
41. Schibicheski Kurelo, B.C.E.; De Souza, G.B.; Da Silva, S.L.; Lepienski, C.M.; Alves Júnior, C.; Chuproski, R.F.; Pintaúde, G. Tribo-Mechanical Behavior of Films and Modified Layers Produced by Cathodic Cage and Glow Discharge Plasma Nitriding Techniques. *Metals* **2023**, *13*, 430. [CrossRef]
42. Markanday, H.; Roy, S.C.; Somers, M.A.J. On the effect of salt bath nitrocarburizing on the cavitation erosion behavior of AISI 304L stainless steel. *Eng. Fail. Anal.* **2024**, *165*, 108752. [CrossRef]
43. Tandon, V.; Patil, A.P.; Rathod, R.C. Influence of Time on Low Temperature Salt Bath Nitriding and its Corrosion Behavior of 316L ASS in PEMFC Environment. *Prot. Met. Phys. Chem. Surf.* **2020**, *56*, 772–779. [CrossRef]
44. Illing, C.; Ren, Z.; Agaponova, A.; Heuer, A.; Ernst, F. Rapid Alloy Surface Engineering through Closed-Vessel Reagent Pyrolysis. *Metals* **2021**, *11*, 1764. [CrossRef]
45. Somers, M.A.J.; Christiansen, T.L. Low temperature surface hardening of stainless steel. In *Thermochemical Surface Engineering of Steels*; Mittemeijer, E.J., Somers, M.A.J., Eds.; Woodhead Publishing: Oxford, UK, 2015; pp. 557–579, ISBN 978-0-85709-592-3. [CrossRef]
46. Spies, H.-J. Corrosion behaviour of nitrided, nitrocarburised and carburised steels. In *Thermochemical Surface Engineering of Steels*; Mittemeijer, E.J., Somers, M.A.J., Eds.; Woodhead Publishing: Oxford, UK, 2015; pp. 267–309, ISBN 978-0-85709-592-3. [CrossRef]
47. Borgioli, F. The Corrosion Behavior in Different Environments of Austenitic Stainless Steels Subjected to Thermochemical Surface Treatments at Low Temperatures: An Overview. *Metals* **2023**, *13*, 776. [CrossRef]
48. Olsson, C.O.A.; Landolt, D. Passive films on stainless steels—Chemistry, structure and growth. *Electrochim. Acta* **2003**, *48*, 1093–1104. [CrossRef]
49. Maurice, V.; Marcus, P. Progress in corrosion science at atomic and nanometric scales. *Prog. Mater. Sci.* **2018**, *95*, 132–171. [CrossRef]
50. Schmuki, P. From Bacon to barriers: A review on the passivity of metals and alloys. *J. Solid State Electrochem.* **2002**, *6*, 145–164. [CrossRef]
51. Asami, K.; Hashimoto, K. Importance of initial surface film in the degradation of stainless steels by atmospheric exposure. *Corros. Sci.* **2003**, *45*, 2263–2283. [CrossRef]
52. Habibzadeh, S.; Li, L.; Shum-Tim, D.; Davis, E.C.; Omanovic, S. Electrochemical polishing as a 316L stainless steel surface treatment method: Towards the improvement of biocompatibility. *Corros. Sci.* **2014**, *87*, 89–100. [CrossRef]
53. Cheon, H.; Kim, K.-S.; Kim, S.; Heo, S.-B.; Lim, J.-H.; Kim, J.-H.; Yoon, S.-Y. Effect of Deformation Structure of AISI 316L in Low-Temperature Vacuum Carburizing. *Metals* **2021**, *11*, 1762. [CrossRef]
54. Ma, L.; Pascalidou, E.-M.; Wiame, F.; Zanna, S.; Maurice, V.; Marcus, P. Passivation mechanisms and pre-oxidation effects on model surfaces of FeCrNi austenitic stainless steel. *Corros. Sci.* **2020**, *167*, 108483. [CrossRef]
55. Jiang, R.; Wang, Y.; Wen, X.; Chen, C.; Zhao, J. Effect of time on the characteristics of passive film formed on stainless steel. *Appl. Surf. Sci.* **2017**, *412*, 214–222. [CrossRef]
56. Örnek, C.; Leygraf, C.; Pan, J. Passive film characterisation of duplex stainless steel using scanning Kelvin probe force microscopy in combination with electrochemical measurements. *NPJ Mater. Degrad.* **2019**, *3*, 8. [CrossRef]
57. Revilla, R.I.; Wouters, B.; Andreatta, F.; Lanzutti, A.; Fedrizzi, L.; De Graeve, I. EIS comparative study and critical Equivalent Electrical Circuit (EEC) analysis of the native oxide layer of additive manufactured and wrought 316L stainless steel. *Corros. Sci.* **2020**, *167*, 108480. [CrossRef]
58. Perumal, G.; Grewal, H.S.; Arora, H.S. Enhanced durability, bio-activity and corrosion resistance of stainless steel through severe surface deformation. *Colloids Surf. B Biointerfaces* **2020**, *194*, 111197. [CrossRef] [PubMed]
59. Gudić, S.; Nagode, A.; Šimić, K.; Vrsalović, L.; Jozić, S. Corrosion Behavior of Different Types of Stainless Steel in PBS Solution. *Sustainability* **2022**, *14*, 8935. [CrossRef]
60. Borgioli, F.; Galvanetto, E.; Bacci, T. Surface Modification of a Nickel-Free Austenitic Stainless Steel by Low-Temperature Nitriding. *Metals* **2021**, *11*, 1845. [CrossRef]
61. Maurice, V.; Marcus, P. Current developments of nanoscale insight into corrosion protection by passive oxide films. *Curr. Opin. Solid State Mater. Sci.* **2018**, *22*, 156–167. [CrossRef]
62. Hakiki, N.B.; Boudin, S.; Rondot, B.; Da Cunha Belo, M. The electronic structure of passive films formed on stainless steels. *Corros. Sci.* **1995**, *37*, 1809–1822. [CrossRef]
63. Fredriksson, W.; Malmgren, S.; Gustafsson, T.; Gorgoi, M.; Edström, K. Full depth profile of passive films on 316L stainless steel based on high resolution HAXPES in combination with ARXPS. *Appl. Surf. Sci.* **2012**, *258*, 5790–5797. [CrossRef]
64. Vignal, V.; Ringeval, S.; Thiébaut, S.; Tabalaiev, K.; Dessolin, C.; Heintz, O.; Herbst, F.; Chassagnon, R. Influence of the microstructure on the corrosion behaviour of low-carbon martensitic stainless steel after tempering treatment. *Corros. Sci.* **2014**, *85*, 42–51. [CrossRef]
65. Wang, Z.; Zhang, L.; Zhang, Z.; Lu, M. Combined effect of pH and H_2S on the structure of passive film formed on type 316L stainless steel. *Appl. Surf. Sci.* **2018**, *458*, 686–699. [CrossRef]

66. Jargelius-Pettersson, R.F.A. Electrochemical investigation of the influence of nitrogen alloying on pitting corrosion of austenitic stainless steels. *Corros. Sci.* **1999**, *41*, 1639–1664. [CrossRef]
67. Ningshen, S.; Mudali, U.K.; Mittal, V.K.; Khatak, H.S. Semiconducting and passive film properties of nitrogen-containing type 316LN stainless steels. *Corros. Sci.* **2007**, *49*, 481–496. [CrossRef]
68. Lei, M.K.; Zhu, X.M. Role of Nitrogen in Pitting Corrosion Resistance of a High-Nitrogen Face-Centered-Cubic Phase Formed on Austenitic Stainless Steel. *J. Electrochem. Soc.* **2005**, *152*, B291–B295. [CrossRef]
69. Tong, S.; Che, H.L.; Lei, M.K. High-resolution TEM characterization of epitaxial passivation for a high nitrogen face-centered-cubic phase formed on AISI 304L austenitic stainless steel in borate buffer solution. *Electrochim. Acta* **2021**, *393*, 139075. [CrossRef]
70. Zhu, X.M.; Guo, Y.; Xing, Z.Q.; Lei, M.K. Effect of Nitrogen on Semiconducting Properties of Passive Films of a High Nitrogen Face-Centered-Cubic Phase Formed on Austenitic Stainless Steel. *J. Electrochem. Soc.* **2012**, *159*, C319–C325. [CrossRef]
71. Heuer, A.H.; Kahn, H.; Ernst, F.; Michal, G.M.; Hovis, D.B.; Rayne, R.J.; Martin, F.J.; Natishan, P.M. Enhanced corrosion resistance of interstitially hardened stainless steel: Implications of a critical passive layer thickness for breakdown. *Acta Mater.* **2012**, *60*, 716–725. [CrossRef]
72. Ha, H.-Y.; Lee, T.-H.; Oh, C.-S.; Kim, S.-J. Effects of Carbon on the Corrosion Behaviour in Fe-18Cr-10Mn-N-C Stainless Steels. *Steel Res. Int.* **2009**, *80*, 488–492. [CrossRef]
73. Niu, W.; Lillard, R.S.; Li, Z.; Ernst, F. Properties of the Passive Film Formed on Interstitially Hardened AISI 316L Stainless Steel. *Electrochim. Acta* **2015**, *176*, 410–419. [CrossRef]
74. Sun, Y. Corrosion behaviour of low temperature plasma carburised 316L stainless steel in chloride containing solutions. *Corros. Sci.* **2010**, *52*, 2661–2670. [CrossRef]
75. Kadowaki, M.; Saengdeejing, A.; Muto, I.; Chen, Y.; Frankel, G.S.; Doi, T.; Kawano, K.; Sugawara, Y.; Hara, N. Roles of Interstitial Nitrogen, Carbon, and Boron in Steel Corrosion: Generation of Oxyanions and Stabilization of Electronic Structure. *J. Electrochem. Soc.* **2020**, *167*, 81503. [CrossRef]
76. Malki, B.; Guillotte, I.; Baroux, B. Deriving Metastable Pourbaix Diagrams of Stainless Steels Using Density Functional Theory Calculations. *J. Electrochem. Soc.* **2023**, *170*, 91501. [CrossRef]
77. Hänninen, H.; Romu, J.; Ilola, R.; Tervo, J.; Laitinen, A. Effects of processing and manufacturing of high nitrogen-containing stainless steels on their mechanical, corrosion and wear properties. *J. Mater. Process. Technol.* **2001**, *117*, 424–430. [CrossRef]
78. Lo, K.H.; Shek, C.H.; Lai, J.K.L. Recent developments in stainless steels. *Mater. Sci. Eng. R Rep.* **2009**, *65*, 39–104. [CrossRef]
79. Sumita, M.; Hanawa, T.; Teoh, S.H. Development of nitrogen-containing nickel-free austenitic stainless steels for metallic biomaterials—Review. *Mater. Sci. Eng. C* **2004**, *24*, 753–760. [CrossRef]
80. Baba, H.; Kodama, T.; Katada, Y. Role of nitrogen on the corrosion behavior of austenitic stainless steels. *Corros. Sci.* **2002**, *44*, 2393–2407. [CrossRef]
81. Flis-Kabulska, I.; Sun, Y.; Flis, J. Monitoring the near-surface pH to probe the role of nitrogen in corrosion behaviour of low-temperature plasma nitrided 316L stainless steel. *Electrochim. Acta* **2013**, *104*, 208–215. [CrossRef]
82. Tong, S.; Che, H.L.; Wang, K.S.; Lei, M.K. Passivation kinetics of a high nitrogen face-centered-cubic phase formed on AISI 304L austenitic stainless steel in borate buffer solutions by photo- and electrochemical methods. *Electrochim. Acta* **2021**, *394*, 139110. [CrossRef]
83. Baba, H.; Katada, Y. Effect of Nitrogen on Crevice Corrosion and Repassivation Behavior of Austenitic Stainless Steel. *Mater. Trans.* **2008**, *49*, 579–586. [CrossRef]
84. Lin, Y.H.; Lan, W.C.; Ou, K.L.; Liu, C.M.; Peng, P.W. Hemocompatibility evaluation of plasma-nitrided austenitic stainless steels at low temperature. *Surf. Coat. Technol.* **2012**, *206*, 4785–4790. [CrossRef]
85. Zhidkov, I.S.; Kukharenko, A.I.; Makarov, A.V.; Savrai, R.A.; Gavrilov, N.V.; Cholakh, S.O.; Kurmaev, E.Z. XPS characterization of surface layers of stainless steel nitrided in electron beam plasma at low temperature. *Surf. Coat. Technol.* **2020**, *386*, 125492. [CrossRef]
86. Oddershede, J.; Christiansen, T.L.; Ståhl, K.; Somers, M.A.J. Extended X-ray absorption fine structure investigation of nitrogen stabilized expanded austenite. *Scr. Mater.* **2010**, *62*, 290–293. [CrossRef]
87. Tong, K.; Ye, F.; Wang, Y.K. Short-range ordered structure and phase stability of supersaturated nitrided layer on austenitic stainless steel. *Acta Mater.* **2019**, *175*, 314–323. [CrossRef]
88. Wang, K.S.; Tong, S.; Lei, M.K. Corrosion and Passivation of High Nitrogen Face-Centered-Cubic Phase Formed on AISI 304L Austenitic Stainless Steel in Borate Buffer Solution. *J. Electrochem. Soc.* **2015**, *162*, C601–C609. [CrossRef]
89. Paredes, E.C.; Bautista, A.; Alvarez, S.M.; Velasco, F. Influence of the forming process of corrugated stainless steels on their corrosion behaviour in simulated pore solutions. *Corros. Sci.* **2012**, *58*, 52–61. [CrossRef]
90. Yao, J.; Macdonald, D.D.; Dong, C. Passive film on 2205 duplex stainless steel studied by photo-electrochemistry and ARXPS methods. *Corros. Sci.* **2019**, *146*, 221–232. [CrossRef]
91. Borgioli, F.; Galvanetto, E.; Bacci, T. Corrosion behaviour of low temperature nitrided nickel-free, AISI 200 and AISI 300 series austenitic stainless steels in NaCl solution. *Corros. Sci.* **2018**, *136*, 352–365. [CrossRef]
92. Zhu, X.M.; Lei, M.K. Pitting corrosion resistance of high nitrogen f.c.c. phase in plasma source ion nitrided austenitic stainless steel. *Surf. Coat. Technol.* **2000**, *131*, 400–403. [CrossRef]
93. Metikoš-Huković, M.; Babić, R.; Grubač, Z.; Petrović, Ž.; Lajçi, N. High corrosion resistance of austenitic stainless steel alloyed with nitrogen in an acid solution. *Corros. Sci.* **2011**, *53*, 2176–2183. [CrossRef]

94. Sun, S.; Wei, S.; Wang, G.; Jiang, Z.; Lian, J.; Ji, C. The Synthesis and Electrochemical Behavior of High-Nitrogen Nickel-Free Austenitic Stainless Steel. *J. Mater. Eng. Perform.* **2014**, *23*, 3957–3962. [CrossRef]
95. Wu, X.Q.; Xu, S.; Huang, J.B.; Han, E.H.; Ke, W.; Yang, K.; Jiang, Z.H. Uniform corrosion and intergranular corrosion behavior of nickel-free and manganese alloyed high nitrogen stainless steels. *Mater. Corros.* **2008**, *59*, 676–684. [CrossRef]
96. Lei, M.K.; Zhu, X.M. Plasma-based low-energy ion implantation of austenitic stainless steel for improvement in wear and corrosion resistance. *Surf. Coat. Technol.* **2005**, *193*, 22–28. [CrossRef]
97. Lei, M.K.; Zhang, Z.L.; Zhu, X.M. Effects of nitrogen-induced hcp martensite formation on corrosion resistance of plasma source ion nitrided austenitic stainless steel. *J. Mater. Sci. Lett.* **1999**, *18*, 1537–1538. [CrossRef]
98. Flis, J.; Kuczynska, M. Effect of Low-Temperature Plasma Nitriding on Corrosion of 304L Stainless Steel in Sulfate and Chloride Solutions. *J. Electrochem. Soc.* **2004**, *151*, B573–B580. [CrossRef]
99. Flis, J.; Gajek, A. Impedance parameters of nitrided 304L stainless steel in an acidified sulphate solution. *J. Electroanal. Chem.* **2001**, *515*, 82–90. [CrossRef]
100. Liu, H.Y.; Che, H.L.; Gao, J.Y.; Li, G.B.; Lei, M.K. Low-pressure hollow cathode plasma source carburizing of AISI 304L austenitic stainless steel at low temperature. *Surf. Coat. Technol.* **2022**, *442*, 128548. [CrossRef]
101. Martin, F.J.; Lemieux, E.J.; Newbauer, T.M.; Bayles, R.A.; Natishan, P.M.; Kahn, H.; Michal, G.M.; Ernst, F.; Heuer, A.H. Carburization-induced passivity of 316 L austenitic stainless steel. *Electrochem. Solid-State Lett.* **2007**, *10*, C76–C78. [CrossRef]
102. Martin, F.J.; Natishan, P.M.; Lemieux, E.J.; Newbauer, T.M.; Rayne, R.J.; Bayles, R.A.; Kahn, H.; Michal, G.M.; Ernst, F.; Heuer, A.H. Enhanced Corrosion Resistance of Stainless Steel Carburized at Low Temperature. *Metall. Mater. Trans. A* **2009**, *40*, 1805–1810. [CrossRef]
103. Li, T.; Chien, S.-C.; Ren, Z.; Windl, W.; Ernst, F.; Frankel, G.S. Understanding the efficacy of concentrated interstitial carbon in enhancing the pitting corrosion resistance of stainless steel. *Acta Mater.* **2021**, *221*, 117433. [CrossRef]
104. Sun, Y. Depth-profiling electrochemical measurements of low temperature plasma carburised 316L stainless steel in 1M H_2SO_4 solution. *Surf. Coat. Technol.* **2010**, *204*, 2789–2796. [CrossRef]
105. Schibicheski Kurelo, B.C.E.; de Souza, G.B.; Serbena, F.C.; Lepienski, C.M.; Borges, P.C. Mechanical properties and corrosion resistance of α_N-rich layers produced by PIII on a super ferritic stainless steel. *Surf. Coat. Technol.* **2020**, *403*, 126388. [CrossRef]
106. Luiz, L.A.; Kurelo, B.C.E.S.; de Souza, G.B.; de Andrade, J.; Marino, C.E.B. Effect of nitrogen plasma immersion ion implantation on the corrosion protection mechanisms of different stainless steels. *Mater. Today Commun.* **2021**, *28*, 102655. [CrossRef]
107. Hamashima, S.; Nishimoto, A. Thickening of S-Phase and Sα-Phase of Various Stainless Steels Treated by Low Temperature Plasma Nitriding Using Screen. *Mater. Trans.* **2022**, *63*, 1170–1178. [CrossRef]
108. Borgioli, F. Formation of expanded phases in ferritic stainless steel nitrided at low temperatures. *Surf. Coat. Technol.* **2024**, *477*, 130309. [CrossRef]
109. Kishimoto, O.; Nishimoto, A. Low Temperature Direct Current Plasma Nitriding of Ferritic Stainless Steel with Metal Screen. In *IFHTSE 2024: Proceedings of the 29th International Federation for Heat Treatment and Surface Engineering World Congress*; ASM International: Cleveland, OH, USA, 2024; pp. 114–121. [CrossRef]
110. Michler, T.; Grischke, M.; Bewilogua, K.; Dimigen, H. Properties of duplex coatings prepared by plasma nitriding and PVD Ti–C:H deposition on X20Cr13 ferritic stainless steel. *Thin Solid Films* **1998**, *322*, 206–212. [CrossRef]
111. Bielawski, J.; Baranowska, J.; Szczecinski, K. Microstructure and properties of layers on chromium steel. *Surf. Coat. Technol.* **2006**, *200*, 6572–6577. [CrossRef]
112. Larisch, B.; Brusky, U.; Spies, H.-J. Plasma nitriding of stainless steels at low temperatures. *Surf. Coat. Technol.* **1999**, *116–119*, 205–211. [CrossRef]
113. Alphonsa, J.; Mukherjee, S.; Raja, V.S. Study of plasma nitriding and nitrocarburising of AISI 430F stainless steel for high hardness and corrosion resistance. *Corros. Eng. Sci. Technol.* **2018**, *53*, 51–58. [CrossRef]
114. Schibicheski Kurelo, B.C.E.; Lepienski, C.M.; de Oliveira, W.R.; de Souza, G.B.; Serbena, F.C.; Cardoso, R.P.; das Neves, J.C.K.; Borges, P.C. Identification of Expanded Austenite in Nitrogen-Implanted Ferritic Steel through In Situ Synchrotron X-ray Diffraction Analyses. *Metals* **2023**, *13*, 1744. [CrossRef]
115. de Sousa, R.R.M.; de Araújo, F.O.; da Costa, J.A.P.; de Oliverira, A.M.; Melo, M.S.; Alves, C., Jr. Cathodic Cage Nitriding of AISI 409 Ferritic Stainless Steel with the Addition of CH_4. *Mater. Res.* **2012**, *15*, 260–265. [CrossRef]
116. Alphonsa, I.; Chainani, A.; Raole, P.M.; Ganguli, B.; John, P.I. A study of martensitic stainless steel AISI 420 modified using plasma nitriding. *Surf. Coat. Technol.* **2002**, *150*, 263–268. [CrossRef]
117. Subrahmanyam, S.; Kumar, R.S. Investigation of microstructure and mechanical properties of liquid nitrided AISI 420 and AISI 430 stainless steels. *AIP Conf. Proc.* **2023**, *2888*, 20029. [CrossRef]
118. Spies, H.-J.; Eckstein, C.; Zimdars, H. Structure and corrosion behaviour of stainless steels after plasma and gas nitriding. *Surf. Eng.* **2002**, *18*, 459–460. [CrossRef]
119. de Araújo Junior, E.; Bandeira, R.M.; Manfrinato, M.D.; Moreto, J.A.; Borges, R.; dos Santos Vales, S.; Suzuki, P.A.; Rossino, L.S. Effect of ionic plasma nitriding process on the corrosion and micro-abrasive wear behavior of AISI 316L austenitic and AISI 470 super-ferritic stainless steels. *J. Mater. Res. Technol.* **2019**, *8*, 2180–2191. [CrossRef]
120. Li, L.; Liu, R.; Liu, Q.; Wu, Z.; Meng, X.; Fang, Y. Effects of Initial Microstructure on the Low-Temperature Plasma Nitriding of Ferritic Stainless Steel. *Coatings* **2022**, *12*, 1404. [CrossRef]

121. Speidel, M.O. Corrosion Science of Stainless Steels. In *Stainless Steels '91, Proceedings of International Conference on Stainless Steels, Chiba, Japan, 10–13 June 1991*; Iron and Steel Institute of Japan: Tokyo, Japan, 1991; Volume 1, pp. 25–35.
122. Gontijo, L.C.; Machado, R.; Casteletti, L.C.; Kuri, S.E.; Nascente, P.A.P. X-ray diffraction characterisation of expanded austenite and ferrite in plasma nitrided stainless steels. *Surf. Eng.* **2010**, *26*, 265–270. [CrossRef]
123. Espitia, L.A.; Varela, L.; Pinedo, C.E.; Tschiptschin, A.P. Cavitation erosion resistance of low temperature plasma nitrided martensitic stainless steel. *Wear* **2013**, *301*, 449–456. [CrossRef]
124. Fernandes, F.A.P.; Picone, C.A.; Totten, G.E.; Casteletti, L.C. Corrosion Behavior of Plasma Nitrided and Nitrocarburised Supermartensitic Stainless Steel. *Mater. Res.* **2018**, *21*, e20160793. [CrossRef]
125. Borgioli, F.; Fossati, A.; Raugei, L.; Galvanetto, E.; Bacci, T. Low temperature glow-discharge nitriding of stainless steels. In Proceedings of the 7th European Stainless Steel Conference: Science and Market, Como, Italy, 21–23 September 2011; Associazione Italiana di Metallurgia: Milan, Italy, 2011.
126. Scheuer, C.J.; Zanetti, F.I.; Cardoso, R.P.; Brunatto, S.F. Ultra-low—To high-temperature plasma-assisted nitriding: Revisiting and going further on the martensitic stainless steel treatment. *Mater. Res. Express* **2018**, *6*, 026529. [CrossRef]
127. Espitia, L.A.; Dong, H.; Li, X.-Y.; Pinedo, C.E.; Tschiptschin, A.P. Cavitation erosion resistance and wear mechanisms of active screen low temperature plasma nitrided AISI 410 martensitic stainless steel. *Wear* **2015**, *332–333*, 1070–1079. [CrossRef]
128. Figueroa, C.A.; Alvarez, F.; Zhang, Z.; Collins, G.A.; Short, K.T. Structural modifications and corrosion behavior of martensitic stainless steel nitrided by plasma immersion ion implantation. *J. Vac. Sci. Technol. A* **2005**, *23*, 693–698. [CrossRef]
129. Schibicheski Kurelo, B.C.E.; de Souza, G.B.; Serbena, F.C.; de Oliveira, W.R.; Marino, C.E.B.; Taminato, L.A. Performance of nitrogen ion-implanted supermartensitic stainless steel in chlorine- and hydrogen-rich environments. *Surf. Coat. Technol.* **2018**, *351*, 29–41. [CrossRef]
130. Dalibon, E.; Charadia, R.; Cabo, A.; Brühl, S.P. Short Time Ion Nitriding of AISI 420 Martensitic Stainless Steel to Improve Wear and Corrosion Resistance. *Mater. Res.* **2019**, *22*, e20190415. [CrossRef]
131. Borgioli, F.; Galvanetto, E.; Bacci, T.; Pradelli, G. Influence of the treatment atmosphere on the characteristics of glow-discharge treated sintered stainless steels. *Surf. Coat. Technol.* **2002**, *149*, 192–197. [CrossRef]
132. Scheuer, C.J.; Cardoso, R.P.; Mafra, M.; Brunatto, S.F. AISI 420 martensitic stainless steel low-temperature plasma assisted carburizing kinetics. *Surf. Coat. Technol.* **2013**, *214*, 30–37. [CrossRef]
133. Scheuer, C.J.; Possoli, F.A.A.; Borges, P.C.; Cardoso, R.P.; Brunatto, S.F. AISI 420 martensitic stainless steel corrosion resistance enhancement by low-temperature plasma carburizing. *Electrochim. Acta* **2019**, *317*, 70–82. [CrossRef]
134. Figueroa, C.A.; Alvarez, F.; Mitchell, D.R.G.; Collins, G.A.; Short, K.T. Previous heat treatment inducing different plasma nitriding behaviors in martensitic stainless steels. *J. Vac. Sci. Technol. A* **2006**, *24*, 1795–1801. [CrossRef]
135. Toscano, T.D.; Cardoso, R.P.; Brunatto, S.F. A Novel Concept of Hybrid Treatment for High-Hardenability Steels: Concomitant Hardening and Paraequilibrium Thermochemical Treatment to Produce Interstitially Hardened/Stabilized Austenite Surfaces. *Steel Res. Int.* **2020**, *91*, 2000189. [CrossRef]
136. Scheuer, C.J.; Cardoso, R.P.; Brunatto, S.F. Low-temperature Plasma Assisted Thermochemical Treatments of AISI 420 Steel: Comparative Study of Obtained Layers. *Mater. Res.* **2015**, *18*, 1392–1399. [CrossRef]
137. Tang, D.; Sun, S.; Zhang, C.; Zhan, H.; Ding, Z.; Chen, D.; Cui, G. Gas Nitriding of AISI 420 Martensitic Stainless Steel during the Incubation Period of CrN Precipitation. *J. Mater. Eng. Perform.* **2024**. [CrossRef]
138. Manova, D.; Mändl, S.; Neumann, H.; Rauschenbach, B. Wear behaviour of martensitic stainless steel after PIII surface treatment. *Surf. Coat. Technol.* **2005**, *200*, 137–140. [CrossRef]
139. Mändl, S.; Fritzsche, B.; Manova, D.; Hirsch, D.; Neumann, H.; Richter, E.; Rauschenbach, B. Wear reduction in AISI 630 martensitic stainless steel after energetic nitrogen ion implantation. *Surf. Coat. Technol.* **2005**, *195*, 258–263. [CrossRef]
140. Scheuer, C.J.; Cardoso, R.P.; Brunatto, S.F. Sequential low-temperature plasma-assisted thermochemical treatments of the AISI 420 martensitic stainless steel. *Surf. Coat. Technol.* **2021**, *421*, 127459. [CrossRef]
141. Liu, R.L.; Yan, F.; Wei, C.Y.; Yan, M.F. Characteristics of carbon-expanded α phase layer on AISI 431 stainless steel using experimental and fist-principles calculation methods. *Surf. Coat. Technol.* **2019**, *375*, 66–73. [CrossRef]
142. Rovani, A.C.; Breganon, R.; de Souza, G.S.; Brunatto, S.F.; Pintaúde, G. Scratch resistance of low-temperature plasma nitrided and carburized martensitic stainless steel. *Wear* **2017**, *376–377*, 70–76. [CrossRef]
143. Li, J.; Tao, X.; Wu, W.; Xie, G.; Yang, Y.; Zhou, X.; Zhang, S. Effect of arc current on the microstructure, tribological and corrosion performances of AISI 420 martensitic stainless steel treated by arc discharge plasma nitriding. *J. Mater. Sci.* **2023**, *58*, 2294–2309. [CrossRef]
144. Corengia, P.; Ybarra, G.; Moina, C.; Cabo, A.; Broitman, E. Microstructure and corrosion behaviour of DC-pulsed plasma nitrided AISI 410 martensitic stainless steel. *Surf. Coat. Technol.* **2004**, *187*, 63–69. [CrossRef]
145. Li, C.X.; Bell, T. Corrosion properties of plasma nitrided AISI 410 martensitic stainless steel in 3.5% NaCl and 1% HCl aqueous solutions. *Corros. Sci.* **2006**, *48*, 2036–2049. [CrossRef]
146. Xi, Y.; Liu, D.; Han, D. Improvement of corrosion and wear resistances of AISI 420 martensitic stainless steel using plasma nitriding at low temperature. *Surf. Coat. Technol.* **2008**, *202*, 2577–2583. [CrossRef]
147. Li, C.X.; Bell, T. A comparative study of low temperature plasma nitriding, carburising and nitrocarburising of AISI 410 martensitic stainless steel. *Mater. Sci. Technol.* **2007**, *23*, 355–361. [CrossRef]

148. Scheuer, C.J.; Cardoso, R.P.; Brunatto, S.F. An overview on plasma-assisted thermochemical treatments of martensitic stainless steels. *Surf. Topogr. Metrol. Prop.* **2023**, *11*, 13001. [CrossRef]
149. Brühl, S.P.; Charadia, R.; Simison, S.; Lamas, D.G.; Cabo, A. Corrosion behavior of martensitic and precipitation hardening stainless steels treated by plasma nitriding. *Surf. Coat. Technol.* **2010**, *204*, 3280–3286. [CrossRef]
150. Loto, R.T.; Loto, C.; Aiguwurhuo, O.; Evana, U. Data on the corrosion resistance quenched 420 martensitic stainless steel and annealed 316 austenitic stainless steel in dilute H_2SO_4 and HCl acid concentration. *IOP Conf. Ser. Mater. Sci. Eng.* **2020**, *872*, 12057. [CrossRef]
151. Borgioli, F.; Fossati, A.; Galvanetto, E.; Bacci, T.; Pradelli, G. Glow discharge nitriding of AISI 316L austenitic stainless steel: Influence of treatment pressure. *Surf. Coat. Technol.* **2006**, *200*, 5505–5513. [CrossRef]
152. Borgioli, F.; Galvanetto, E.; Bacci, T. Influence of surface morphology and roughness on water wetting properties of low temperature nitrided austenitic stainless steels. *Mater. Charact.* **2014**, *95*, 278–284. [CrossRef]
153. Stinville, J.C.; Cormier, J.; Templier, C.; Villechaise, P. Modeling of the lattice rotations induced by plasma nitriding of 316L polycrystalline stainless steel. *Acta Mater.* **2015**, *83*, 10–16. [CrossRef]
154. Czerwiec, T.; Tsareva, S.; Andrieux, A.; Bruyère, S.; Marcos, G. Effects of surface topography at different scales on the dispersion of the wetting data for sessile water droplets on nitrided austenitic stainless steels. *Surf. Coat. Technol.* **2022**, *441*, 128510. [CrossRef]
155. Bottoli, F.; Jellesen, M.S.; Christiansen, T.L.; Winther, G.; Somers, M.A.J. High temperature solution-nitriding and low-temperature nitriding of AISI 316: Effect on pitting potential and crevice corrosion performance. *Appl. Surf. Sci.* **2018**, *431*, 24–31. [CrossRef]
156. Maistro, G.; Yao, Y.; Klement, U.; Nyborg, L.; Cao, Y. On surface carbides in low-temperature carburized austenitic stainless steels. *Mater. Charact.* **2020**, *167*, 110462. [CrossRef]
157. Cisquini, P.; Ramos, S.V.; Viana, P.R.P.; Lins, V.d.F.C.; Franco, A.R.; Vieira, E.A. Effect of the roughness produced by plasma nitrocarburizing on corrosion resistance of AISI 304 austenitic stainless steel. *J. Mater. Res. Technol.* **2019**, *8*, 1897–1906. [CrossRef]
158. Borgioli, F.; Galvanetto, E.; Bacci, T. Effects of surface modification by means of low temperature plasma nitriding on wetting and corrosion behavior of austenitic stainless steel. *Coatings* **2020**, *10*, 98. [CrossRef]
159. Czerwiec, T.; He, H.; Weber, S.; Dong, C.; Michel, H. On the occurrence of dual diffusion layers during plasma-assisted nitriding of austenitic stainless steel. *Surf. Coat. Technol.* **2006**, *200*, 5289–5295. [CrossRef]
160. Christiansen, T.; Dahl, K.V.; Somers, M.A.J. Nitrogen diffusion and nitrogen depth profiles in expanded austenite: Experimental assessment, numerical simulation and role of stress. *Mater. Sci. Technol.* **2008**, *24*, 159–167. [CrossRef]
161. Czerwiec, T.; He, H.; Marcos, G.; Thiriet, T.; Weber, S.; Michel, H. Fundamental and Innovations in Plasma Assisted Diffusion of Nitrogen and Carbon in Austenitic Stainless Steels and Related Alloys. *Plasma Process. Polym.* **2009**, *6*, 401–409. [CrossRef]
162. Jafarpour, S.M.; Dalke, A.; Biermann, H. New Approach for Plasma Nitrocarburizing of Stainless Steels by a Modified Reactor Configuration Using a Plasma-Activated Solid Carbon Precursor. *Steel Res. Int.* **2024**, 2400247. [CrossRef]
163. Werner, K.V.; Che, H.L.; Lei, M.K.; Christiansen, T.L.; Somers, M.A.J. Low Temperature Carburizing of Stainless Steels and the Development of Carbon Expanded Austenite. *HTM Journal Heat Treat. Mater.* **2022**, *77*, 3–15. [CrossRef]
164. Borgioli, F.; Fossati, A.; Matassini, G.; Galvanetto, E.; Bacci, T. Low temperature glow-discharge nitriding of a low nickel austenitic stainless steel. *Surf. Coat. Technol.* **2010**, *204*, 3410–3417. [CrossRef]
165. Borgioli, F.; Galvanetto, E.; Bacci, T. Low temperature nitriding of AISI 300 and 200 series austenitic stainless steels. *Vacuum* **2016**, *127*, 51–60. [CrossRef]
166. Tao, X.; Li, X.; Dong, H.; Matthews, A.; Leyland, A. Evaluation of the sliding wear and corrosion performance of triode-plasma nitrided Fe-17Cr-20Mn-0.5N high-manganese and Fe-19Cr-35Ni-1.2Si high-nickel austenitic stainless steels. *Surf. Coat. Technol.* **2021**, *409*, 126890. [CrossRef]
167. Che, H.L.; Tong, S.; Wang, K.S.; Lei, M.K.; Somers, M.A.J. Co-existence of γ'_N phase and γ_N phase on nitrided austenitic Fe–Cr–Ni alloys- I. experiment. *Acta Mater.* **2019**, *177*, 35–45. [CrossRef]
168. Che, H.L.; Christiansen, T.L.; Lei, M.K.; Somers, M.A.J. Co-existence of γ'_N phase and γ_N phase in nitrided austenitic Fe-Cr-Ni alloys—II: A pragmatic modeling approach. *Acta Mater.* **2022**, *235*, 118094. [CrossRef]
169. Che, H.L.; Lei, M.K.; Somers, M.A.J. A simple model for nitrogen-induced lattice expansion of γ'_N and γ_N phases in Fe–Cr–Ni alloys with different chromium contents. *Philos. Mag. Lett.* **2020**, *100*, 435–441. [CrossRef]
170. Che, H.L.; Lei, M.K. Microstructure of perfect nitrogen-expanded austenite formed by unconstrained nitriding. *Scr. Mater.* **2021**, *194*, 113705. [CrossRef]
171. Che, H.L.; Yang, X.; Lei, M.K.; Somers, M.A.J. Co-existence of γ'_N phase and γ_N phase on nitrided austenitic Fe-Cr-Ni alloys—III. An investigation of the evolution of long-range ordered domains. *Acta Mater.* **2023**, *253*, 118971. [CrossRef]
172. Che, H.L.; Yang, X.; Lei, M.K. Pancake-like antiphase domains in perfect nitrogen-expanded austenite by TEM characterization. *Mater. Res. Express* **2023**, *10*, 106507. [CrossRef]
173. Lei, M.K. Phase transformations in plasma source ion nitrided austenitic stainless steel at low temperature. *J. Mater. Sci.* **1999**, *34*, 5975–5982. [CrossRef]
174. Tao, X.; Qi, J.; Rainforth, M.; Matthews, A.; Leyland, A. On the interstitial induced lattice inhomogeneities in nitrogen-expanded austenite. *Scr. Mater.* **2020**, *185*, 146–151. [CrossRef]
175. Tong, K.; Ye, F.; Che, H.; Lei, M.K.; Miao, S.; Zhang, C. High-density stacking faults in a supersaturated nitrided layer on austenitic stainless steel. *J. Appl. Crystallogr.* **2016**, *49*, 1967–1971. [CrossRef]

176. Tao, X.; Liu, X.; Matthews, A.; Leyland, A. The influence of stacking fault energy on plasticity mechanisms in triode-plasma nitrided austenitic stainless steels: Implications for the structure and stability of nitrogen-expanded austenite. *Acta Mater.* **2019**, *164*, 60–75. [CrossRef]
177. Che, H.L.; Yang, X.; Liu, H.Y.; Lei, M.K. Gradient self-organized dislocation in expanded austenite layer during low-temperature nitriding. *Mater. Res. Express* **2023**, *10*, 76512. [CrossRef]
178. Sah, J.V.; Dwivedi, P.K.; Mukherjee, S.; Jhala, G.; Joseph, A. Influence of γ'_N and ε'_N phases on the properties of AISI 304L after low-temperature plasma nitrocarburizing. *J. Vac. Sci. Technol. A* **2023**, *41*, 33101. [CrossRef]
179. Lei, M.K.; Huang, Y.; Zhang, Z.L. In situ Transformation of Nitrogen-induced h.c.p. Martensite in Plasma Source Ion–nitrided Austenitic Stainless Steel. *J. Mater. Sci. Lett.* **1998**, *17*, 1165–1167. [CrossRef]
180. Fossati, A.; Galvanetto, E.; Bacci, T.; Borgioli, F. Improvement of corrosion resistance of austenitic stainless steels by means of glow-discharge nitriding. *Corros. Rev.* **2011**, *29*, 209–221. [CrossRef]
181. Tsujikawa, M.; Yamauchi, N.; Ueda, N.; Sone, T.; Hirose, Y. Behavior of carbon in low temperature plasma nitriding layer of austenitic stainless steel. *Surf. Coat. Technol.* **2005**, *193*, 309–313. [CrossRef]
182. Williamson, D.L.; Davis, J.A.; Wilbur, P.J. Effect of austenitic stainless steel composition on low-energy, high-flux, nitrogen ion beam processing. *Surf. Coat. Technol.* **1998**, *103–104*, 178–184. [CrossRef]
183. Manova, D.; Mändl, S. Initial phase formation during nitriding of austenitic stainless steel. *Surf. Coat. Technol.* **2023**, *456*, 129258. [CrossRef]
184. Mändl, S.; Manova, D. Comparison of Nitriding Behavior for Austenitic Stainless Steel 316Ti and Super Austenitic Stainless Steel 904L. *Metals* **2024**, *14*, 659. [CrossRef]
185. Bell, T. Surface engineering of austenitic stainless steel. *Surf. Eng.* **2002**, *18*, 415–422. [CrossRef]
186. Borgioli, F.; Galvanetto, E.; Bacci, T. Surface modification of austenitic stainless steel by means of low pressure glow-discharge treatments with nitrogen. *Coatings* **2019**, *9*, 604. [CrossRef]
187. Li, X.Y. Low Temperature Plasma Nitriding of 316 Stainless Steel—Nature of S Phase and Its Thermal Stability. *Surf. Eng.* **2001**, *17*, 147–152. [CrossRef]
188. Li, X.Y.; Thaiwatthana, S.; Dong, H.; Bell, T. Thermal stability of carbon S phase in 316 stainless steel. *Surf. Eng.* **2002**, *18*, 448–451. [CrossRef]
189. Fossati, A.; Borgioli, F.; Galvanetto, E.; Bacci, T. Glow-discharge nitriding of AISI 316L austenitic stainless steel: Influence of treatment time. *Surf. Coat. Technol.* **2006**, *200*, 3511–3517. [CrossRef]
190. Sun, Y. Hybrid plasma surface alloying of austenitic stainless steels with nitrogen and carbon. *Mater. Sci. Eng. A* **2005**, *404*, 124–129. [CrossRef]
191. Sun, Y.; Li, X.; Bell, T. Low temperature plasma carburising of austenitic stainless steels for improved wear and corrosion resistance. *Surf. Eng.* **1999**, *15*, 49–54. [CrossRef]
192. Huang, Z.; Guo, Z.-X.; Liu, L.; Guo, Y.-Y.; Chen, J.; Zhang, Z.; Li, J.-L.; Li, Y.; Zhou, Y.-W.; Liang, Y.-S. Structure and corrosion behavior of ultra-thick nitrided layer produced by plasma nitriding of austenitic stainless steel. *Surf. Coat. Technol.* **2021**, *405*, 126689. [CrossRef]
193. Stio, M.; Martinesi, M.; Treves, C.; Borgioli, F. Cultures and co-cultures of human blood mononuclear cells and endothelial cells for the biocompatibility assessment of surface modified AISI 316L austenitic stainless steel. *Mater. Sci. Eng. C* **2016**, *69*, 1081–1091. [CrossRef] [PubMed]
194. Yazıcı, M.; Çomaklı, O.; Yetim, T.; Yetim, A.F.; Çelik, A. The effect of plasma nitriding temperature on the electrochemical and semiconducting properties of thin passive films formed on 316L stainless steel implant material in SBF solution. *Surf. Coat. Technol.* **2015**, *261*, 181–188. [CrossRef]
195. Fossati, A.; Borgioli, F.; Galvanetto, E.; Bacci, T. Corrosion resistance properties of glow-discharge nitrided AISI 316L austenitic stainless steel in NaCl solutions. *Corros. Sci.* **2006**, *48*, 1513–1527. [CrossRef]
196. Schibicheski Kurelo, B.C.E.; de Souza, G.B.; Serbena, F.C.; Lepienski, C.M.; Chuproski, R.F.; Borges, P.C. Improved saline corrosion and hydrogen embrittlement resistances of superaustenitic stainless steel by PIII nitriding. *J. Mater. Res. Technol.* **2022**, *18*, 1717–1731. [CrossRef]
197. Kamachi Mudali, U.; Shankar, P.; Ningshen, S.; Dayal, R.K.; Khatak, H.S.; Raj, B. On the pitting corrosion resistance of nitrogen alloyed cold worked austenitic stainless steels. *Corros. Sci.* **2002**, *44*, 2183–2198. [CrossRef]
198. Escalada, L.; Dalibon, E.L.; Brühl, S.P.; Manova, D.; Mändl, S.; Simison, S. Influence of Inclusions in the Corrosion Behavior of Plasma Nitrided Stainless Steel. *Adv. Eng. Mater.* **2023**, *25*, 2201112. [CrossRef]
199. Pardo, A.; Merino, M.C.; Coy, A.E.; Viejo, F.; Arrabal, R.; Matykina, E. Pitting corrosion behaviour of austenitic stainless steels—Combining effects of Mn and Mo additions. *Corros. Sci.* **2008**, *50*, 1796–1806. [CrossRef]
200. Saravanan, P.; Raja, V.S.; Mukherjee, S. Effect of alloyed molybdenum on corrosion behavior of plasma immersion nitrogen ion implanted austenitic stainless steel. *Corros. Sci.* **2013**, *74*, 106–115. [CrossRef]
201. De Las Heras, E.; Ybarra, G.; Lamas, D.; Cabo, A.; Dalibon, E.L.; Brühl, S.P. Plasma nitriding of 316L stainless steel in two different N_2-H_2 atmospheres—Influence on microstructure and corrosion resistance. *Surf. Coat. Technol.* **2017**, *313*, 47–54. [CrossRef]
202. Borgioli, F.; Fossati, A.; Galvanetto, E.; Bacci, T. Glow-discharge nitriding of AISI 316L austenitic stainless steel: Influence of treatment temperature. *Surf. Coat. Technol.* **2005**, *200*, 2474–2480. [CrossRef]

203. Zatkalíková, V.; Drímalová, P.; Balin, K.; Slezák, M.; Markovičová, L. Electrochemical Behavior of Plasma-Nitrided Austenitic Stainless Steel in Chloride Solutions. *Materials* **2024**, *17*, 4189. [CrossRef] [PubMed]
204. Stio, M.; Martinesi, M.; Treves, C.; Borgioli, F. In vitro response of human peripheral blood mononuclear cells to AISI 316L austenitic stainless steel subjected to nitriding and collagen coating treatments. *J. Mater. Sci. Mater. Med.* **2015**, *26*, 100. [CrossRef] [PubMed]
205. Martinesi, M.; Bruni, S.; Stio, M.; Treves, C.; Bacci, T.; Borgioli, F. Biocompatibility evaluation of surface-treated AISI 316L austenitic stainless steel in human cell cultures. *J. Biomed. Mater. Res. Part A* **2007**, *80*, 131–145. [CrossRef] [PubMed]
206. Martinesi, M.; Stio, M.; Treves, C.; Borgioli, F. Biocompatibility studies of low temperature nitrided and collagen-I coated AISI 316L austenitic stainless steel. *J. Mater. Sci. Mater. Med.* **2013**, *24*, 1501–1513. [CrossRef] [PubMed]
207. Lei, M.K.; Zhu, X.M. In vitro corrosion resistance of plasma source ion nitrided austenitic stainless steels. *Biomaterials* **2001**, *22*, 641–647. [CrossRef] [PubMed]
208. Spies, H.-J.; Eckstein, C.; Biermann, H.; Franke, A. Corrosion behaviour of stainless steels after low temperature thermochemical treatment. *Materwiss. Werksttech.* **2010**, *41*, 133–141. [CrossRef]
209. Sah, J.; Joseph, A.; Jhala, G.; Mukherjee, S. On the Effects of H_2 and Ar on Dual Layer Formed by Plasma Nitrocarburizing on Austenitic Stainless Steels. *J. Mater. Eng. Perform.* **2022**, *31*, 2664–2677. [CrossRef]
210. Sun, Y. Enhancement in corrosion resistance of austenitic stainless steels by surface alloying with nitrogen and carbon. *Mater. Lett.* **2005**, *59*, 3410–3413. [CrossRef]
211. Borowski, T. Enhancing the Corrosion Resistance of Austenitic Steel Using Active Screen Plasma Nitriding and Nitrocarburising. *Materials* **2021**, *14*, 3320. [CrossRef]
212. Adachi, S.; Yamaguchi, T.; Ueda, N. Formation and Properties of Nitrocarburizing S-Phase on AISI 316L Stainless Steel-Based WC Composite Layers by Low-Temperature Plasma Nitriding. *Metals* **2021**, *11*, 1538. [CrossRef]
213. Buhagiar, J.; Dong, H. Corrosion properties of S-phase layers formed on medical grade austenitic stainless steel. *J. Mater. Sci. Mater. Med.* **2012**, *23*, 271–281. [CrossRef] [PubMed]
214. Formosa, D.; Hunger, R.; Spiteri, A.; Dong, H.; Sinagra, E.; Buhagiar, J. Corrosion behaviour of carbon S-phase created on Ni-free biomedical stainless steel. *Surf. Coat. Technol.* **2012**, *206*, 3479–3487. [CrossRef]
215. Adachi, S.; Yamaguchi, T.; Tanaka, K.; Nishimura, T.; Ueda, N. Effects of Solid-Solution Carbon and Eutectic Carbides in AISI 316L Steel-Based Tungsten Carbide Composites on Plasma Carburizing and Nitriding. *Metals* **2023**, *13*, 1350. [CrossRef]
216. Buhagiar, J.; Spiteri, A.; Sacco, M.; Sinagra, E.; Dong, H. Augmentation of crevice corrosion resistance of medical grade 316LVM stainless steel by plasma carburising. *Corros. Sci.* **2012**, *59*, 169–178. [CrossRef]
217. Wang, J.; Lin, Y.; Yan, J.; Zeng, D.; Huang, R.; Hu, Z. Modification of AISI 304 Stainless Steel Surface by the Low Temperature Complex Salt Bath Nitriding at 430 °C. *ISIJ Int.* **2012**, *52*, 1118–1123. [CrossRef]
218. Sun, Y. Response of cast austenitic stainless steel to low temperature plasma carburizing. *Mater. Des.* **2009**, *30*, 1377–1380. [CrossRef]
219. Ceschini, L.; Chiavari, C.; Lanzoni, E.; Martini, C. Low-temperature carburised AISI 316L austenitic stainless steel: Wear and corrosion behaviour. *Mater. Des.* **2012**, *38*, 154–160. [CrossRef]
220. Tian, R.; Sun, J.; Wang, L. Plasma-nitrided austenitic stainless steel 316L as bipolar plate for PEMFC. *Int. J. Hydrogen Energy* **2006**, *31*, 1874–1878. [CrossRef]
221. Lin, K.; Li, X.; Sun, Y.; Luo, X.; Dong, H. Active screen plasma nitriding of 316 stainless steel for the application of bipolar plates in proton exchange membrane fuel cells. *Int. J. Hydrogen Energy* **2014**, *39*, 21470–21479. [CrossRef]
222. Liu, C.; Li, C.; Ye, Z.; Suo, Z.; Jiang, F.; Gu, J. Investigation of evolution of γ_N phase and its effect on conductivity and corrosion resistance of plasma-nitrided 316 L stainless steel bipolar plate for proton exchange membrane fuel cell. *Surf. Topogr. Metrol. Prop.* **2024**, *12*, 25001. [CrossRef]
223. Kuczynska-Wydorska, M.; Flis, J. Corrosion and passivation of low-temperature nitrided AISI 304L and 316L stainless steels in acidified sodium sulphate solution. *Corros. Sci.* **2008**, *50*, 523–533. [CrossRef]
224. Reinders, P.M.; Bräuer, G. A model to predict the S-phase thickness and the change in corrosion behavior toward H_2SO_4 of 316L austenitic stainless steel after plasma nitriding. *Surf. Coat. Technol.* **2023**, *475*, 130135. [CrossRef]
225. Corujeira Gallo, S.; Dong, H. Corrosion behaviour of direct current and active screen plasma carburised AISI 316 stainless steel in boiling sulphuric acid solutions. *Corros. Eng. Sci. Technol.* **2011**, *46*, 8–16. [CrossRef]
226. Rosalbino, F.; Scavino, G.; Ubertalli, G. Passivity and its breakdown on low temperature plasma carburized AISI 204Cu stainless steel in chloride-containing solution. *Mater. Corros.* **2018**, *69*, 563–571. [CrossRef]
227. Shi, W.; Wang, J.; Jiang, R.; Xiang, S. Anticorrosion Properties of the Low-Temperature Glow Plasma Nitriding Layer on AISI 904L Austenitic Stainless Steel in Hydrofluoric Acid Obtained at Various NH_3 Pressures. *Coatings* **2020**, *10*, 1156. [CrossRef]
228. Jiang, R.; Zou, G.; Shi, W.; Liang, Y.; Xiang, S. Corrosion Behavior of Plasma-Nitrided 904L Austenitic Stainless Steel in Hydrofluoric Acid. *J. Mater. Eng. Perform.* **2019**, *28*, 1863–1872. [CrossRef]
229. Pinedo, C.E.; Varela, L.B.; Tschiptschin, A.P. Low-temperature plasma nitriding of AISI F51 duplex stainless steel. *Surf. Coat. Technol.* **2013**, *232*, 839–843. [CrossRef]
230. Chiu, L.H.; Su, Y.Y.; Chen, F.S.; Chang, H. Microstructure and Properties of Active Screen Plasma Nitrided Duplex Stainless Steel. *Mater. Manuf. Process.* **2010**, *25*, 316–323. [CrossRef]

231. Tschiptschin, A.P.; Varela, L.B.; Pinedo, C.E.; Li, X.Y.; Dong, H. Development and microstructure characterization of single and duplex nitriding of UNS S31803 duplex stainless steel. *Surf. Coat. Technol.* **2017**, *327*, 83–92. [CrossRef]
232. Christiansen, T.; Somers, M.A.J. Low temperature gaseous nitriding and carburising of stainless steel. *Surf. Eng.* **2005**, *21*, 445–455. [CrossRef]
233. Shen, H.; Wang, L.; Sun, J. Effect of plasma nitriding at low temperature on the corrosion resistance and conductivity of 2205 duplex stainless steel. *Surf. Eng.* **2021**, *37*, 749–754. [CrossRef]
234. Alphonsa, J.; Raja, V.S.; Mukherjee, S. Study of plasma nitriding and nitrocarburizing for higher corrosion resistance and hardness of 2205 duplex stainless steel. *Corros. Sci.* **2015**, *100*, 121–132. [CrossRef]
235. de Oliveira, W.R.; Kurelo, B.C.E.S.; Ditzel, D.G.; Serbena, F.C.; Foerster, C.E.; de Souza, G.B. On the S-phase formation and the balanced plasma nitriding of austenitic-ferritic super duplex stainless steel. *Appl. Surf. Sci.* **2018**, *434*, 1161–1174. [CrossRef]
236. Li, X.; Dou, W.; Tian, L.; Dong, H. Combating the Tribo-Corrosion of LDX2404 Lean Duplex Stainless Steel by Low Temperature Plasma Nitriding. *Lubricants* **2018**, *6*, 93. [CrossRef]
237. Kahn, H.; Heuer, A.H.; Michal, G.M.; Ernst, F.; Sharghi-Moshtaghin, R.; Ge, Y.; Natishan, P.M.; Rayne, R.J.; Martin, F.J. Interstitial hardening of duplex 2205 stainless steel by low temperature carburisation: Enhanced mechanical and electrochemical performance. *Surf. Eng.* **2012**, *28*, 213–219. [CrossRef]
238. Calabokis, O.P.; de la Rosa, Y.N.; Lepienski, C.M.; Cardoso, R.P.; Borges, P.C. Crevice and pitting corrosion of low temperature plasma nitrided UNS S32750 super duplex stainless steel. *Surf. Coat. Technol.* **2021**, *413*, 127095. [CrossRef]
239. Possoli, F.A.A.; Souza, A.P.N.; Bernardelli, E.A.; Borges, P.C. Tribocorrosion assessment of low-temperature plasma nitrided super duplex stainless steel. *Surf. Coat. Technol.* **2024**, *479*, 130572. [CrossRef]
240. Bielawski, J.; Baranowska, J. Formation of nitrided layers on duplex steel—Influence of multiphase substrate. *Surf. Eng.* **2010**, *26*, 299–304. [CrossRef]
241. Pinedo, C.E.; Tschiptschin, A.P. Low temperature plasma carburizing of AISI 316L austenitic stainless steel and AISI F51 duplex stainless steel. *Rev. Esc. Minas* **2013**, *66*, 209–214. [CrossRef]
242. Lei, K.; Bai, J.; Wang, B. Low temperature nitriding behavior in annealed 2205 duplex stainless steel. *Heat Treat. Surf. Eng.* **2024**, *6*, 2330740. [CrossRef]
243. Dib, J.; Gómez, B.; Strubbia, R.; Ares, A.; Méndez, C.; Fuster, V.; Hereñú, S. Characterization of Plasma Nitrided Duplex Stainless Steel: Influence of Prior Shot Peening and Nitriding Atmosphere. *J. Mater. Eng. Perform.* **2023**, *32*, 406–414. [CrossRef]
244. Zhao, S.; Wang, L. Formation and properties of nitrided layer on 2205 duplex stainless steel by anodic plasma-nitriding assisted with hollow cathode discharge. *J. Mater. Res. Technol.* **2024**, *31*, 3652–3660. [CrossRef]
245. Pintaude, G.; Rovani, A.C.; das Neves, J.C.K.; Lagoeiro, L.E.; Li, X.; Dong, H.S. Wear and Corrosion Resistances of Active Screen Plasma-Nitrided Duplex Stainless Steels. *J. Mater. Eng. Perform.* **2019**, *28*, 3673–3682. [CrossRef]
246. Pereira Neto, J.O.; Silva, R.O.D.; Silva, E.H.D.; Moreto, J.A.; Bandeira, R.M.; Manfrinato, M.D.; Rossino, L.S. Wear and Corrosion Study of Plasma Nitriding F53 Super duplex Stainless Steel. *Mater. Res.* **2016**, *19*, 1241–1252. [CrossRef]
247. Riazi, H.; Ashrafizadeh, F.; Hosseini, S.R.; Ghomashchi, R.; Liu, R. Characterization of simultaneous aged and plasma nitrided 17-4 PH stainless steel. *Mater. Charact.* **2017**, *133*, 33–43. [CrossRef]
248. Bernardelli, E.A.; Borges, P.C.; Fontana, L.C.; Floriano, J.B. Role of plasma nitriding temperature and time in the corrosion behaviour and microstructure evolution of 15-5 PH stainless steel. *Kov. Mater.* **2010**, *48*, 110–115. [CrossRef]
249. Wang, Z.; Grimm, M.; Lindner, T.; Schubert, F.; Winkler, K.; Berger, R.; Lampke, T. Wear and corrosion properties of low-temperature nitrocarburized 17-4PH SLM components. *Surf. Coat. Technol.* **2024**, *494*, 131399. [CrossRef]
250. Dong, H.; Esfandiari, M.; Li, X.Y. On the microstructure and phase identification of plasma nitrided 17-4PH precipitation hardening stainless steel. *Surf. Coat. Technol.* **2008**, *202*, 2969–2975. [CrossRef]
251. Wang, J.; Lin, Y.; Zeng, D.; Yan, J.; Fan, H. Effects of the Process Parameters on the Microstructure and Properties of Nitrided 17-4PH Stainless Steel. *Metall. Mater. Trans. B* **2013**, *44*, 414–422. [CrossRef]
252. Esfandiari, M.; Dong, H. The corrosion and corrosion–wear behaviour of plasma nitrided 17-4PH precipitation hardening stainless steel. *Surf. Coat. Technol.* **2007**, *202*, 466–478. [CrossRef]
253. Han, Z.; Zhuang, W.; Lai, P.; Wang, J.; Guo, X.; Zhang, L. General corrosion behavior and mechanism of low-temperature plasma nitrided 17–4PH stainless steel in high temperature water. *Mater. Charact.* **2024**, *209*, 113702. [CrossRef]
254. Han, Z.; Lu, J.; Yin, C.; Lai, P.; Zhuang, W.; Li, L.; Wang, J.; Zhang, L.; Guo, X. Composition, microstructure, and phase evolution of 17-4PH stainless steel with a work-hardened layer in the low-temperature plasma nitriding process. *Surf. Coat. Technol.* **2022**, *451*, 128950. [CrossRef]
255. Liu, D.; Liu, D.; Wu, Y.; Yang, J.; Xu, X.; Li, M.; Li, S.; Ma, A.; Liang, Y. Insight into nitriding behavior and corrosion mechanism in 17-4PH steel: The influence of nanocrystalline structure. *J. Mater. Res. Technol.* **2023**, *27*, 3761–3776. [CrossRef]
256. Pinedo, C.E.; Larrotta, S.I.V.; Nishikawa, A.S.; Dong, H.; Li, X.-Y.; Magnabosco, R.; Tschiptschin, A.P. Low temperature active screen plasma nitriding of 17–4 PH stainless steel. *Surf. Coat. Technol.* **2016**, *308*, 189–194. [CrossRef]
257. Bottoli, F.; Winther, G.; Christiansen, T.L.; Somers, M.A.J. Influence of Microstructure and Process Conditions on Simultaneous Low-Temperature Surface Hardening and Bulk Precipitation Hardening of Nanoflex®. *Metall. Mater. Trans. A* **2015**, *46*, 5201–5216. [CrossRef]
258. Kochmański, P.; Długozima, M.; Baranowska, J. Structure and Properties of Gas-Nitrided, Precipitation-Hardened Martensitic Stainless Steel. *Materials* **2022**, *15*, 907. [CrossRef] [PubMed]

259. Lee, I. Combination of plasma nitriding and nitrocarburizing treatments of AISI 630 martensitic precipitation hardening stainless steel. *Surf. Coat. Technol.* **2019**, *376*, 8–14. [CrossRef]
260. Heuer, A.H.; Kahn, H.; O'Donnell, L.J.; Ernst, F.; Michal, G.M.; Rayne, R.J.; Martin, F.J.; Natishan, P.M. Carburization-Enhanced Passivity of PH13-8 Mo: A Precipitation-Hardened Martensitic Stainless Steel. *Electrochem. Solid-State Lett.* **2010**, *13*, C37. [CrossRef]
261. Wang, D.; Chen, C.-W.; Dalton, J.C.; Yang, F.; Sharghi-Moshtaghin, R.; Kahn, H.; Ernst, F.; Williams, R.E.A.; McComb, D.W.; Heuer, A.H. "Colossal" interstitial supersaturation in delta ferrite in stainless steels—I. Low-temperature carburization. *Acta Mater.* **2015**, *86*, 193–207. [CrossRef]
262. Wang, D.; Kahn, H.; Ernst, F.; Heuer, A.H. "Colossal" interstitial supersaturation in delta ferrite in stainless steels: (II) low-temperature nitridation of the 17-7 PH alloy. *Acta Mater.* **2017**, *124*, 237–246. [CrossRef]
263. Long, H.; Zhou, X.; Ma, Y.; Li, K.; Ren, J. The Effect of Heat Treatment on the Plasma Nitriding of Hot-Rolled 17–7 PH Stainless Steel. *Metals* **2024**, *14*, 1061. [CrossRef]
264. Esfandiari, M.; Dong, H. Improving the surface properties of A286 precipitation-hardening stainless steel by low-temperature plasma nitriding. *Surf. Coat. Technol.* **2007**, *201*, 6189–6196. [CrossRef]
265. Fernandes, F.A.P.; Christiansen, T.L.; Somers, M.A.J. Low Temperature Gaseous Nitriding of a Stainless Steel Containing Strong Nitride Formers. In Proceedings of the Heat Treat & Surface Engineering Conference & Expo, Chennai, India, 16–18 May 2013; ASM International: Chennai, India, 2013.
266. Christiansen, T.L.; Dahl, K.V.; Somers, M.A.J. New Stainless Steel Alloys for Low Temperature Surface Hardening? *BHM Berg- und Hüttenmännische Monatshefte* **2015**, *160*, 406–412. [CrossRef]
267. Scheuer, C.J.; Cardoso, R.P.; Mafra, M.; Brunatto, S.F. Effects of the Voltage and Pressure on the Carburizing of Martensitic Stainless Steel in Pulsed DC Glow Discharge. *Mater. Res.* **2021**, *24*, e20210154. [CrossRef]
268. Jafarpour, S.M.; Mandel, M.; Krüger, L.; Biermann, H.; Dalke, A. Functional properties of expanded austenite generated on AISI 316L by plasma nitrocarburizing using different active screen materials. *Mater. Res. Express* **2024**, *11*, 116501. [CrossRef]
269. *ASTM G5-14*; Standard Reference Test Method for Making Potentiodynamic Anodic Polarization Measurements. ASTM International: West Conshohocken, PA, USA, 2014.
270. Zhang, X.L.; Jiang, Z.H.; Yao, Z.P.; Song, Y.; Wu, Z.D. Effects of scan rate on the potentiodynamic polarization curve obtained to determine the Tafel slopes and corrosion current density. *Corros. Sci.* **2009**, *51*, 581–587. [CrossRef]
271. Kurz, S.; Seemann, P.; Gümpel, P. Electrochemical investigation of passive layer formation and degradation on 1.4301 at neutral Ph—Significance of experimental parameters. In Proceedings of the 7th European Stainless Steel Conference: Science and Market, Como, Italy, 21–23 September 2011; Associazione Italiana di Metallurgia: Milan, Italy, 2011.
272. Frangini, S.; De Cristofaro, N. Analysis of the galvanostatic polarization method for determining reliable pitting potentials on stainless steels in crevice-free conditions. *Corros. Sci.* **2003**, *45*, 2769–2786. [CrossRef]